12-2013

Alternative Steel Reinforcement in Mechanically Stabilized Earth (MSE) Walls

Daniel T. Pond
Utah State University

ALTERNATIVE STEEL REINFORCEMENT IN

MECHANICALLY STABILIZED EARTH (MSE) WALLS

by

Daniel T. Pond

A thesis submitted in partial fulfillment
of the requirements for the degree

of

MASTER OF SCIENCE

In

Civil and Environmental Engineering

Approved:

_____   _____
Dr. James A. Bay   Dr. John D. Rice
Major Professor   Committee Member

_____   _____
Dr. Paul Barr   Dr. Mark R. McLellan
Committee Member   Vice President for Research and
                                          Dean of the School of Graduate Studies

Utah State University
Logan, Utah

2013

ABSTRACT

Exploration of Mechanically Stabilized Earth (MSE)

Using Alternative Steel Reinforcement

by

Daniel T. Pond, Master of Science

Utah State University, 2013

Major Professor: Dr. James A. Bay
Department: Civil and Environmental Engineering

Mechanically Stabilize Earth (MSE) is a method in which soil tensile strength and shear resistance are increased by the pullout capacity and friction at the soil-reinforcement interfaces of the reinforcement used. The traditional forms of reinforcement include bars, galvanized strips, welded wire mats or steel grids, and geosynthetics.

Corrosion is the decaying and destroying of metal. It is an issue that needs to be accounted for when doing engineering designs for retaining walls with steel reinforcement. This study investigates alternative steel reinforcement shapes and their efficiencies related to corrosion and pullout resistance. Crimped wire is one of the shapes evaluated. Previously, a full-scale MSE wall was design and constructed at Utah State University (USU) using crimped wire. These crimps were measured to obtain deflections from the wall. Also, RECO straps are compared to round bars for corrosion and pullout resistance. RECO straps have a rectangular cross-section while round bars have a

circular cross-section. Regarding corrosion, circular cross-section is beneficial over rectangular cross-sections. This data is to help find the most economical and efficient shape and size of reinforcement in MSE walls.

(155 pages)

PUBLIC ABSTRACT

Exploration of Mechanically Stabilized Earth (MSE)

Using Alternative Steel Reinforcement

Mechanically Stabilize Earth (MSE) is a method in which soil tensile strength and shear resistance is increased by using reinforcement. The traditional forms of reinforcement include bars, galvanized strips, welded wire mats or steel grids, and geosynthetics.

When steel is used as reinforcement in MSE walls, it gets corroded or decayed. Certain shapes of reinforcement will have less corrosion because less surface area is exposed. Pullout resistance is the ability to resist a tensile force. This can be affected by the design and shape of the steel. This study simulates different overburden depths or pressures for pullout resistance and evaluates standard corrosion rates.

Daniel T. Pond

ACKNOWLEDGMENTS

I would like to thank my committee members, Drs. John Rice and Paul Barr, for the interest and support in my education as well as my project. I would also like to thank my major advisor, Dr. Jim Bay. It was great to work with him because of his enthusiasm and love for Geotechnical Engineering. I would also like to thank Dr. Joe Caliendo for recommending me for the project. I was a little intimidated to do a thesis but Dr. Caliendo encouraged me to take a chance and so I have!

Many thanks to Ken Jewkes and all the time he put in. He was knowledgeable in helping us create and do design modifications to our equipment. He willingly shared his tools which aided in the advancement of the project.

Utah State University and I would like to thank Hilfiker Retaining Walls for financial and technical support in the project. They have contributed much to Utah State University's Civil Engineering Department and their graduate students.

I would like to thank all my family and friends who have supported me. I would also like to thank my dad for his enthusiasm in my education.

Daniel T. Pond

CONTENTS

LIST OF TABLES

LIST OF FIGURES

CHAPTER 1

INTRODUCTION

1.1 Executive Summary

A retaining wall is a structure which retains or resists soil and rock loads. There are many methods to design a retaining wall. Gravity, cantilever, and mechanically stabilize earth (MSE) retaining walls are a few types. Gravity walls are constructed with concrete or stone masonry and rely on the weight of the wall to resist the soil forces. Cantilever walls are made of reinforced concrete and have a thin stem and a base slab. The loads are cantilevered to the base of the wall where it is transferred to the ground below. MSE walls are a method in which reinforcement is used at different elevations of the wall. The reinforcement reduces the load on the wall. The soil tensile strength and shear resistance is increased by the pullout capacity and friction at the soil-reinforcement interfaces of the reinforcement used. MSE walls are often less costly than gravity or cantilever walls. There two categories of reinforcement in MSE walls, extensible and inextensible material. Extensible materials such as geosynthetics are plastic polymer mesh and grids. Inextensible materials include steel bars, galvanized strips, welded wire mats or steel grids.

In this project, we look at two ways to increase efficiency in MSE walls. One method is using round bars versus using a rectangular bar like a RECO strap. This is more efficient because there is less surface area exposed to the ground and thus less corrosion occurs. The second method includes using crimped mats. Using crimped mats allows the steel reinforcement to have extensible properties like geosythetic material.

1.2 Organization

    This thesis includes seven chapters. Chapter 2 is a literature review and includes the background and technical information on AASHTO LRFD design, K-Stiffness method, and pullout resistance. Chapter 3 presents crimp deformations from the USU wall and predictions of the crimp reinforcement stiffness. Chapter 4 includes the various steel shapes of reinforcement tested for pullout resistance, the process and results. Chapter 5 includes the connection capacity of the reinforcement to the wall facing. Chapter 6 contains the galvanized crimps section. It focuses on the integrity of the galvanization coating and the stiffness measurements. Finally, Chapter 7 includes the summary, conclusions, and recommendations related to this thesis.

CHAPTER 2

LITERATURE REVIEW

2.1 Background

Reinforcement material can be classified into two types based on modulus: inextensible materials and extensible materials. Inextensible materials include wire mesh, steel strips, bar mat, and welded wire or steel grids. Extensible materials include non-metallic material such as geosynthetics. Extensibility is a property that allows the material to extend or deform. Metals are stiff and do not deform as easily so they are considered inextensible. Pullout resistance is the strength of the friction between the reinforcement and the soil particles. It is discussed in the last section.

In this chapter, we look at two methods for designing MSE walls, the AASHTO LRFD Bridge Design Specifications and K-Stiffness Method. The method developed by AASHTO considers the external stability of wall system and internal stability of reinforced soil mass behind the facing. The K-Stiffness method was developed empirically from case studies to predict reinforcement tension as a function of the stiffness of the reinforcement. This method provides a transition between geosynthetic and steel reinforced soil walls.

2.2 AASHTO LRFD Bridge Design Specifications for MSE Walls

2.2.1 General

The AASHTO load reduction factored design (LFRD) bridge design specifications for MSE walls presented in this thesis is taken from the AASHTO LRFD Bridge Design Specifications 5th edition, 2010 manual.

2.2.2 Minimum Length of Soil Reinforcement

MSE walls require a reinforcement length of at least 70% of the wall height as measured from the leveling pad. The reinforcement length should be increased as surcharges and other external loads require. The commentary states that the requirement of a uniform reinforcement length equal to 70% of the height has no theoretical justification, only that it has been the basis of many successful designs to-date.

A uniform reinforcement length throughout the height of the wall is required. If evidence is presented that a variation of length is satisfactory, then it is acceptable. To meet pullout requirements, or to address seismic or impact loads, the uppermost reinforcement layers maybe be lengthened above 70% of the wall height. To meet overall global stability requirements the lowermost reinforcement layers may be lengthened beyond 70% of the wall height. For walls on competent foundation soil such that Standard Penetration Test (SPT) greater than 50, the bottom reinforcements layers can be decreased to a minimum of 40% of the wall height.

2.2.3 Internal Stability

The Simplified Method used for load calculations in MSE wall design is presented. To find the maximum loads we first need to calculate the vertical stresses at each reinforcement layer and then multiply that by a lateral earth pressure coefficient.   Theses vertical stresses are used to compute the horizontal stresses. Figure 2.1 shows the geometry of an MSE wall.

Vertical stress calculations are shown in Equation 2.1.

$$\sigma_v = \gamma_r Z + q \tag{2.1}$$
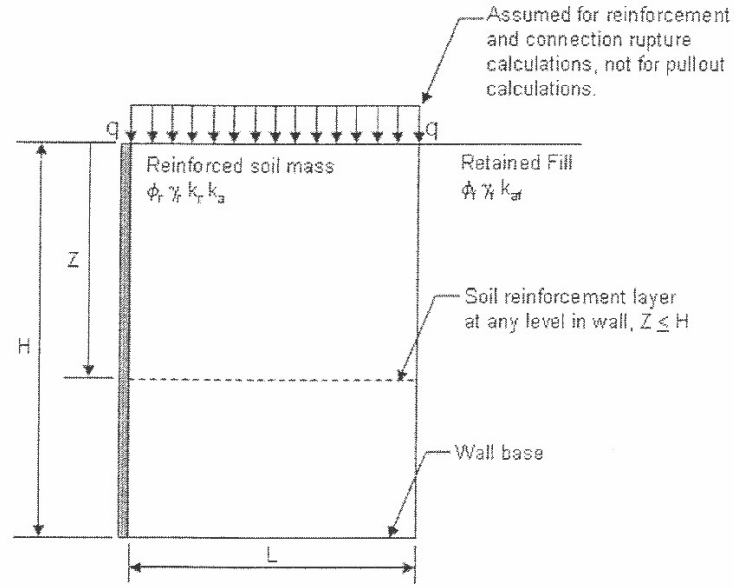
Fig. 2.1. Geometry of typical MSE wall design (AASHTO Fig. 11.10.10.1-1)

where γ_r is the is the unit weight of the reinforced soil mass, Z is the depth of the

reinforcement layer measured from the top of the wall, q is the surcharge or any external

load applied to the top of the wall. Equation 2.2 shows how to calculate the horizontal

stresses.

$$\sigma_H = \gamma_P(\sigma_v k_r) \tag{2.2}$$

where γ_P is the load factor for vertical earth pressure EV from Table 3.4.1-2 in the

AASHTO LRFD Bridge Design Specifications manual, σ_v is the vertical stress calculated

from Equation 2.1, and k_r is the lateral stress coefficient found on Figure 2.2.

Assuming Rankine conditions, for a vertical wall, k_a is calculated using Equation 2.3.

This method assumes there is no wall friction, which is a typical assumption in MSE wall

design.

$$k_a = tan^2(45 - \frac{\varphi}{2}) \tag{2.3}$$
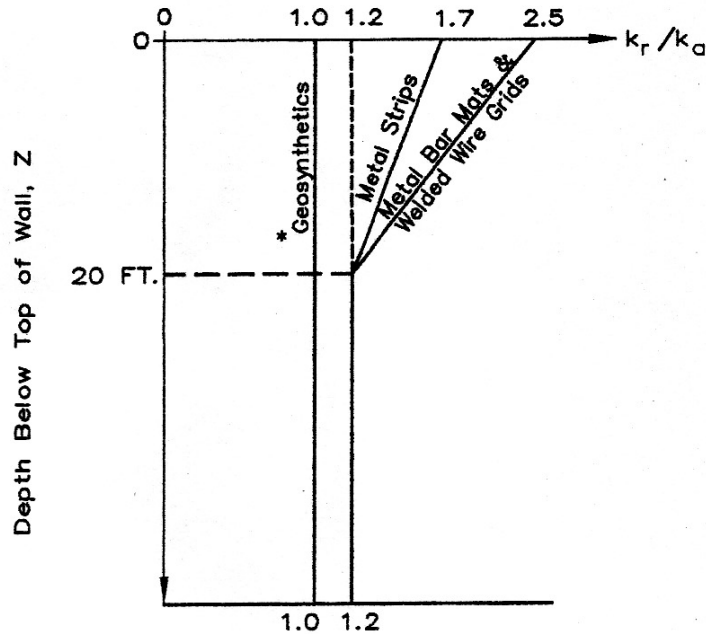
*Does not apply to polymer strip reinforcement

Fig. 2.2. Variation of the coefficient of lateral stress ratio k_r/k_a with depth in a MSE wall (AASHTO Fig. 11.10.6.2.1-3)

where φ is the friction angle of the soil behind the face of the MSE wall. The applied factored load per unit wall width to the reinforcements, T_{max}, is calculated with Equation 2.4 (AASHTO Equation 11.10.6.2.1-2).

$$T_{max} = \sigma_H S_v \tag{2.4}$$

where σ_H is the factored horizontal soil stress at the reinforcement, S_v is the vertical spacing of the reinforcement. A vertical spacing greater than 2.7 feet should not be used unless there is enough data to support larger spacings.

The location for the locus of maximum stress is shown Figures 2.3 and 2.4 for inextensible and extensible reinforcement.

The reinforcement pullout resistance is checked at each depth of reinforcement and only the effective pullout length beyond the active zone is to be considered. The minimum length, L_e, beyond the active zone is 3 ft and the total length, L, is equal to $L_a + L_e$. The length of embedment is calculated using Equation 2.5 (AASHTO Equation 11.10.6.2.1-1).

$$3 \leq L_e = \frac{T_{max}}{\Phi F^* \alpha \sigma_v C R_c} \tag{2.5}$$

where T_{max} is the maximum tensile load per unit wall width of wall, Φ is the resistance factor for reinforcement pullout found in Table 11.5.6-1 of the AASHTO LRFD Bridge Design Specifications manual, F^* is the pullout friction factor, α is the scale effect correction factor, σ_v is the unfactored vertical stress at the reinforcement level in the resistant zone and calculated in Equation 2.1, C is the reinforcement surface area geometry (2 for strip, grid, and sheet type reinforcements), and R_c is reinforcement coverage ratio shown in Equation 2.6.

F^* and C are determined from product-specific pullout tests, but it can also be estimated empirically. AASHTO gives both the default values for backfill which meets the AASHTO requirements. These default values are shown in Table 2.1 and Figure 2.5.

Table 2.1. Default values for α (AASHTO Table 11.10.6.3.2-1)

Reinforcement Type	Default Value for α
All Steel Reinforcements	1.0
Geogrids	0.8
Geotextiles	0.6
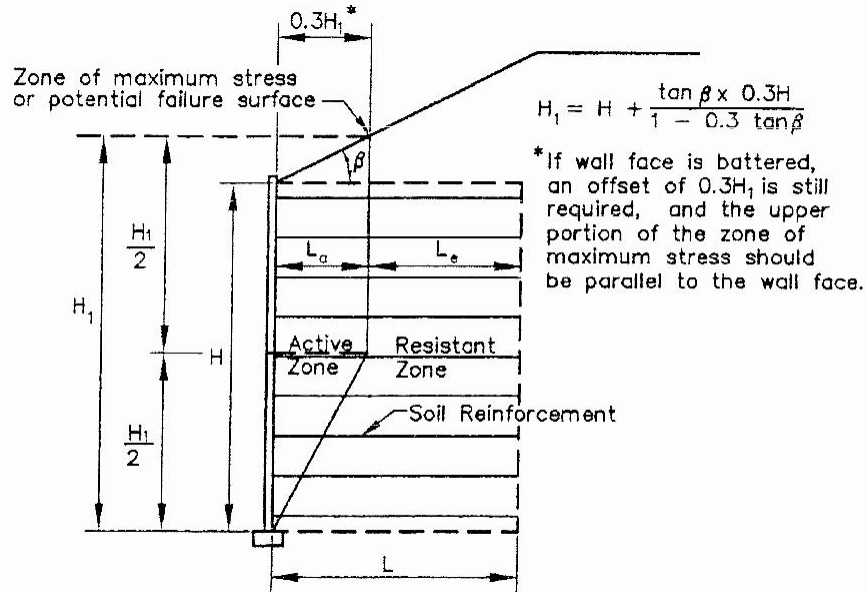
Fig. 2. 3. Location of locus of maximum stress in inextensible reinforcement (AASHTO Figure 11.10.6.3.1-1a)
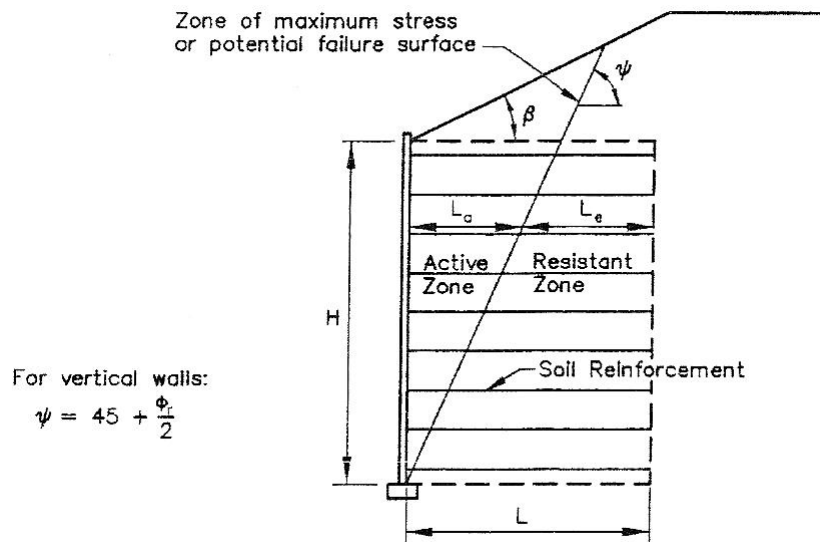
Fig. 2.4. Location of locus of maximum stress in extensible reinforcement (AASHTO Figure 11.10.6.3.1-1b)

The value R_c is the ratio of the overall width of the grid reinforcement mat divided by

the horizontal spacing between the individual reinforcement mats. R_c is calculated in

Equation 2.6. Figure 2.6 shows how the R_c values b and S_h are measured.

$$R_c = \frac{b}{S_h} \tag{2.6}$$

Default Values for Pullout Friction Factor, F*
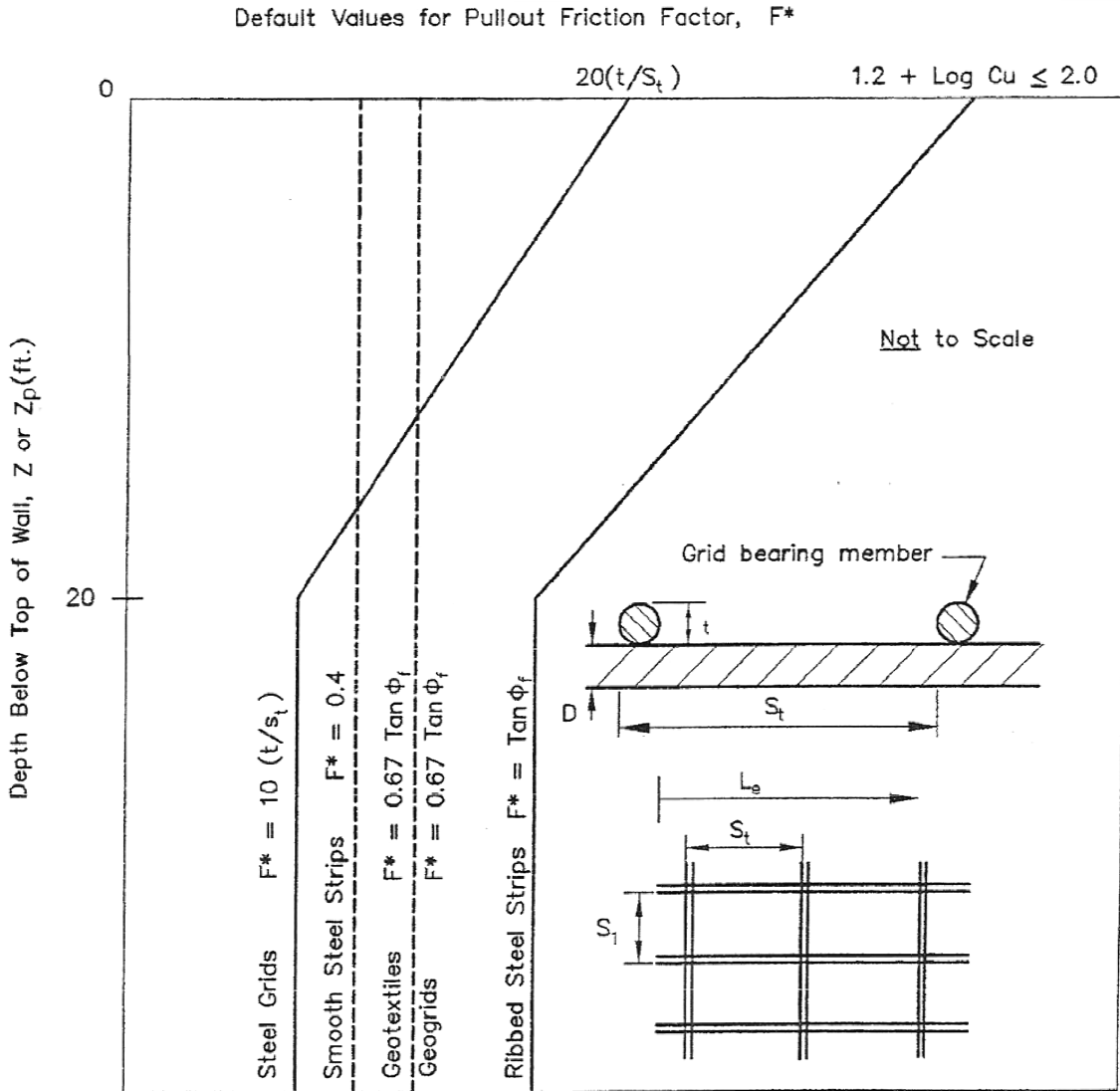
Fig. 2.5. Default values for F* (AASHTO Figure 11.10.6.3.2-1)

The strength of the reinforcement is calculated in Equation 2.7 (AASHTO Equation

11.10.6.4.1-1). This equation checks if the factored allowable tension in the

reinforcement is greater than the factored tensions caused by the loads in the walls. If the check is not met the wall must be redesigned.

$$T_{max} \leq \Phi T_{al} R_c \tag{2.7}$$

where T_{max} is the factored load to the reinforcement, Φ is the resistance factor for the reinforcement tension, specified in Table 11.5.6-1 in the AASHTO LRFD Bridge Design Specifications manual, T_{al} is the nominal long-term reinforcement design strength shown in Equation 2.8 (AASHTO Equation 11.10.6.4.3a-1), and R_c is the reinforcement coverage ratio shown previously in Equation 2.6.

$$T_{al} = \frac{A_c F_y}{b} \tag{2.8}$$

where A_c is the area of reinforcement corrected for corrosion loss, F_y is the minimum yield strength of the steel, and b is the unit width of reinforcement.
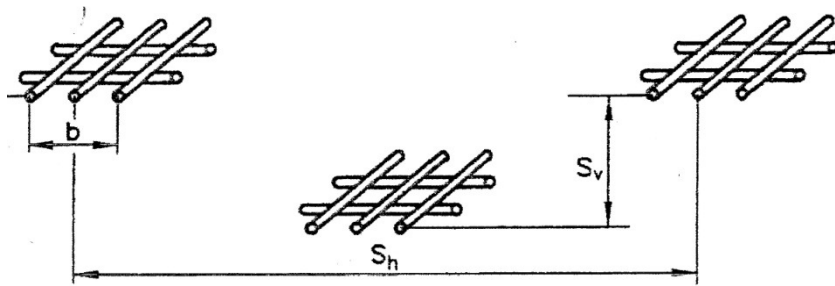
Fig. 2.6. Shows the geometry and measurements for wire mats (AASHTO Fig. 11.10.6.4.1-1)

The term A_c refers to the long-term area or the area after corrosion over the design life of the steel reinforcement in the MSE wall. It is shown in Equation 2.9.

$$A_c = \frac{D_c^2 \pi}{4} \tag{2.9}$$
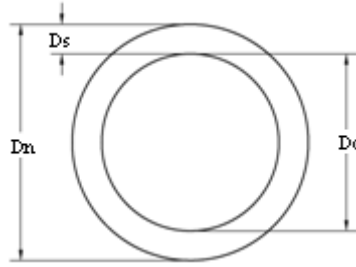
Fig. 2.7. Orientation of D_c dimensions

where D_c is the thickness of metal reinforcement, in this case diameter, at the end of the service life. It is the nominal thickness subtracted by the sacrificial steel on the outer surface area shown by Figure 2.7.

The associated values for sacrificial steel due to corrosion are as follows:

Loss of Galvanizing   =   0.58 mil./yr. for first 2 years
                        =   0.16 mil./yr. for subsequent years

Loss of Carbon Steel =   0.47 mil./yr. after zinc depletion

These values are used when the soil backfill is considered nonaggressive. To be considered nonaggressive they must have a pH equal to 5 through 10, have a resistivity greater than or equal to 3000 ohm-cm, have a choride content less than or equal to 100 ppm, have a sulfate content less than or equal to 200 ppm, and have an organic content less than or equal to 1 percent.

2.3 K-Stiffness Method

2.3.1 Background

The K-Stiffness method was created by Tony M. Allen and Richard J. Bathurst. It was developed empirically through the analysis of numerous full-scale wall histories. For the K-Stiffness method, most of the reinforcement loads from the case histories were estimated through measuring reinforcement strains and converted to a load with

reinforcement stiffness values. After the correct load levels were determined, the

reinforcement loads obtained from the full-scale wall case histories were compared to the

values predicted by the current methodologies. The existing design methodologies were

found to provide very poor predictions of the reinforcement load for the geosynthetic

walls being overly conservative and only marginally acceptable predictions for steel

reinforced structures.

The method considers the stiffness of all the wall components to estimate the

distribution and magnitude of T_{max}, which is the predicted maximum tension force for the

reinforcement layer. T_{max} is more accurately predicted on the internal design of

geosynthetic reinforced MSE walls. Some of the variables considered are the

reinforcement stiffness properties, geometry, spacing, etc. The design method should

result in cost savings for geosynthetic walls. The goal of the new methodology is to

provide a wall design with the least cost, but still maintaining acceptable and predictable

long-term performance. The K-Stiffness method will be presented in the following

sections.

2.3.2 Internal Design

The primary equation for the K-Stiffness method for internal design calculates T_{max}^i,

which is the maximum load per running unit length of wall in the reinforcement layer i,

given in Equation 2.10.

$$T_{max}^i = S_v^i \sigma_h D_{tmax} \Phi \qquad (2.10)$$

where S_v^i is the average vertical spacing of the reinforcement, σ_h is the lateral earth

pressure acting over the tributary area, D_{tmax} is the load distribution factor based on layer

location that modifies the reinforcement load, Φ is the influence factor that consists of

global reinforcement stiffness over the entire wall height, Φ_g, the local stiffness factor of the reinforcement layer compared to the average stiffness of all the reinforcement layers, Φ_{local}, respectively, the facing stiffness, Φ_{fs}, and the facing batter factor, Φ_{fb}. The equation for the lateral earth pressure is given in Equation 2.11.

$$\sigma_h = \frac{1}{2}K\gamma(H + S) \tag{2.11}$$

where γ is the unit weight of the soil, H is the height of the wall, S is the equivalent height of uniform surcharge pressure q (i.e., $S = \frac{q}{\gamma}$), and K is the coefficient of lateral earth pressure calculated in Equation 2.12.

$$K = K_0 = 1 - \sin\varphi_{ps} \tag{2.12}$$

where φ_{ps} is the peak plane strain friction angle. Thus Equation 2.7 is simplified and shown in Equation 2.13.

$$T_{max}^i = \frac{1}{2}K\gamma(H + S)S_v^i D_{tmax}\Phi \tag{2.13}$$

The influence factor is calculated using Equation 2.14.

$$\Phi = \Phi_g\,\Phi_{local}\Phi_{fs}\Phi_{fb} \tag{2.14}$$

The global stiffness factor, Φ_g, it is computed as the global stiffness factor, S_{global}, is divided by atmospheric pressure, P_a = 101 kPa, shown in Equation 2.15.

$$\Phi_g = \alpha\left(\frac{S_{global}}{P_a}\right)^\beta \tag{2.15}$$

where α and β are constant coefficients, both equal to 0.25. S_{global} is computed in Equation 2.16.

$$S_{global} = \frac{J_{ave}}{(H/n)} = \frac{\sum_{i=1}^{n}J_i}{H} \tag{2.16}$$

where J_{ave} is the average tensile stiffness of all "n" reinforcements layers over the wall height, J_i is the tensile stiffness of an individual reinforcement layer expressed in units of force per unit length of wall, H is the height of the wall.
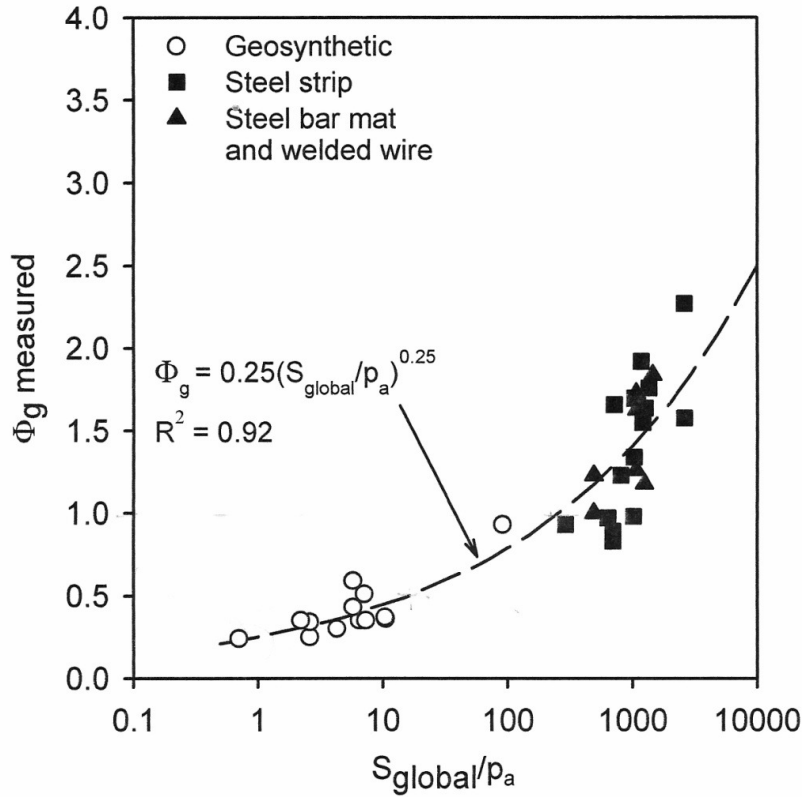
Fig. 2.8. Measure (Φ_g) vs. normalized global reinforcement stiffness value $\left(\frac{S_{global}}{P_a}\right)$ (K-Stiffness Figure 7.4)

The K-Stiffness method provides data from geosynthetic wall case histories that enable back-calculation of global stiffness factor values, Φ_g(measured), from measured maximum reinforcement load, T_{mxmx}, values, shown in Figure 2.8.

$$\Phi_g(measured) = \frac{T_{mxmx}}{S_v^i \sigma_h D_{tmax} \Phi_{local} \Phi_{fs} \Phi_{fb}} \qquad (2.17)$$

where T_{mxmx} is the maximum reinforcement load in the wall and D_{tmax}, Φ_{local}, Φ_{fs}, and

Φ_{fb} are equal to 1 for a steel, vertical, wire-facing wall.

The local stiffness factor, Φ_{local}, relates the stiffness of the reinforcement layer

(S_{local}) with respect to the average stiffness of all the reinforcement layers (S_{global}). It is

shown in Equation 2.18.

$$\Phi_{local} = \left(\frac{S_{local}}{S_{global}}\right)^a \tag{2.18}$$

where the term a is equal to 0 for steel reinforcements and 1 for geosynthetic reinforced

soil walls. S_{local} is calculated in Equation 2.19.

$$S_{local} = \left(\frac{J}{S_v}\right)_i \tag{2.19}$$
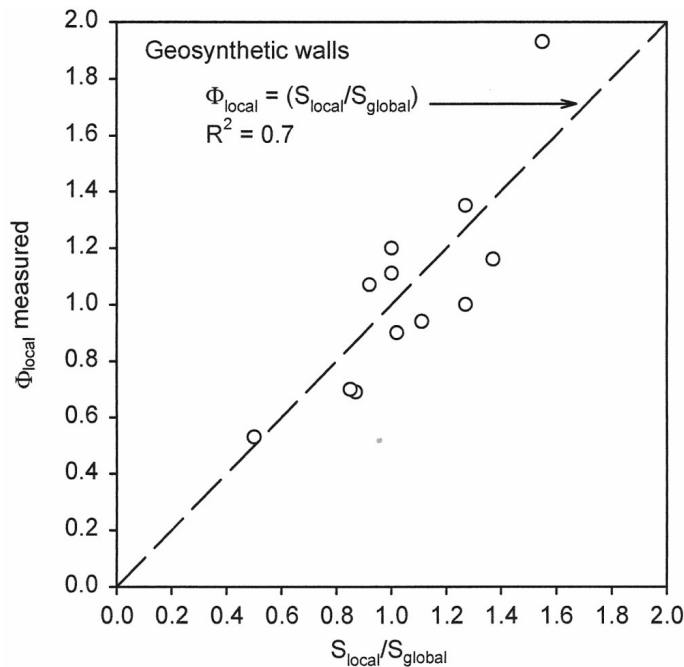
Fig. 2.9. Measured Φ_{local} factor versus $\dfrac{S_{local}}{S_{global}}$ (K-Stiffness Figure 7.6)

Since crimped wire mats are a relatively new type of reinforcement implemented on full scale walls, there is not much data for the stiffness values. Thus, back-calculation must be done to obtain the stiffness values using the K-Stiffness method and the measured maximum tensile load in the wall. This can be done using Equation 2.20 and Figure 2.9.

$$\Phi_{local}(measured) = \frac{T_{mxmx}}{S_v^i \sigma_h D_{tmax} \Phi_g \Phi_{fs} \Phi_{fb}} \tag{2.20}$$

Φ_{fs} is the facing stiffness factor. This factor considers the loads transferred to the facing mechanisms used in the MSE wall design. As more load is transferred to the facing element the global stiffness reinforcement decreases. Inextensible steel reinforced walls generally have a high global stiffness value relative to the stiffness of the facing. Thus, the facing element contribute little and does not need to be considered. If extensible material is used, the stiffness of the facing elements will contribute to the MSE design and should be considered. For these designs Φ_{fs} will equal 1 for all inextensible steel reinforced walls.

The facing batter factor, Φ_{fb}, relates the slope of the wall and Coulomb earth pressure theory. Limit equilibrium methodologies attempt to capture this effect through the Coulomb earth pressure coefficient. However, the Coulomb earth pressure coefficient tends to reduce reinforcement loads excessively for heavily battered walls. The influence of reduced confining pressure near the wall face cannot be captured explicitly by limit equilibrium methods. The facing batter factor is calculated empirically in Equation 2.21.

$$\varphi_{fb} = \left(\frac{K_{abh}}{K_{avh}}\right)^d \tag{2.21}$$

where K_{abh} is the horizontal component of the active earth pressure coefficient

accounting for the wall face batter, K_{avh} is the horizontal component of the active earth

pressure coefficient, assuming the wall is vertical and d is a constant coefficient. If the

wall is assumed to be vertical, Φ_{fb} approaches 1. Using regression analysis, the exponent

d was found to be approximately 0.25.

2.3.3 Influence Factor, D_{tmax}

The influence factor, D_{tmax}, accounts for variation of the tensile load relative to the

height of the wall. General loading of soil tends to slope linearly with depth resulting in a

triangular distribution. The K-Stiffness design method assumes a trapezoidal shape load

distribution. The maximum loads for extensible reinforcement material are seen a depths

of 0.4H to 0.8H below the top of the wall. It is shown in Figure 2.10.
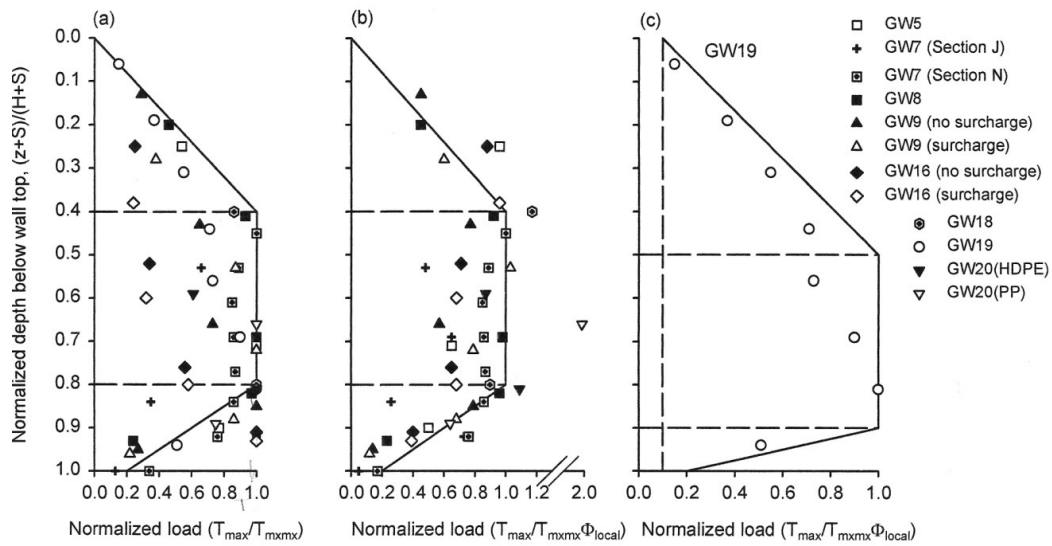
Fig. 2.10. Distribution $\boldsymbol{D_{tmax}}$ as a function of normalized depth (K-Stiffness Figure 7.3)

In Figure 2.10a, T_{max}^i, the maximum tensile load, is normalized with respect to

T_{mxmx}. In Figure 2.10b, T_{max}^i is normalized with respect to T_{mxmx} and Φ_{local}. A stiff

polymer strap reinforcement was used for Figure 2.10c. The crimped wire mat

reinforcement referred to in this paper is assumed to be a flexible extensible

reinforcement and will tend to follow the distribution pattern shown in Figure 2.10b.

2.4 Other Related MSE Wall Systems

2.4.1 Background

Pullout resistance is the tensile force that is measured due to friction of the soil and

reinforcement on each other. Typically as there is more overburden pressure or as soil is

deeper in the ground, the pullout resistance increases. For this section of the thesis, I will

be summarizing what others have done related to pullout resistance.

2.4.2 Factors affecting kinked steel grids reinforcement in MSE structures

This section covers the article "Factors affecting kinked steel grids reinforcement in

MSE structures," written by N. Tin, and published in the Geotextiles and Geomembranes

journal in 2010. This study performs pullout tests on triangular kinks and U-shaped

kinks to check which shape of kink should be used on the steel grid. The kinks are made

using a metal break machine. The reinforcements included both one and two kinks for

the triangular and U-shaped steel grids. Figure 2.11 shows the different combinations

and shapes.

The pullout tests pressures of 30 kPa, 60 kPa, 90 kPa, and 120 kPa were applied. To

achieve an active state limit state for a wall, a lateral movement of H/1000 is required,

where H is the height of the wall in meters. When the overburden pressure is applied the

displacement of the reinforcement is measured to see if it conforms to an active state

condition. The pullout box has rigid sides which don't allow for lateral movement, thus

there is no tension or extension of the reinforcement. If there were no rigid support there

would be an increase in tension due to the overburden pressure. The deformation of the test conducted is from overburden pressure. Retaining walls are not rigid therefore this condition is not consistent.

The one and two U-shaped kinks had displacements due to the applied pressure of only 1mm and 1.5 mm, respectively. These are too small to meet the displacement requirements for an active limit state. Different dimensions and angles were used with the triangular kink which is shown in Figure 2.12. A triangular kink with a dimension of 25.4 mm and 120º did not yield enough displacement. A triangular kink of 45º was broken during a small displacement of pullout thus a 50.8 mm length for each side with an angle of 90º was selected for the study. The triangular kink is thought to be more practical and convenient than the U-shaped kink. Figure 2.12 shows the dimensions of the kinks.

The largest pullout resistance was found in the grid with two triangular kinks, followed by the steel grid with one triangular kink, and then the steel grid with no kink. Frictional resistance and bearing resistance are the two components of pullout resistance. The kinks added to the bearing resistance and thus the pullout resistance. Higher pullout displacements were found in multiple kinks compared to only one kink. The triangular shape with one kink met the required movement for active conditions for pressures of 30 kPa and 60 kPa. The triangular shape with two kinks met the required movement for active conditions for pressures of 30 kPa, 60 kPa, 90 kPa, and 120 kPa. Again, this shows the displacement of the reinforcement in a rigid pullout box due to the applied pressure. These results are shown in Figure 2.13. When the required movements for

active conditions are met the lateral earth pressure and amount of reinforcement can be reduced.
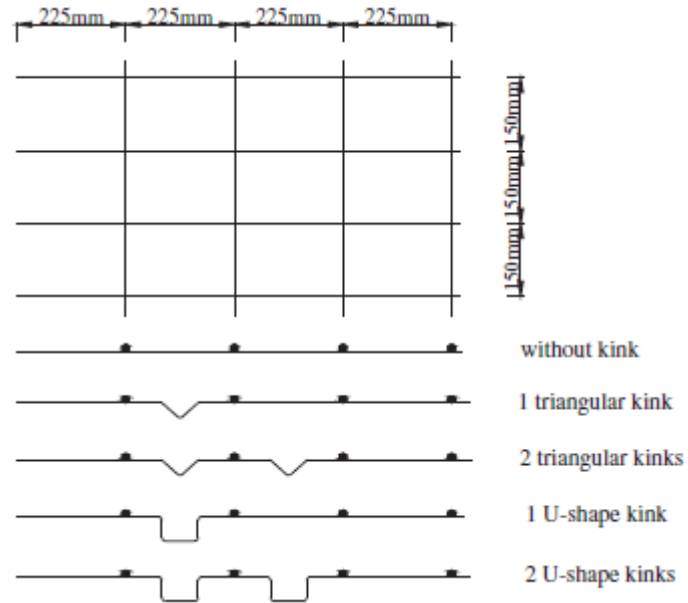
Fig. 2.11. Different shapes of kinks from (Tin, 2010)
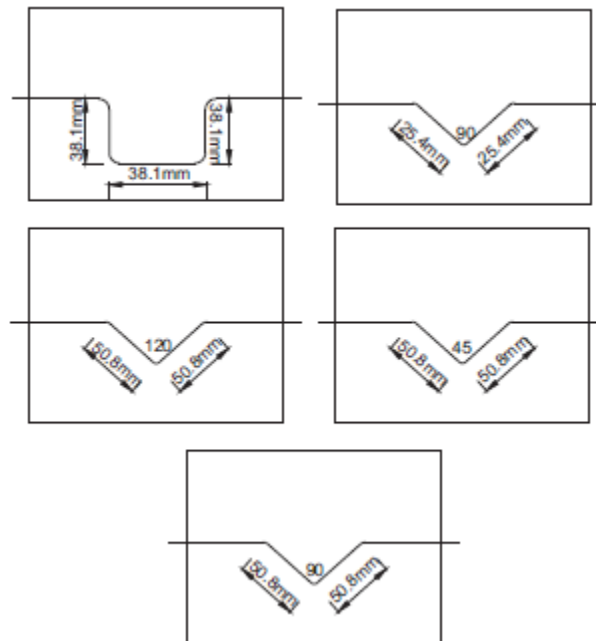
Fig. 2.12. Dimensions for each kink from (Tin, 2010)

Structure of Steel grid	Normal pressure (kPa)	Observed movements (mm)	Required movements for active conditions (Terzaghi, 1934)(H/1000) (mm)	Comparisons
No kink	30, 60, 90, 120	0	—	Not ok
1 triangular kink	30	2.5	1.5	Ok
	60	3.5	3	Ok
	90	4	4.5	Not ok
	120	5	6	Not ok
2 triangular kinks	30	4	1.5	Ok
	60	5	3	Ok
	90	5.5	4.5	Ok
	120	6	6	Ok

Fig. 2.13. Lateral movement of the steel grid in the pullout test from (Tin, 2010)

2.4.3 Pullout resistance of bearing reinforcement embedded in coarse-grained soils

This section covers the article titled "Pullout resistance of bearing reinforcement embedded in coarse-grained soils" written by Cherdsak Suksiripattanapong (2012). Since 2008, a new steel reinforcement design has been produced in Thailand, where the study was done; at less expensive costs because of the high import costs. The article studies the influence of soil properties (friction angle, grain size, and gradation) and dimension and spacing of the transverse members on the pullout mechanism and the pullout bearing resistance. Three existing pullout bearing failure mechanisms for the plane strain condition are proposed; they include general shear failure, punching shear failure, and modified punching shear failure. The maximum bearing stress of a single isolated transverse member is shown in Equation 2.22.

$$\sigma_{bmax} = N_q \sigma_n \qquad (2.22)$$

where N_q is the bearing capacity factor, depending on the mode of failure and σ_n is the normal stress. N_q is presented in terms of soil friction angle, φ, for the three failure

mechanisms, which are general shear failure (Equation 2.23), punching shear failure

(Equation 2.24), and modified punching shear failure (Equation 2.25).

$$N_{q(general)} = \exp[\pi \tan\varphi] \tan^2(\frac{\pi}{4} + \frac{\varphi}{2}) \tag{2.23}$$

$$N_{q(punching)} = \exp\left[(\frac{\pi}{2} + \varphi) \tan\varphi\right] \tan(\frac{\pi}{4} + \frac{\varphi}{2}) \tag{2.24}$$

$$N_{q(modified)} = \frac{1}{\cos\varphi} \exp[\pi \tan\varphi] \tan^2(\frac{\pi}{4} + \frac{\varphi}{2}) \tag{2.25}$$

The reinforcement has longitudinal and 3 transverse members shown in Figure 2.14.

The transverse members are a set of hot rolled, steel, equal angles designed to give

bearing resistance. It is simple to install, convenient to transport and possess high pullout

and rupture resistances with less volume (weight). The 3 soil types that were used had

different grain size distributions, friction angles, and different average grain sizes, D_{50}.

There were a well-graded gravel (GW), well-graded sand (SW), and crushed rock (GP)

according to the Unified Soil Classification System (USCS). Also, a poorly graded sand

(SP) is used in this article (Horpibulsuk, 2010). The friction angles were 45, 42, and 40

for GW, SW, and GP, respectively. The dimensions and spacing, S, of the transverse

members were varied. The transverse members ranged between 1 and 4. The bearing

reinforcement is connected to the facing panel at the tie point (2 U-shaped steel pieces)

by a locking bar (a deformed bar), possibly a concrete rebar, shown in Figure 2.15. The

study doesn't say how the angles are connected to the bar. Figure 2.14 and Figure 2.15

show the geometry of the reinforcement. This mechanically stabilized earth (MSE) wall

is designated as "Bearing Reinforcement Earth (BRE) wall" (Suksiripattanapong, 2012).

There were different lengths chosen for the test. The leg lengths, B and length L, were 25, 40, and 50 mm and 100, 150, and 200 mm, respectively. The applied normal stresses used were 30, 50, and 90 kPa. This study assumes 3 different types of failure for the plane strain condition, which are general shear failure, punching shear failure, and modified punching shear failure. Zone 1 (S/B $\leq$ 3.75) is block failure where all the transverse members act like a rough block. Zone 2 (3.75 < S/B < 25) is member interference failure. Zone 3 (S/B > 25) is individual failure. The maximum bearing stress for each transverse member is determined by the mode of failure and the friction angle, φ. The maximum pullout force increased as the maximum normal stress increased. The well-graded gravel (GW) gave the highest pullout friction force due to its higher friction angle of 45. The crushed rock (GP) and poorly graded sand (SW) had the same pullout force for the same normal stress even with different grain sizes distribution curves and D_{50} values.

Both GP and SW had the same friction angle which mostly affects the pullout force. The friction between the soil and the transverse member, δ, was greater than the soil friction angle because of the roughness and rigidity of the steel deformed bar. The δ/φ ratio is approximately 1.47 for all the soils tested.

The pullout mechanism is mainly controlled by the B/D_{50} and normal stress, regardless of being well-graded or poorly-graded. By assuming that the general shear and modified punching shear are the upper and lower boundaries, the bearing capacity factor, N_q, can be calculated which helps predict the maximum pullout resistance of a single transverse member.
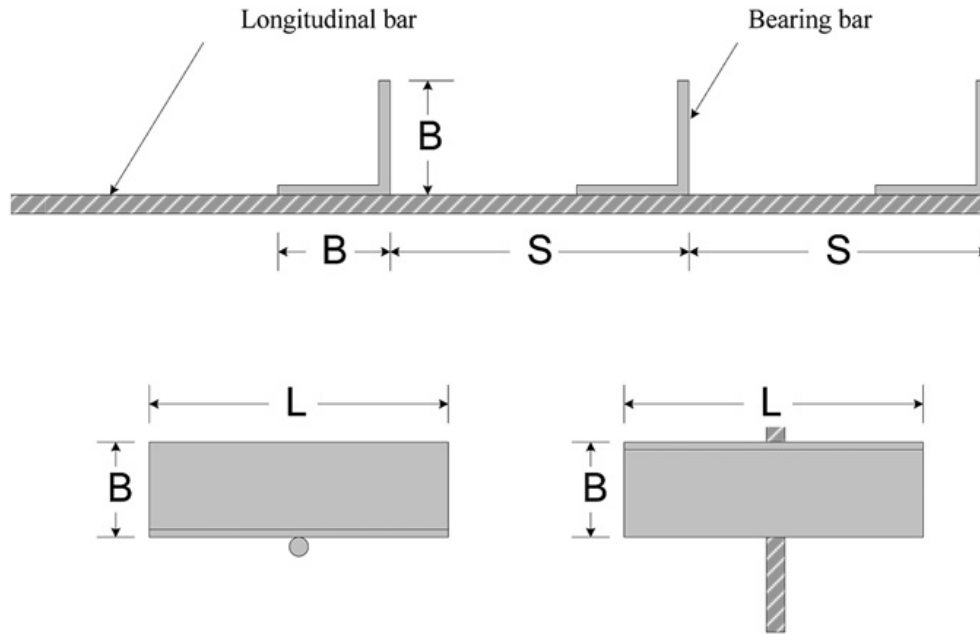
Fig. 2.14. Configuration of bearing reinforcement from (Suksiripattanapong, 2012)
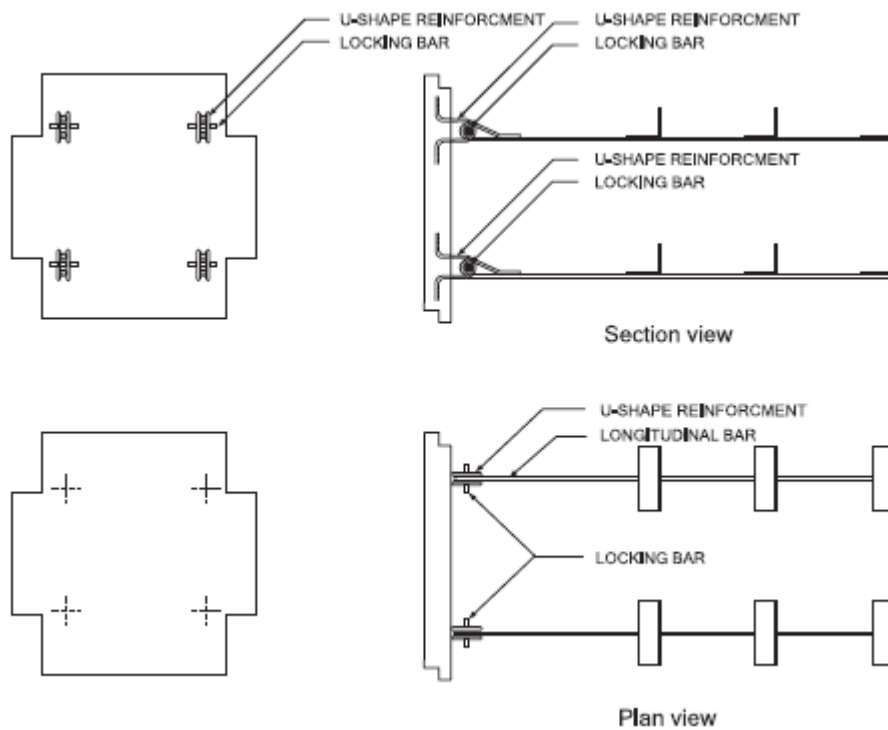
Fig. 2.15. Connection of the bearing reinforcement to the wall facing from (Suksiripattanapong, 2012)

2.4.4 Effects of wetting on the pullout resistance of geogrids in compacted silty sand

This section covers the article titled "Effects of Wetting on the Pullout Resistance of Geogrids in Compacted Silty Sand" written by Cheng-Wei Chen and Jason Y. Wu (2012). In this article, pullout tests are performed on geogrids with various applied stresses using silty sand with both dry and wet conditions. Often MSE failures happen because of rainfall and improper drainage control. This study helps our understanding and analysis of MSE walls under severe rainfall conditions.

The geogrids used were two types of woven biaxial, Type A and Type B. Both were made of high strength polyester (PET) yarns and coated with polyvinyl chloride (PVC). The sample was inundated with 20 liters of water for 48 hours before a pullout was applied. Figures 2.16 and 2.17 show Type A and Type B geogrid pullout results of both dry and wet conditions.

From the pullout results, you can see that the geogrids lost more than 50 percent of their strength after the sample was inundated. Figure 2.18 shows a linear relationship of the observed maximum pullout resistance achieved, as a function of the normal stress applied. For identical normal stresses, the wetting effect caused less displacement to mobilize peak pullout resistance and was more significant for conditions with lower stresses. The types of geogrid and applied normal stresses appear to have a minor effect on the reduction of pullout resistance when the soil samples were near saturated.
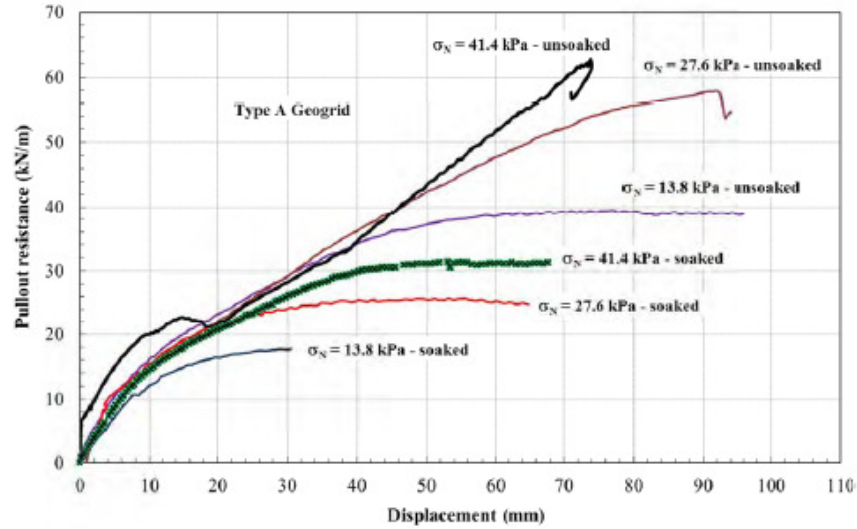
Fig. 2.16. Comparison of pullout resistance, before and after wetting, in Type A geogrid from (Chen and Wu, 2012)
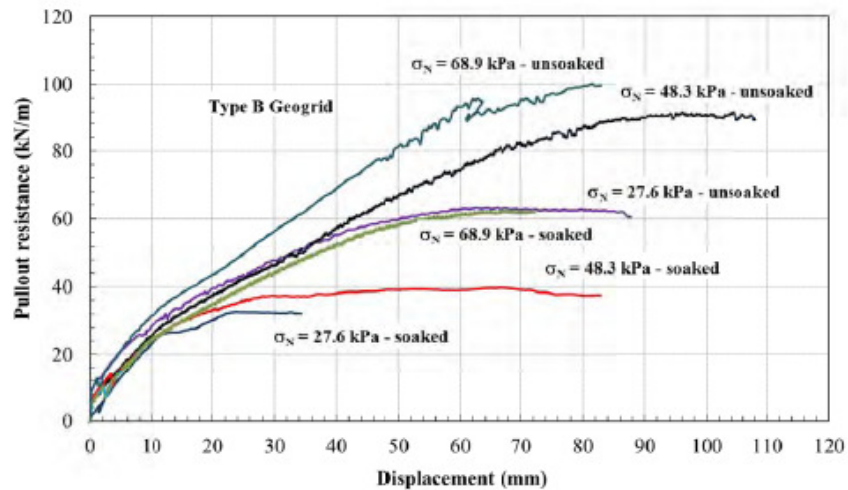
Fig. 2.17. Comparison of pullout resistance, before and after wetting, in Type B geogrid from (Chen and Wu, 2012)
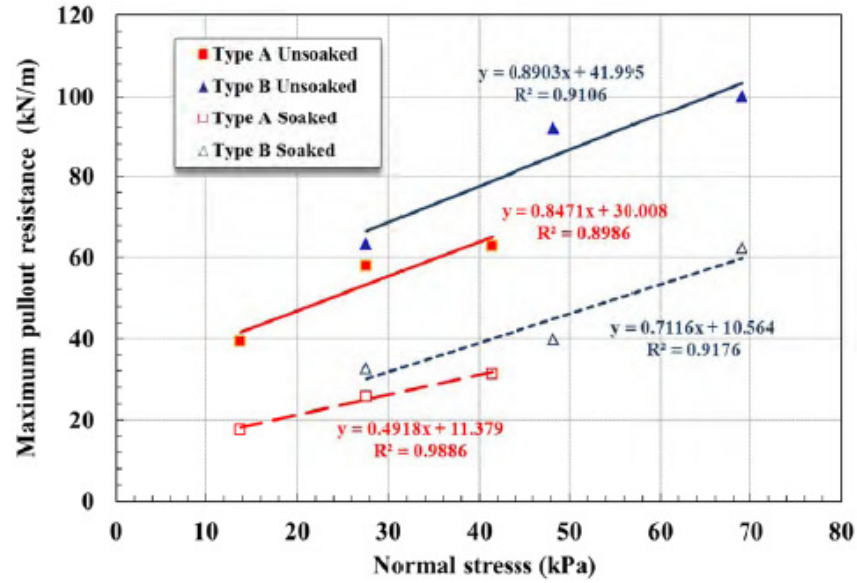
Fig. 2.18. Variation of the maximum pullout resistance versus normal stress for the soil-geogrid systems tested before and after wetting from (Chen and Wu, 2012)

CHAPTER 3

CRIMP DEFORMATION AND LABORATORY CRIMP STIFFNESS

MEASUREMENTS

3.1 Introduction

This chapter covers laboratory and field measurements of crimp deformation and stiffness. We look how the crimps in the MSE wall were positioned and how they were exhumed and extracted in section 3.2. The field measured crimp deflection data is shown in section 3.3. In section 3.4 the lab crimp deformation and stiffness measurements data are shown and how we conducted the test. We also show the predicted stiffness we obtained. Section 3.5 is titled where we fall in K-Stiffness. This section shows how our results compare to the K-Stiffness approach and its case studies.

3.2 Exhuming The Utah State University MSE Wall

The USU wall was constructed August 9th -13th of 2011. The location chosen was in the hillside of an abandoned gravel pit on the corner of 1400 North and 1200 East in Logan, Utah. The purpose of constructing the MSE wall was to record tensile stresses throughout the wall and make comparisons of observed wall behavior against design predictions, using AASHTO LRFD and K-Stiffness methods. Instrumentation was used to measure tension and wall deformations of the wall during and after construction. The wall was exhumed July 16th -21st of 2012. The purpose of exhuming the wall was to measure the crimp deformations, perform laboratory stiffness tests, and predict the stiffness of the USU wall.

The height of the USU wall was 20 ft tall. Reinforcement was layered every 2 ft thus the lift thickness was 2 ft. There were 10 layers of wire mats and each had a length of 13 ft. The top five layers consisted of a W3.5 wire mat while the bottom five layers had W5.0 wires, shown in Figure 13. The W3.5 and W5.0 wires is shown if Figure 19. A wire mat consisted of four longitudinal wires perpendicular to the face of the wall and 6 transverse wires running parallel to the wall. The longitudinal wire spacing, S_L, is 16 inches. The transverse wire spacing, S_T, is 24 inches. The crimp had a radius of 1.5 inches. In the top five layers there were no crimps in the first interval while the bottom five layers had no crimps in the last interval. This spacing and crimp geometry is shown in Figures 15-16.

To identify positions of specific crimps in the mats, the following convention was used. Layer 1 was defined as the top grid down to layer 10 at the bottom. A layer was defined as all the grids at a given elevation. Each grid had four longitudinal wires. Three grids were used at each layer so there would be 12 longitudinal wires per layer. The 12 longitudinal wires were the rows. Row one began at the farthest right longitudinal wire when facing the wall. An interval was defined on the longitudinal wires. Interval 1 was found between the front first (closest wire to face of the wall) and second transverse wires. Between the second and third transverse wires was interval 2. A crimp labeled 1 – 1 – 2 would be found on the top layer, farthest row to the right (when facing the wall), and the 2nd interval. Each layer had four crimps.
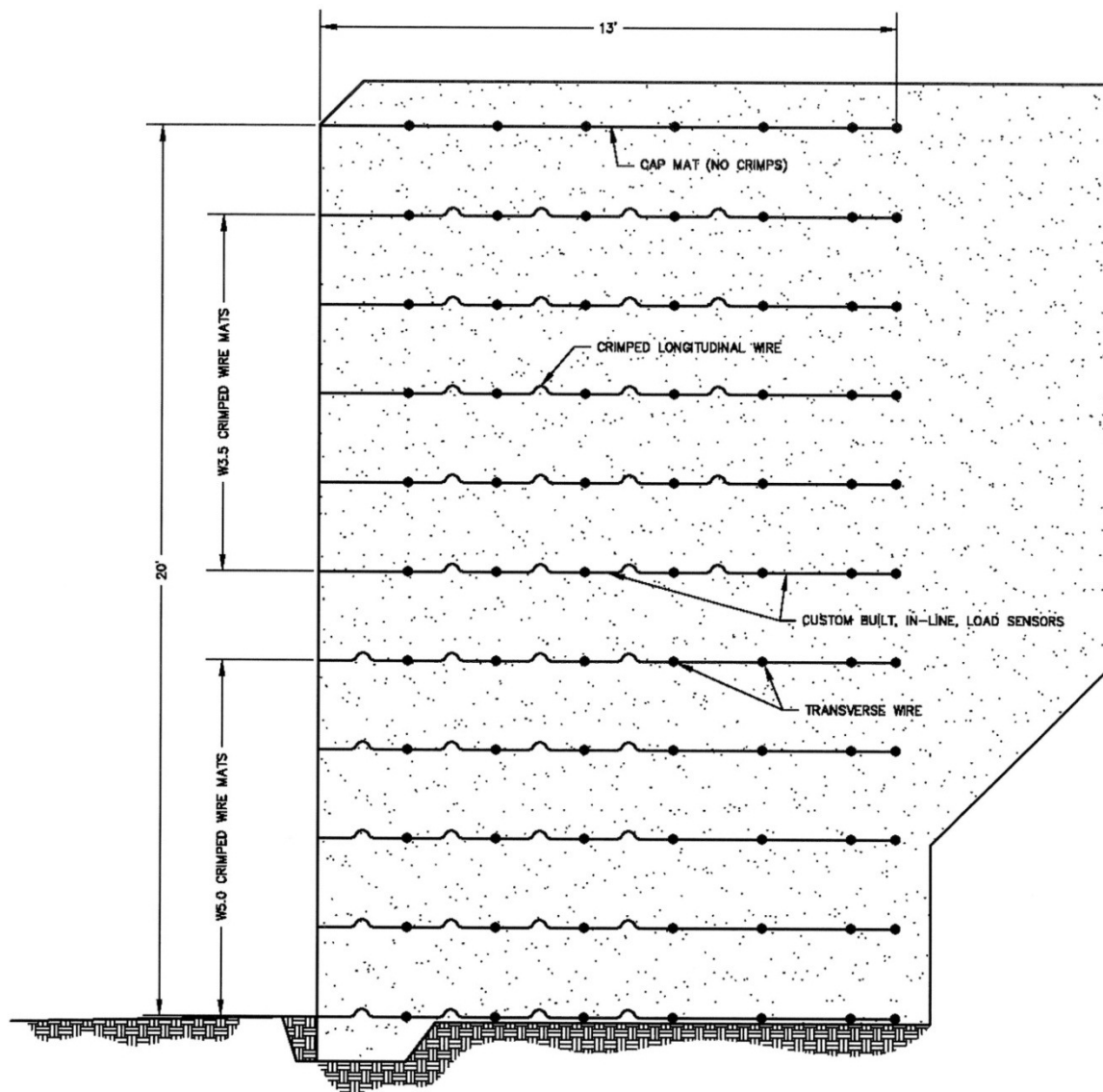
Fig. 3.19. Elevation view of the USU wall (Jensen, 2013)
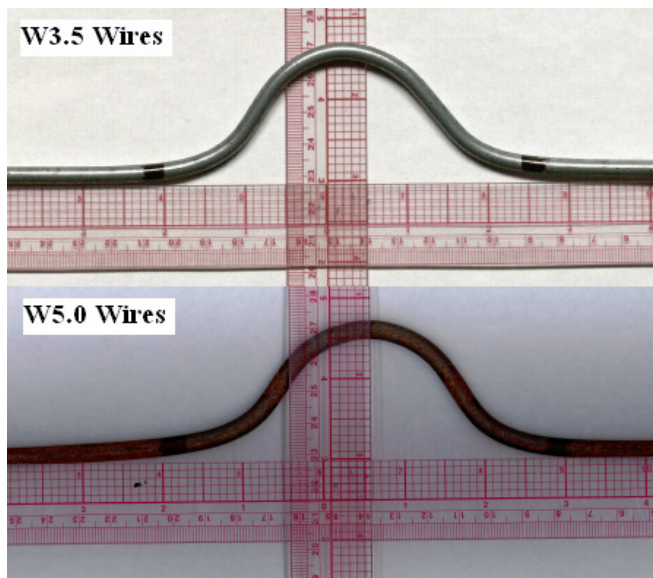
Fig. 3.20. W3.5 and W5.0 wires

Fig. 3.21. Extracting the crimp mats and labeling them
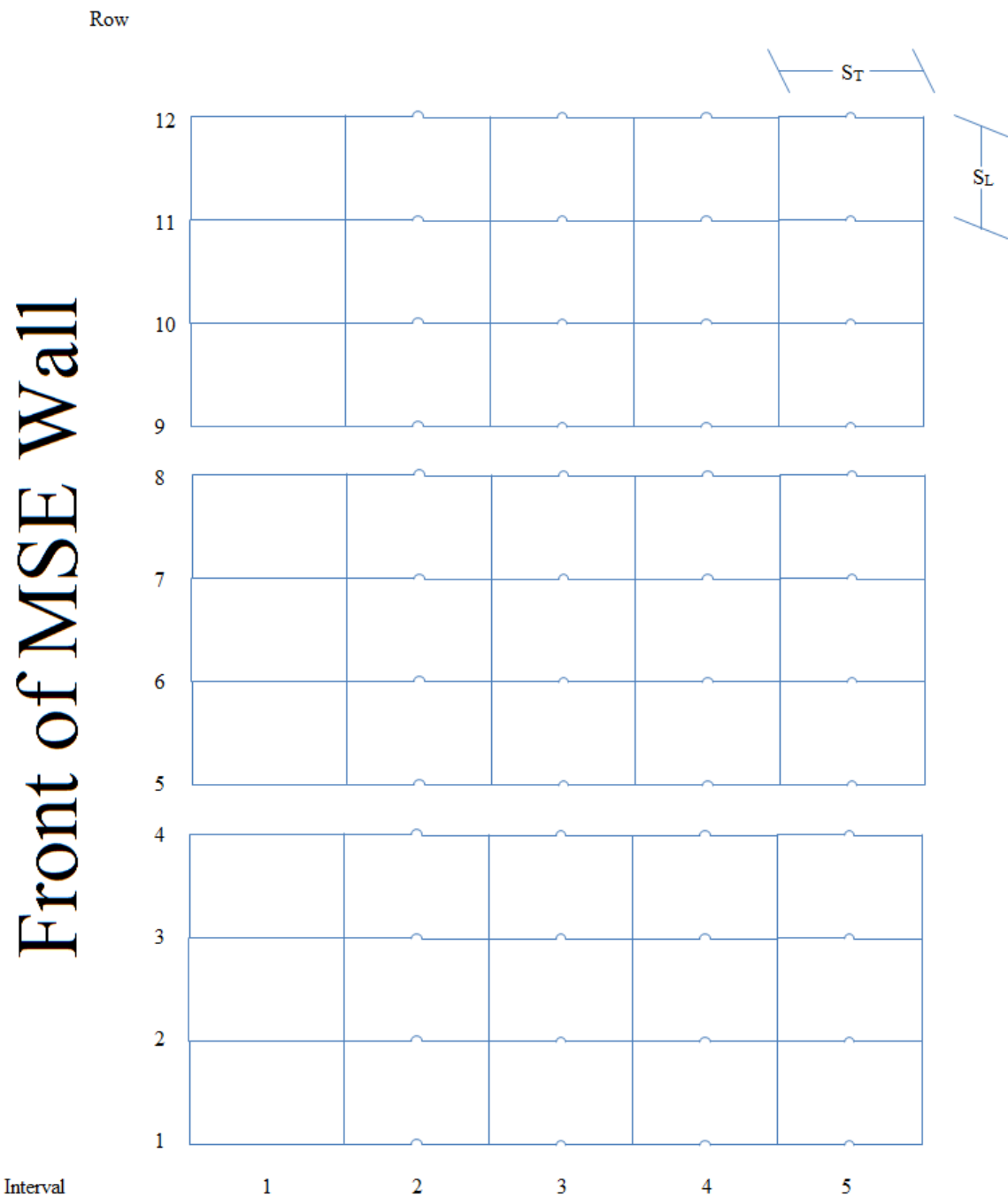
Fig. 3.22. Top 5 Layers of MSE Wall (Layers 1-5)

Row
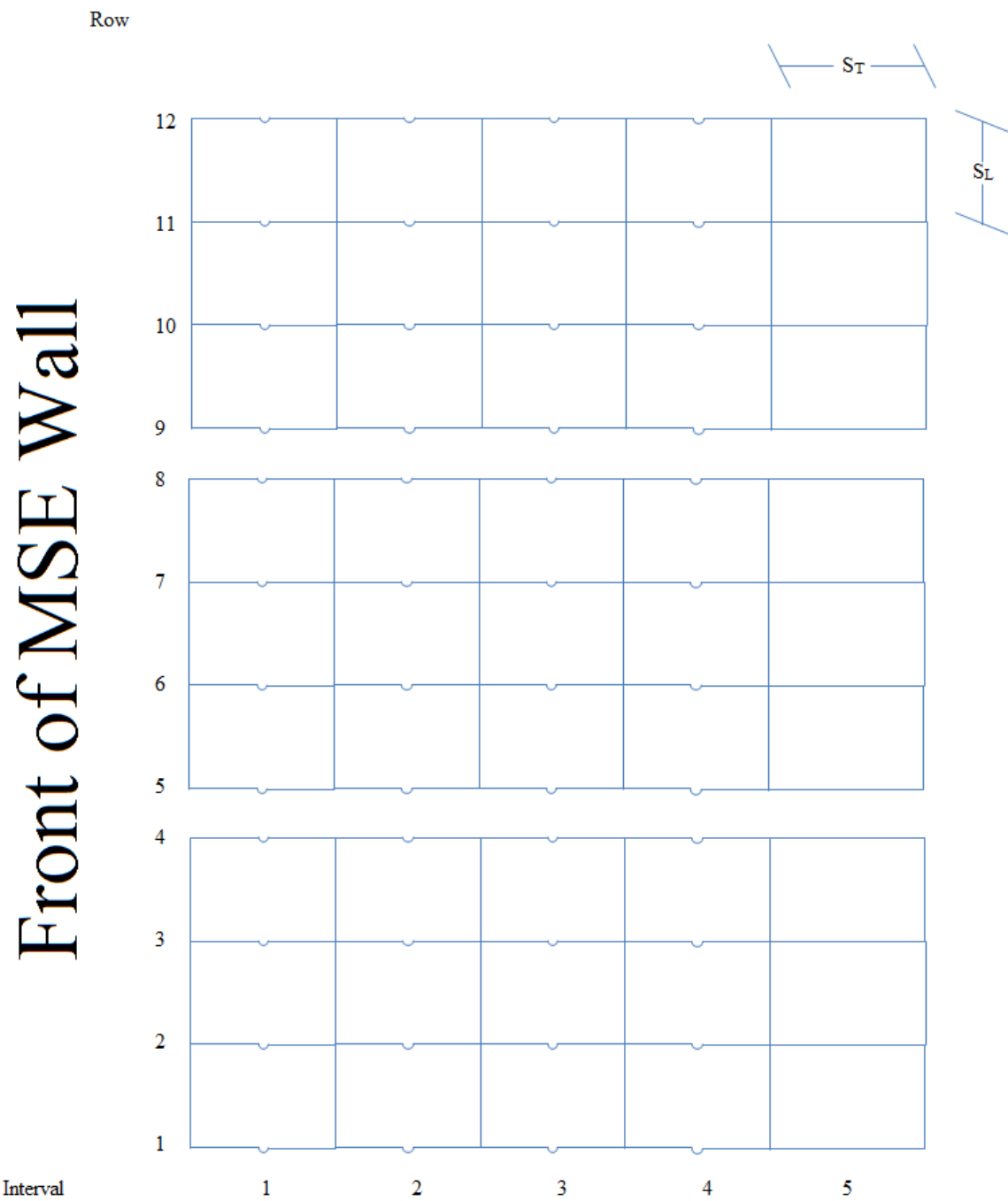
Fig. 3.23. Bottom 5 Layers of MSE Wall (Layer 6-10)

Fig. 3.24. Exhuming of USU Wall

Fig. 3.25. Exhuming USU Wall using a water hose

An excavator was used to help dig out the buried steel grids, shown in Figure 3.24. A backhoe aided in the exhuming phase as well. Shovels and picks were used as more of the grids became exposed and as the lift thickness decreased in hopes of being more delicate with the crimped sections. However, some of the crimps were damaged as the excavator dug. A wire cutter was used to cut the longitudinal wires in rows because it would be faster in retrieving the grids and continue in the demolishing.

As exhumation continued, discussion initiated of using a water truck and high pressure hose to remove the soil around the mats. Using a water hose would prevent damage to the crimps as they were extracted. Once the water truck arrived, we began spraying the soil in the wall to accelerate the exhumation and extraction of the crimp mats, shown in Figure 3.25. All the damage to the crimps occurred on the top 5 layers. Because of the use of the water tank and more experience in digging out the crimps, there was no damage done to the lower layers 6-10. With four crimps per row and 12 rows, there are 48 crimps per layer. Forty-two crimps were damaged on the top five layers. This equals 17.5% of the crimps of the top five layers or 8.75% of all 10 layers of crimps.

3.3 Measured Crimp Deformation

Each crimp was marked using a stencil to allow accurate measurements of the crimp deformations as shown in Figure 3.26. The initial length of the mark was 4.432 in. The measurements were recorded using calipers. With the known length before construction and after exhumation we could calculate the actual deformation.

Table 3.2 shows the average deflections found in the crimps in each layer according to interval and layer. More data is shown in the appendices.

Table 3.2. Crimp Deflections

Layer	Average Interval Deflection, in.					Deflection, in.	
	1	2	3	4	5	Total	Average
1	*	0.632	0.624	0.611	0.430	2.297	0.574
2	*	0.716	0.541	0.546	0.321	2.124	0.531
3	*	0.795	0.779	0.717	0.525	2.817	0.704
4	*	0.857	0.781	0.457	0.457	2.552	0.638
5	*	0.845	0.713	0.312	0.273	2.142	0.535
6	0.619	0.656	0.908	0.265	*	2.447	0.612
7	0.631	0.715	0.463	0.181	*	1.989	0.497
8	0.487	0.581	0.472	0.267	*	1.806	0.452
9	0.493	0.282	0.142	0.113	*	1.030	0.258
10	0.181	0.123	0.055	-0.027	*	0.332	0.083

*indicates there was no crimp

Fig. 3.26. Crimp showing yellow paint before construction (Jensen, 2013)

3.4 Lab Stiffness Measurements of W3.5 and W5.0 Wires

To help us predict the stiffness in the USU wall we performed lab stiffness measurements on the W3.5 and W5.0 wires. Approximately 0.33 in. of deformation occurred during compaction when the wall was built. To simulate this we prestressed the crimps until there was 0.33 in. of deformation.

The pullout box was modified so that it could conduct a representative stiffness test. The pullout box had no rigid plates inside during pullout tests. To have an accurate stiffness test we needed to have a rigid plate to attach the W3.5 and W5.0 wires. This was done by connecting a 1.0 in. diameter bar to the back bulkhead and the plate where the crimps would be screwed in, shown in Figure 3.27. Between the plate and the back bulkhead we added washed mortar sand as we had done previously to added more stiffness to the plate. It was compacted with the 11 amp compactor and compactor foot. Force-Deflection curves were made from the tests. Using the Force-Deflection curves we made the J value-Deflection curves. The J value is a stiffness measurement calculated using Equation 3.2. The Force-Deflection and J value-Deflection curves are shown thru Figures 3.29 to Figure 3.36. Our measured tension and calculated tension forces are shown in Figure 3.28. The measured and calculated tensions correlate well.

The W3.5 wires were located on the top five layers of the wall between depths of 2 ft to 10 ft. On the bottom five layers were the W5.0 wires, corresponding to the depths of 12 ft to 20 ft. To assist in calculating the K-Stiffness measurements of the J value, we ran pullout tests on the W3.5 and W5.0 wires. Approximately 0.33 in. of deflection occurred on layers 1 through 8 on the wall during compaction of the lifts. Layers 9 and 10 did not have that compaction deflection. The post compaction deflection is the average

deflection measured from the crimps at each layer subtracted by the compaction

deflection of 0.33 in., except for layers 9 and 10. It is shown in Equation 3.1.

Fig. 3.27. Pullout box modification for crimp pullout tests

$$\delta^i_{post\ compaction} = \delta^i_{average} - \delta^i_{compaction} \qquad (3.1)$$

where $\delta^i_{post\ compaction}$ is the final deflection after construction, $\delta^i_{average}$ is the measured

crimp deformation, and $\delta^i_{compaction}$ is the deflection during compaction of the wall,

which is equal to 0.33 in. for layers 1-8 and equal to 0 in. for layers 9 and 10. Layer 7

and layer 8's predicted tension value were much greater than the measured tension.

Instead of using the 0.33 in. of deflection we used 0.165 in., which is half of 0.33 in.

The W3.5 and W5.0 wires were prestressed to have a deflection of 0.33 in. The pullout box was filled with the washed mortar sand and applying an overburden of 2 ft, the W3.5 wire was pulled to failure. This test was repeated again but with an overburden depth of 10 ft. The W5.0 wires were pulled to failure at the overburden pressure simulating a depth of 10 ft and 20 ft. Interpolation was performed for the depths of 12, 14, and 16 ft. to calculate the J values. Layers 9 and 10 had less than 0.33 in. of total deflection and no deflection during compaction. Thus getting the Force-Deflection and J value-Deflection curves were done without prestressing the wires. Overburden depths of 12 ft and 20 ft were applied for the pullout tests. The J_{18} and J_{20} was interpolated from the 12 and 20 ft depths with a non prestressed crimps. Equation 3.2 shows the equation for calculating the J values.

$$(J_2)_i = \frac{S_c * F}{\delta_{average}^i} \tag{3.2}$$

where $(J_2)_i$ is the J value at an overburden pressure simulating a depth of 2 ft at a given depth, i, F is the force, S_c is the spacing of the crimps in feet, in our case the spacing was 2 ft, and $\delta_{average}^i$ is the average deflection in the crimps in feet. Curves were plotted for the 2 ft and 10 ft J values. The deflection averages shown in Table 3.4. For the layer depths of 4 ft to 8 ft, interpolation was performed to get a represented value for these depths. Each depth had their individual J values at 2 ft and 10 ft. Equation 3.3 shows the interpolation formula.

$$J_4 = (J_2)_4 + \frac{2}{8} * ((J_{10})_4 - (J_2)_4) \tag{3.3}$$

The vertical stress is calculated assuming a unit weight of 125 pcf for a retaining wall. We measured the deflections that occurred in the wall to help predict the stiffness of the

wall. We performed lab stiffness tests using the W3.5 and W5.0 wires. Using both the deflections and lab stiffness measurements we predicted the stiffness of the wall. Tables 3.5 show terms and their values using the K-Stiffness approach. The K-Stiffness value predicted in the wall was S_{global} = 26927.62 psf and $\frac{S_{global}}{Pa}$ = 12.73, assuming atmospheric pressure, Pa = 2116 psf.

Table 3.3. Equations for J value

Wire	Layer	Depth, ft	J Equation (interpolation)
W3.5	1	2	$J_2 = J_2$
W3.5	2	4	$J_4 = (J_2)_4 + \frac{2}{8} * ((J_{10})_4 - (J_2)_4)$
W3.5	3	6	$J_6 = (J_2)_6 + \frac{4}{8} * ((J_{10})_6 - (J_2)_6)$
W3.5	4	8	$J_8 = (J_2)_8 + \frac{6}{8} * ((J_{10})_8 - (J_2)_8)$
W3.5	5	10	$J_{10} = J_{10}$
W5.0	6	12	$J_{12} = (J_{10})_{12} + \frac{2}{10} * ((J_{20})_{12} - (J_{10})_{12})$
W5.0	7	14	$J_{14} = (J_{10})_{14} + \frac{4}{10} * ((J_{20})_{14} - (J_{10})_{14})$
W5.0	8	16	$J_{16} = (J_{10})_{16} + \frac{6}{10} * ((J_{20})_{16} - (J_{10})_{16})$
W5.0	9	18	$J_{18} = (J_{12})_{18} + \frac{6}{8} * ((J_{20})_{18} - (J_{12})_{18})$
W5.0	10	20	$J_{20} = J_{20}$

Table 3.4. Various Values Associated with Each Depth

Depth, ft	$\delta^i_{average}$, in.	$\delta_{post\ compaction}$, in.	Lab. Estimate J, lb/ft	S_{local}	φ_{local}
2	0.574	0.244196	33409	16704.30	0.620
4	0.531	0.200948	42326	21163.16	0.786
6	0.704	0.374133	33096	16547.82	0.615
8	0.638	0.307933	40242	20121.01	0.747
10	0.535	0.205463	55201	27600.32	1.025
12	0.612	0.281833	62808	31404.02	1.166
14	0.497	0.332208	60178	30089.15	1.117
16	0.452	0.286542	65599	32799.64	1.218
18	0.258	0.2575	59338	29668.93	1.102
20	0.083	0.083008	86356	43177.85	1.603

Table 3.5. Lab. Estimate Tensions and Measured Tensions

Depth, ft	φ	D_{tmax}	Lab. Estimate T^i_{max}, lb/ft	Measured T^i_{max}, lb/ft
2	0.293	0.25	70	153
4	0.371	0.5	178	222
6	0.290	0.75	209	314
8	0.353	1	339	394
10	0.484	1	465	387
12	0.551	1	529	475
14	0.528	1	507	512
16	0.575	1	553	403
18	0.520	0.6	300	267
20	0.757	0.2	145	241
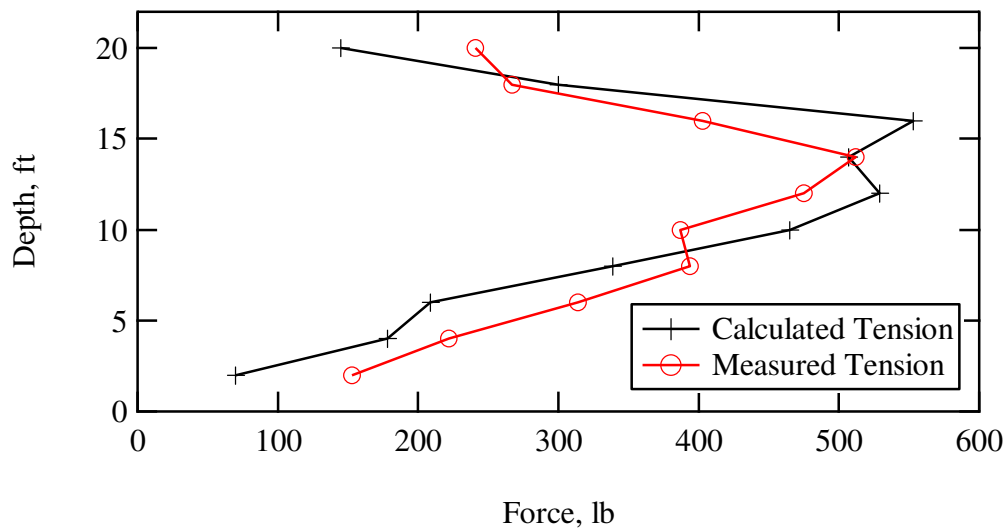
Fig. 3.28. Calculated and Measured Tensions
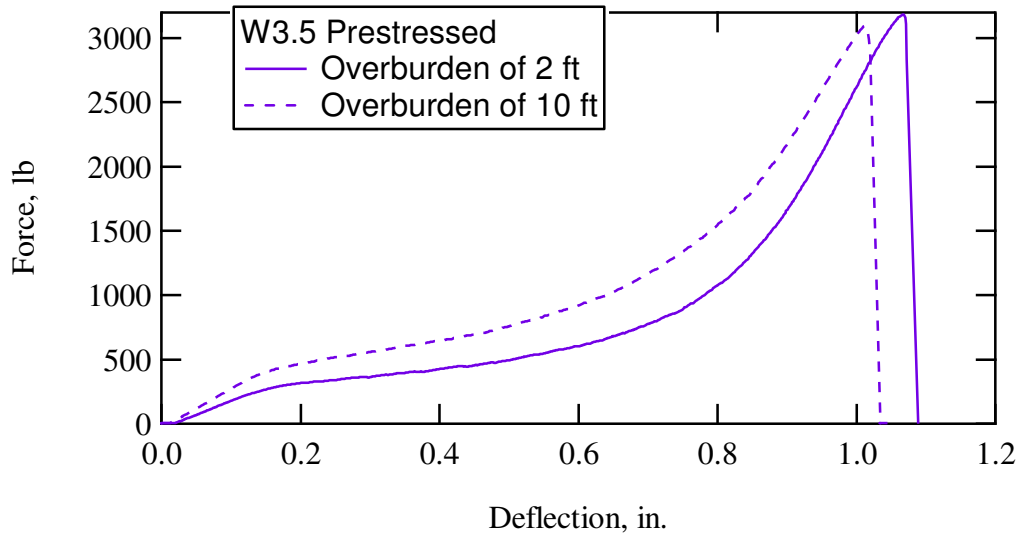
Fig. 3.29. Force versus deflection curve for overburden depths of 2 and 10 ft (Prestressed)
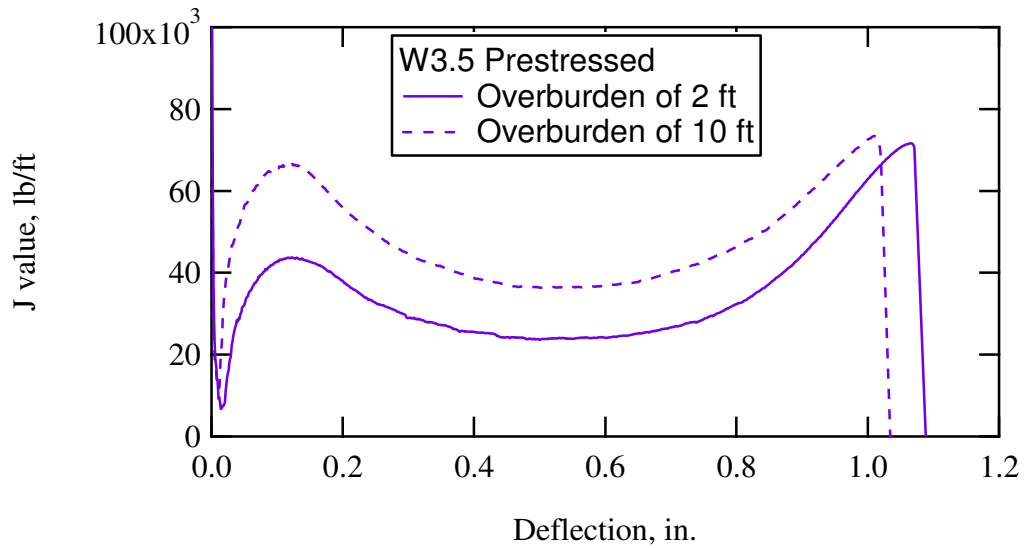
Fig. 3.30. J values versus deflection for depths 2- 10 ft (Prestressed)
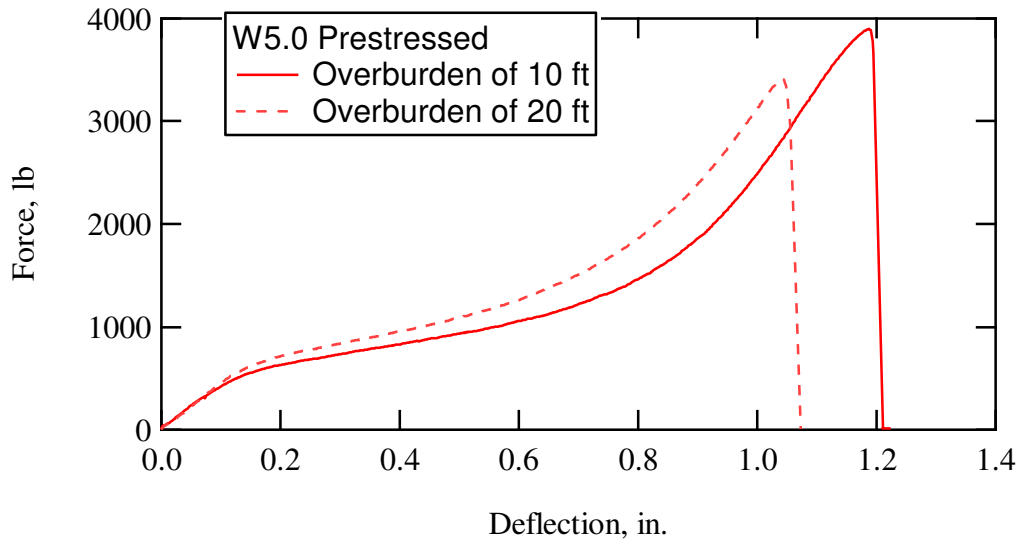
Fig. 3.31. Force versus deflection curve for overburden depths of 10 and 20 ft (Prestressed)
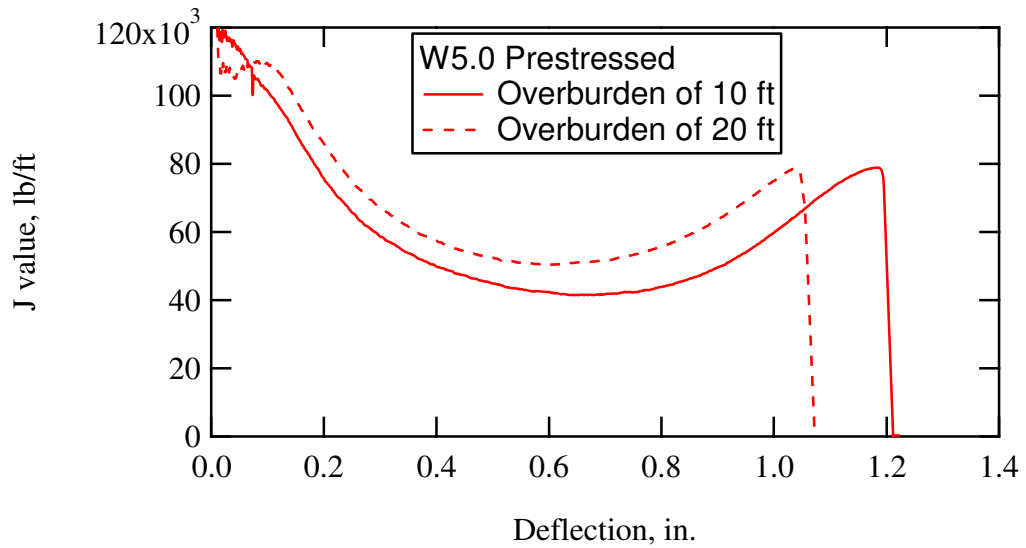
Fig. 3.32. J values versus deflection for depths 10- 20 ft (Prestressed)
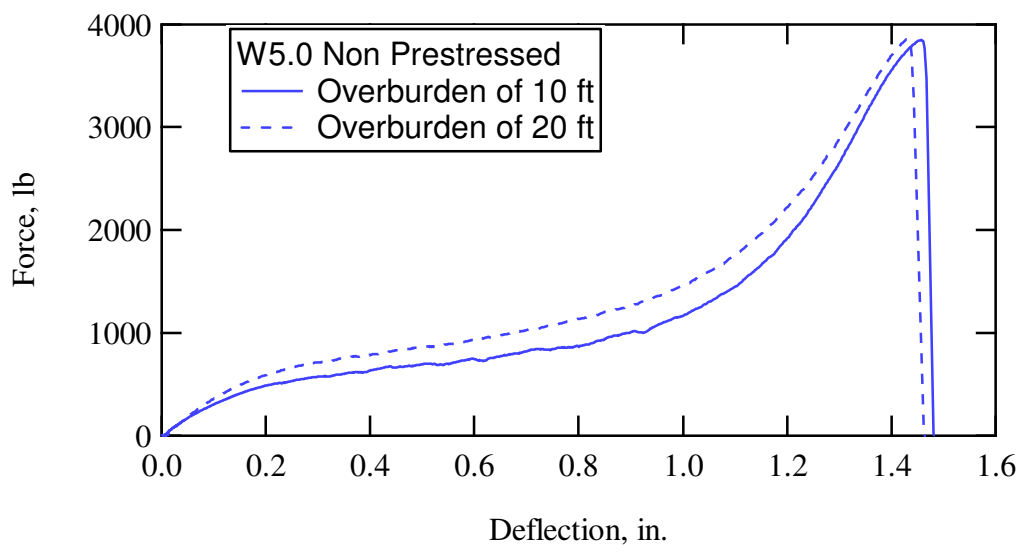
Fig. 3.33. Force versus deflection curve for overburden depths of 10 and 20 ft (Non Prestressed)
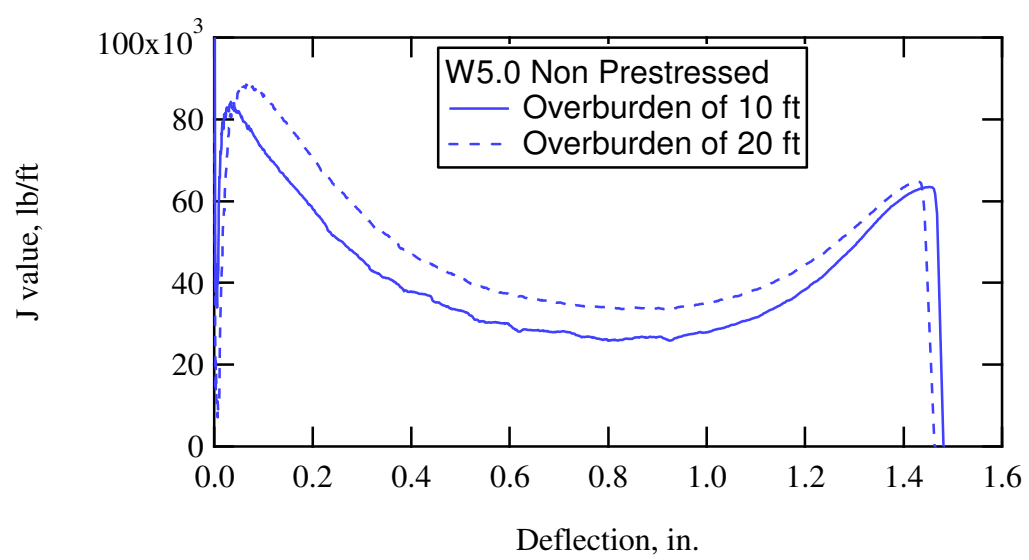
Fig. 3.34. J values versus deflection for depths 18- 20 ft (Non Prestressed)
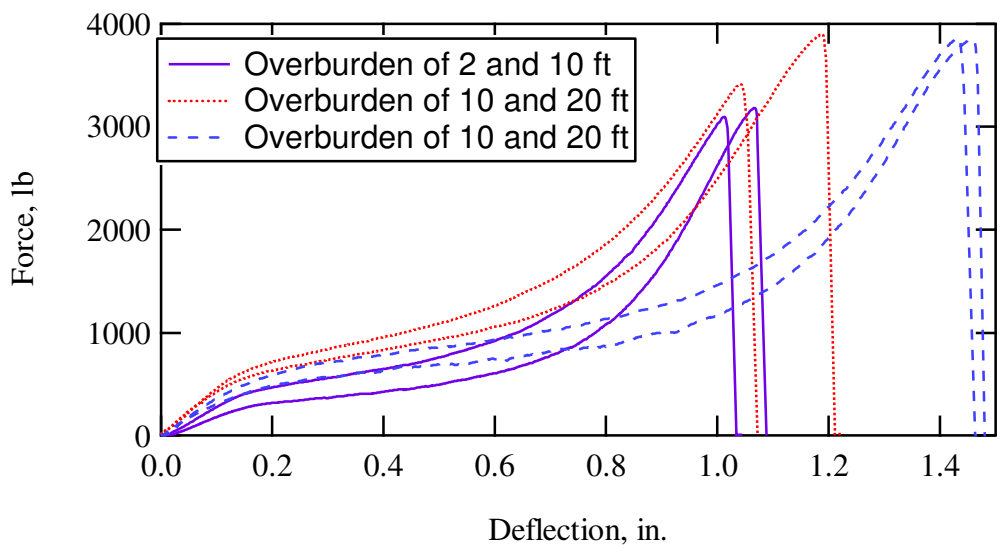
Fig. 3.35. Force versus deflection curve for all depths
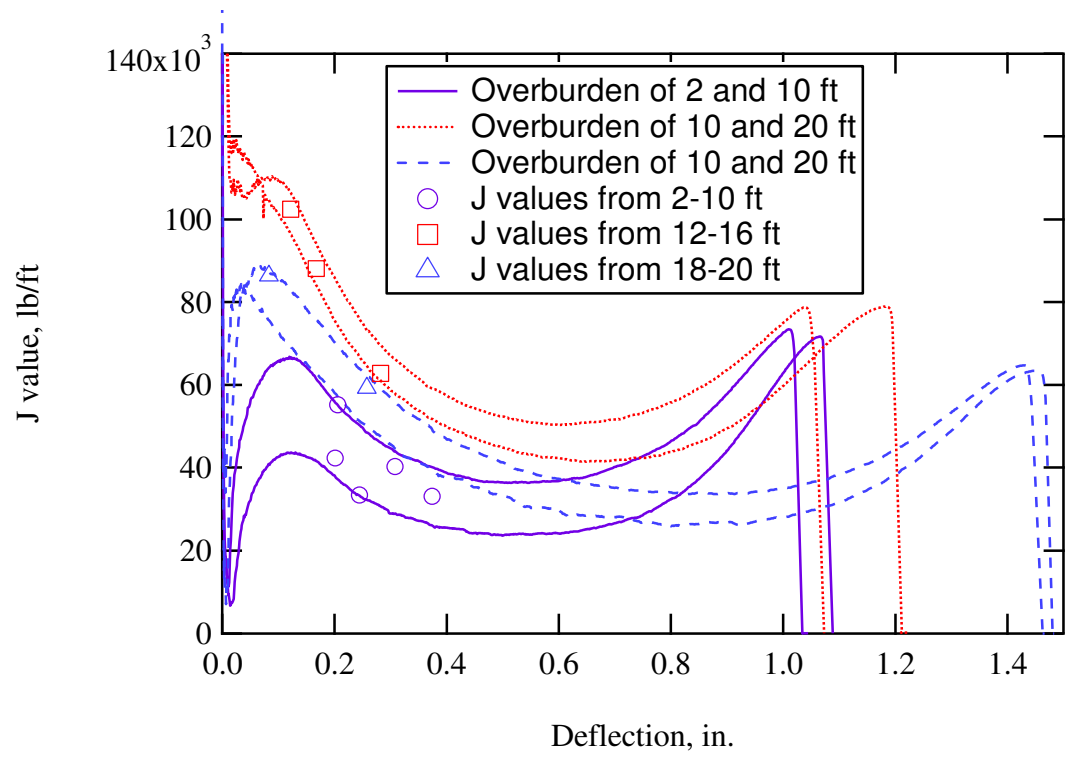
Fig. 3.36. J values versus deflection for all depths

3.5 Where Stiffness Falls in K-Stiffness

The K-Stiffness method is a relatively new concept for designing MSE walls. Some of the more popular methods include the Coherent Gravity Method, the FHWA Structure Stiffness Method, and the Simplified Method. The K-Stiffness method was developed empirically through the analysis of numerous full-scale wall histories. T_{max}^i is more accurately predicted on the internal design of geosynthetic reinforced MSE walls. This should result in a more efficient design for geosynthetic walls. The goal of the new methodology is to provide a wall design with the least cost, but still maintaining acceptable and predictable long-term performance.
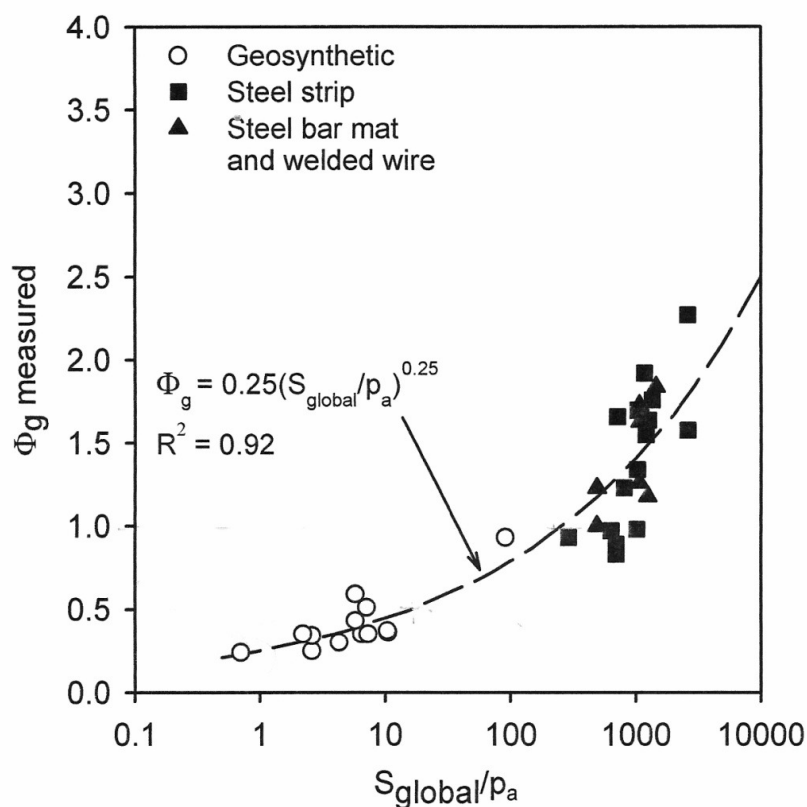
Fig. 3.37. Measure ($\boldsymbol{\Phi}_{g)}$ vs. normalized global reinforcement stiffness value $\left(\dfrac{S_{global}}{P_a}\right)$ (K-Stiffness Figure 7.4)

The K-Stiffness method provides data from geosynthetic wall case histories that enable back-calculation of global stiffness factor values, Φ_g(measured), from measured maximum reinforcement load, T_{mxmx}, values.

The measured stiffness using Φ_g was 0.472. The predicted stiffness we measured was $\frac{S_{global}}{Pa} = 12.73$. Using both values we see the intersection of the stiffness in Figure 3.38. Our measured and predicted stiffness correlates well with the geosynthetic data.
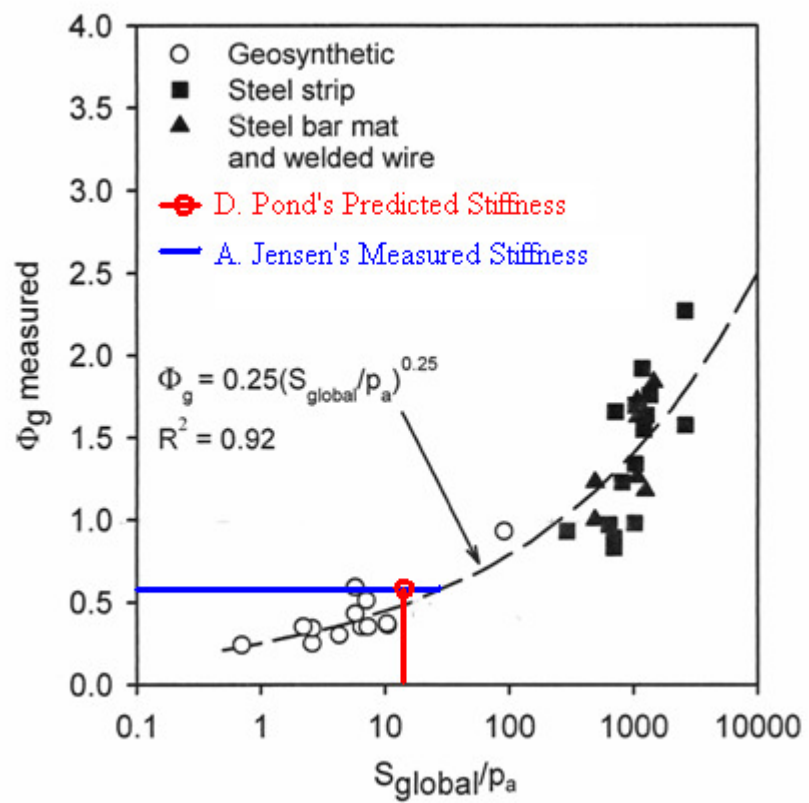
Fig. 3.38. Plot of the measured and predicted stiffness (After K-Stiffness Figure 7.4)

CHAPTER 4

PULLOUT RESISTANCE OF ROUND BARS AND RECO STRAP

4.1 Introduction

Corrosion is the destruction of metal reinforcement due to oxidation. Since corrosion

occurs on the outer surface of metal, rounds bars having the same cross sectional area as

a rectangular bar will have less corrosion. Section 4.2 covers the discussion of round

bars versus a RECO strap in relation to corrosion.

In section 4.3 discusses the different shapes of bars and their properties associated

with pullout resistance. They include cross bars to add bearing capacity thus adding

pullout resistance. And also deformed bars to allow for more deformation before higher

loads are reached.

The pullout test procedure and results are included in section 4.4. Section 4.5

presents the "Progressive" test. The USU wall was built in layers and compacted. As

reinforcement layers were compacted and buried they experience overburden pressure

and thus deformed. The progressive tests simulate the construction of the wall.

4.2 Why Round Bars

Corrosion is the gradual destruction of metal due to oxidation. RECO strap is a

common type of MSE reinforcement for retaining walls. It has a rectangular cross-

sectional area which exposes more surface area than a circular or round bar cross-section.

The RECO strap is more susceptible to corrosion because of their shape. This is why a

round bar is more advantageous for corrosion. A highway retaining wall having a design

life of 75 years would have 75 years of corrosion unless the metal was galvanized. With

galvanization, the metal is credited 15 years reducing corrosion to 60 years. The amount

of corrosion that occurs each year is 0.00047 in. To calculate the corrosion for 60 years

we use:

$$(75\ yr - 15\ yr) * \left(0.00047\frac{in}{yr}\right) = 0.0282\ in \tag{4.1}$$

To compare a RECO strap (50 mm by 4 mm) to a round bar with a diameter of 0.5

in. see Table 4.6. The table shows that there is a loss of 39.3% of steel in the RECO strap

compared to 20.9% in the round bar, nearly a 20% reduction in steel loss. Because of the

reduced steel loss, the tension allowable of the round bar approaches closer to the RECO

strap even though it has a greater initial area. This makes round bars more economical,

efficient, and competitive as an alternative form of reinforcement.

4.3 Types of Bars

There were different bars that were used in testing for pullout resistance. Many 0.5

in. diameter round bars were included. A RECO strap was included to make comparisons

with the round bars. The round bars have different shapes related to different properties

to increase pullout resistance. The cross bars increase pullout resistance by increasing

bearing capacity. To allow for greater deformations while keeping the tension forces

low, bars with tapers and welded washers were used. These bars are shown in Figure

4.39 and Figure 4.40.

A smooth round bar with a diameter of 0.5 in. was tested. The smooth bars that were

tested had cross bars of 8, 4, 2, and 1 in. welded on to add bearing capacity. There was

also a smooth bar with no cross bar we tested to help give us a standard pullout resistance

to reference. To obtain the pullout force of the cross bars alone, the pullout force of the

cross bars were subtracted by the smooth bar with no crossbar.

Table 4.6. Reco Strap vs. Round Bar

	RECO Strap (50 mm by 4 mm)	Round Bar (diameter = 0.5 in.)
Initial Cross-Sectional Area, A_0 (in.^{2})	0.310	0.196
Cross-Sectional Area after 75 yr design life, A_{75} (in.^{2})	$\left(\dfrac{50}{25.4} - 2 * 0.0282\right)$ $* \left(\dfrac{4}{25.4} - 2 * 0.0282\right)$ $= 0.193$	$\pi * \dfrac{(0.5 - 2 * 0.0282)^2}{4}$ $= 0.155$
Area Lost (in.^{2})	0.117	0.041
Area Lost (%)	39.3	20.9
$\sigma_{ultimate}$ (ksi)	65	65

$\sigma_{allowable}$ (ksi)	32.5	32.5
$T_{allowable} = \sigma_{allowable}^* A_{75}$ (kips)	6.27	5.04

The taper bars that were tested were 0.5 in. diameter bars with tapers of 15° and 30°. The purpose of the tapers was to allow for more deformation and lower tension forces. If enough deformation occurs the soil will be in an active state thus making the load in the reinforcement smaller. The welded washer bars had a diameter of 0.5 in. and washer s with either a 1.0 or 0.75 in. diameter. As mentioned earlier, both the taper and welded washers were to see if enough deformation occurs so that the soil will be in an active state. The welded washer bars add a different geometry than the tapers to test for deformation.

The RECO strap is a common form of reinforcement that is used today. This will make it beneficial to compare with the round bars. It is also advantageous to compare because of its rectangular shape. We will be able to see how effective the round bars are. The dimensions of the RECO strap used are 50 mm by 4 mm.
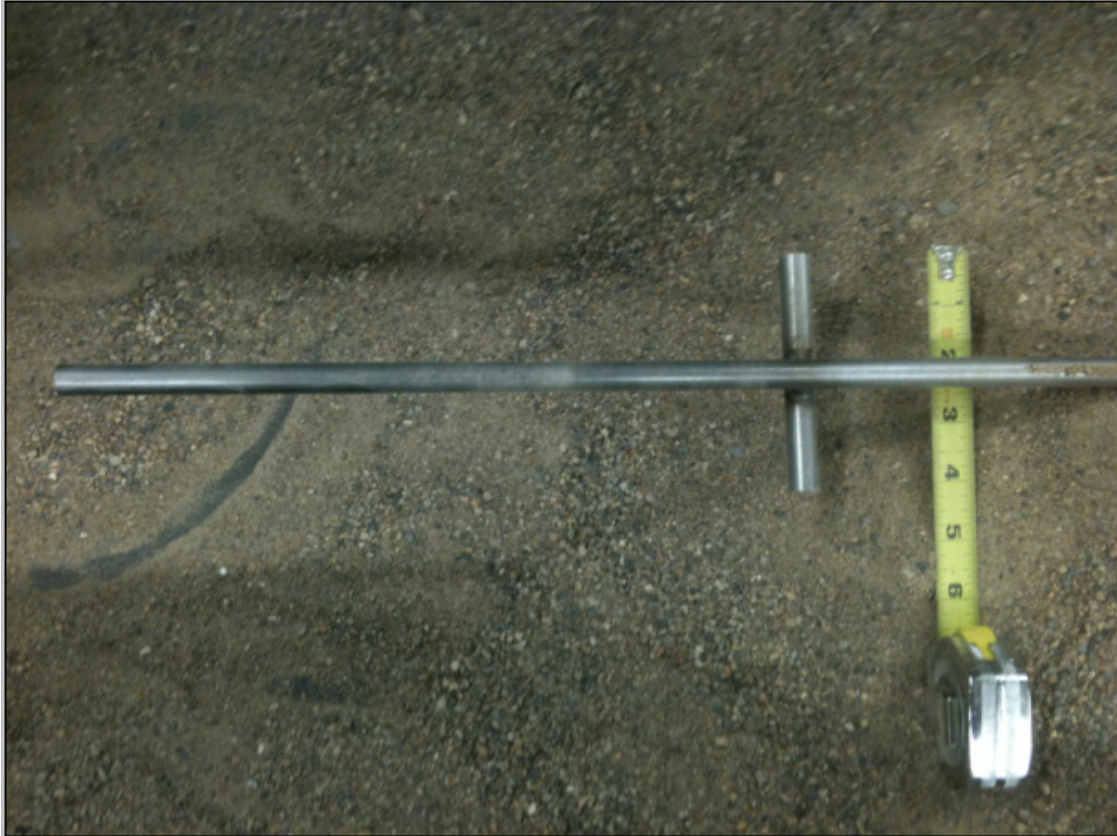
Fig. 4.39. 0.5 in. diameter and cross bar of 4 in.

4.4 Pullout Testing Procedure

The pullout box had dimensions of 18 in. by 87 in., shown in Figure 4.42. The

procedure for testing the reinforcement was done similarly for each test so that consistent

data could be collected and compared.

This process involves pulling reinforcement (bar or strap) in washed mortar sand at

different vertical pressures, simulating different depths of embedment and measuring the

tensile forces and deflections on the bar. To obtain a consistent density the first and

second lifts contained 505 lb and 480 lb, respectively. The washed mortar sand was

compacted to a total unit weight of 110.2 pcf. The first lift had a volume of 4.58 ft^3,

while the second lift had a volume of 4.18 ft^3. Each lift was compacted with an 11 amp

compacter and compaction foot with a mass of 300 lb, shown in Figures 4.41 and 4.43.

A pulley was used to raise and lower the compactor and foot on the rolling lift structure,

shown in Figure 4.44.

The compaction foot has holes where two rods can be inserted. The rods rest on the

edges of the pullout box when the desired compaction is reached, shown in Figure 4.45

and Figure 4.46. After the first lift is compacted, you can now connect the steel

reinforcement, as seen in Figure 4.48. The reinforcement (bar or strap) is connected to

the load sensors and measured to ensure that it is straight and concentric with the load

cell and screw jack. The width of the box from inside edge to inside edge is 18 in.

Therefore we would measure 9 in. from the wall to the center of the steel reinforcement,

shown in Figure 4.59. Then the second lift is poured and compacted, shown in figure

4.50. After the second lift is compacted, an air bladder is placed on top of the sand,

shown in Figure 4.51. A lid, some channels, and nuts are assembled on the box, seen in

Figure 4.52 and Figure 4.53. The air bladder hose is then connected to the pressure

control board which expels the various pressures, shown in Figure 4.54 and Figure 4.55.

The depths that were desired for the tests to be run at were 2.5, 5, 10, 20, and 40 ft. Their

corresponding vertical pressures were 1.86 psi, 4.03 psi, 8.37 psi, 17.05 psi, and 34.4 psi

(33.85 psi was used because of leakage). Equation 4.2 was used to calculate the vertical

pressures from the depths:

$$P = d * \gamma_{wall} - z * \gamma_{soil} \qquad (4.2)$$

where P is the vertical pressure, d is the various depths of overburden, γ_{wall} is the unit

weight of a retaining wall which is 125 pcf, z is the distance from the top of the box to

the center of the bar which is 4.806 in. or 0.4004 ft, and γ_{soil} is the unit weight of the washed mortar sand which is 110.2 pcf.

The metal reinforcement is connected to the load cell which connects to the clevis and the screw jack by a pin, seen in Figure 4.56. After the pressure is reached the load cell is zeroed without the pin. The pin is inserted into the clevis and screw jack. Then the LVDT (Linear Variable Differential Transformer), which is the linear position sensor, is zeroed as well. This was done each time and then the test was run. The bars that were compared for these tests include a 0.5 in. diameter smooth bar, a 0.5 in. diameter crossbar with lengths of 8 in., 4 in., 2 in., and 1 in., a 0.5 in. diameter bar with a 15° taper, a 0.5 in. diameter bar with a 30° taper, a 0.5 in. diameter bar with a 0.75 in. welded washer, a 0.5 in. diameter bar with a 1.0 in. welded washer, and a RECO strap.
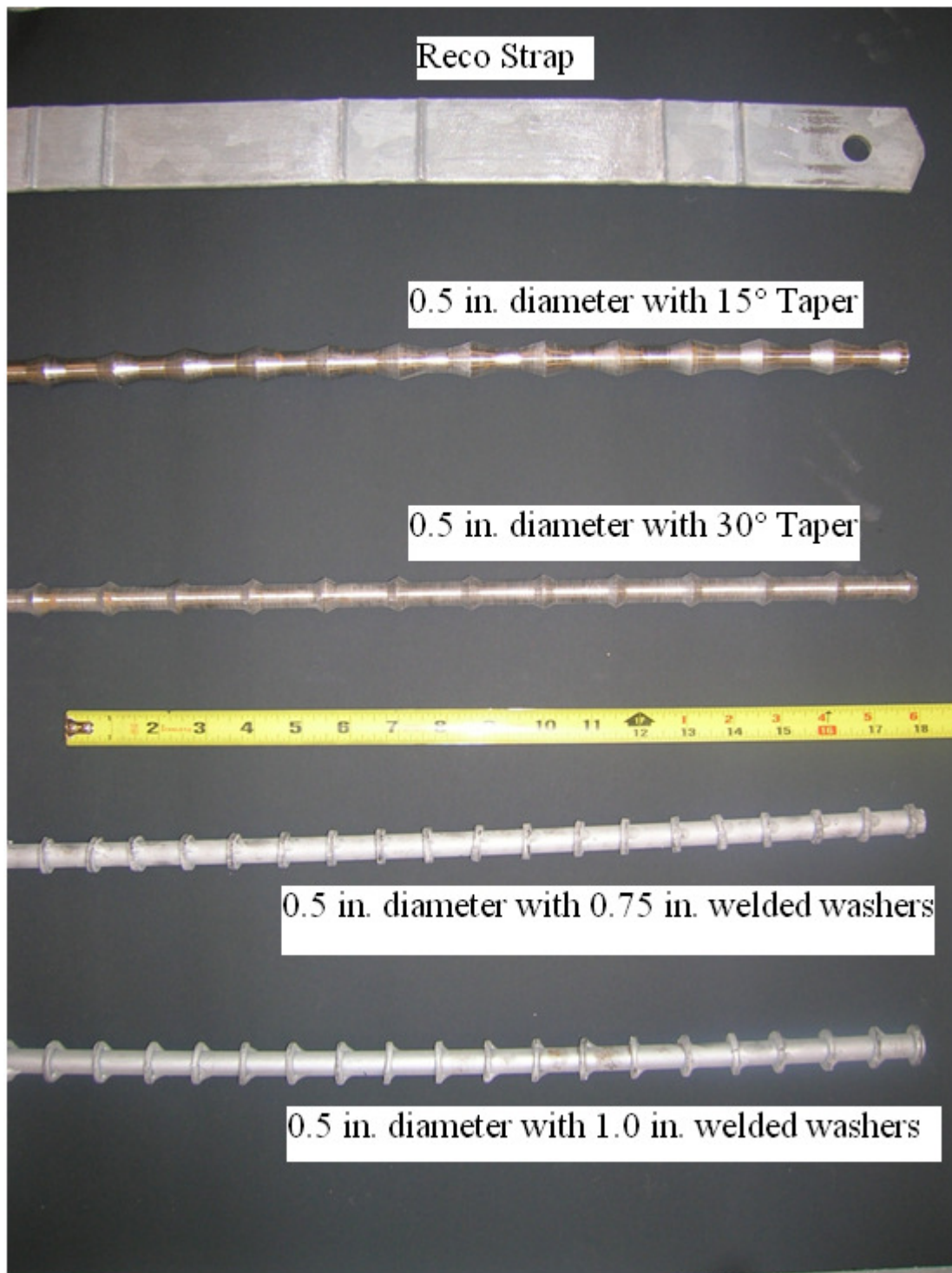
Fig. 4.40. Different types of bars

Fig. 4.41. Close up of compactor and compaction foot

Fig. 4.42. Pullout box showing dimensions of 18 in. by 87 in.
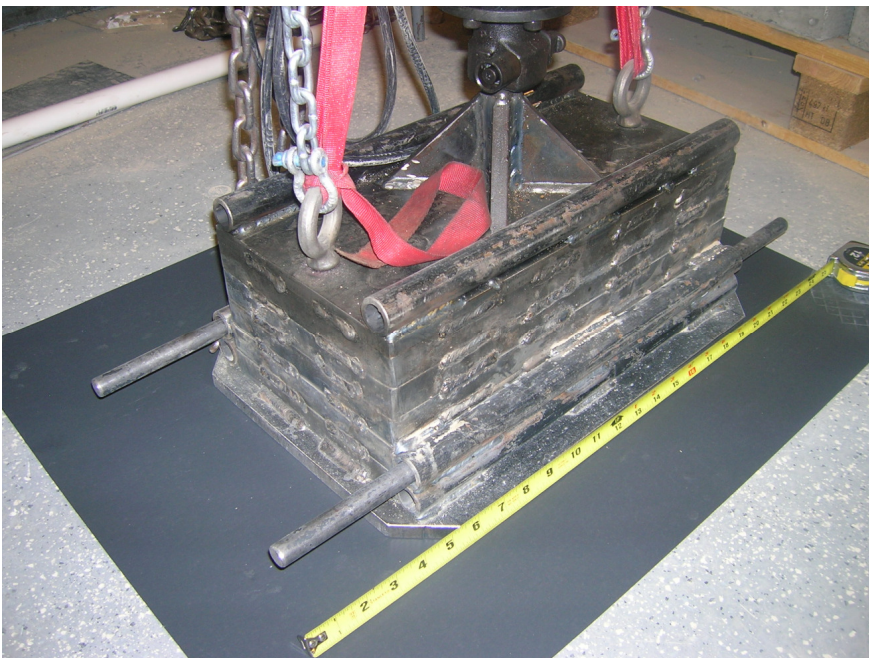
Fig. 4.43. Close up of compaction foot

Fig. 4.44. Rolling lift structure with pulley and compacter and compaction foot

(a) Before Compaction of 1st lift

(b) After Compaction of 1st lift
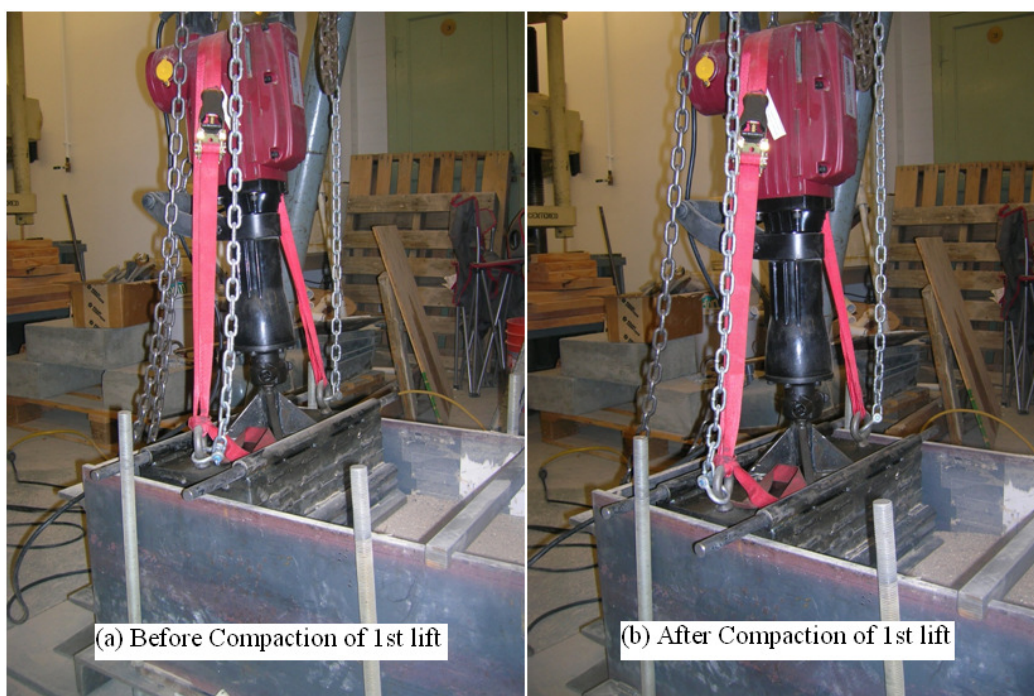
Fig. 4.45. Using compactor on 1st lift
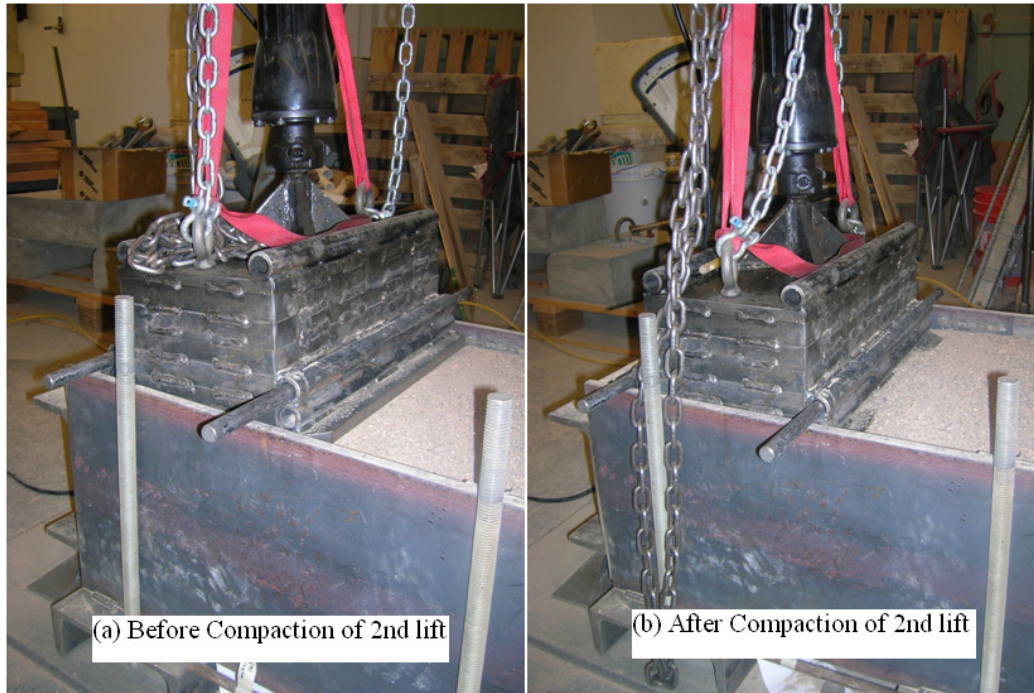
Fig. 4.46. Using compactor on 2nd lift

Fig. 4.47. Side view of compacter after compaction

Fig. 4.48. Top view of pullout box after compaction of first lift
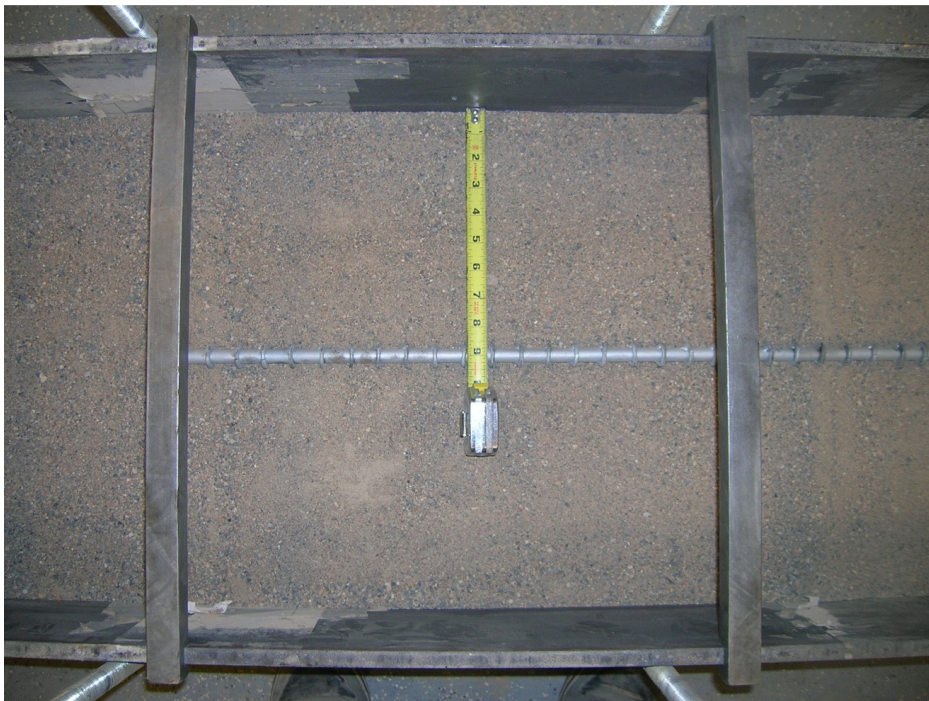
Fig. 4.49. The bar is measured to ensure concentric loading

Fig. 4.50. Pullout box after second lift is compacted

Fig. 4.51. Air bladder is placed on the lifts of sand after compaction

Fig. 4.52. The pullout box lid is the placed on top of the bladder

Fig. 4.53. The pullout box is ready for testing
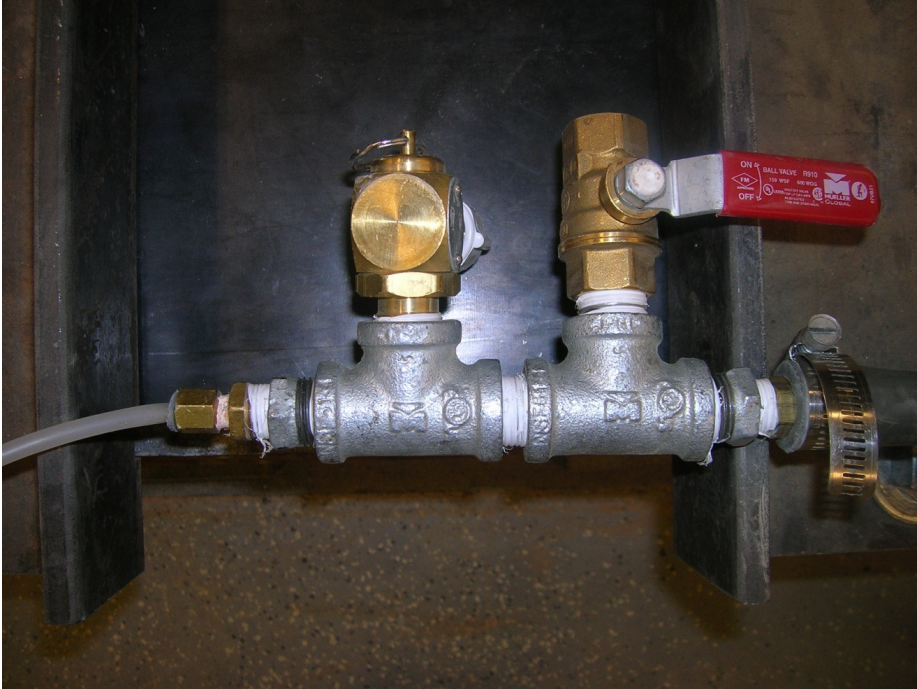
Fig. 4.54. Close up of the pressure connection to the air bladder hose

Fig. 4.55. Pressure control panel
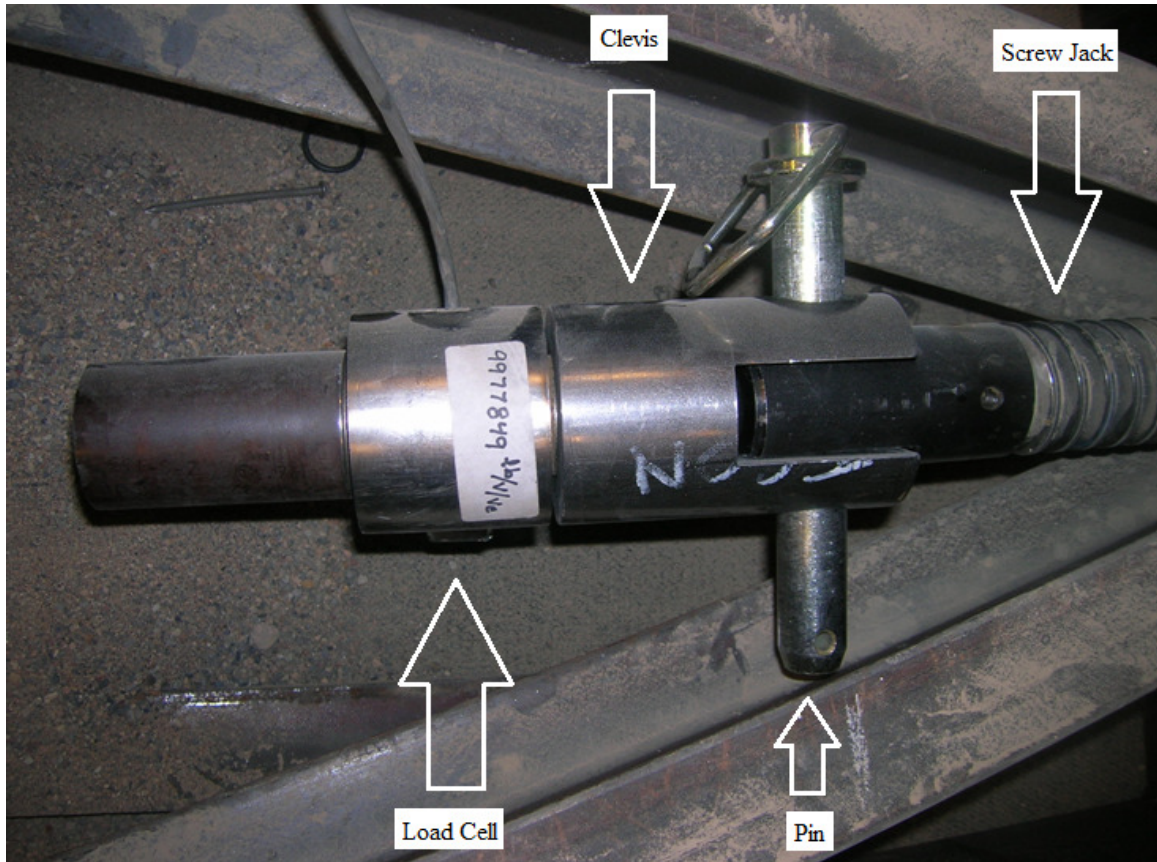
Fig. 4.56. Connection of load cell to screw jack

4.4.1 Cross Bars Pullout Resistance

In order to measure the effect of the cross bars, we first performed pullout tests on smooth bars. This was done so that we could take the cross bar pullout resistance and subtract the smooth bar resistance to see the resistance of the cross bar alone. The smooth and cross bars had a diameter of 0.5 in. We pulled the bar at pressures simulating the depths of 2.5 ft, 5 ft, 10 ft, 20 ft, and 40 ft. The cross bar included the smooth bar with the actual cross bar of the diameter of 0.5 in. welded perpendicular to the main bar and perpendicular to the load. The lengths tested were 8 in., 4 in., 2 in., and 1 in. cross bars. The 8 in. cross bar was tested first. It was the only bar that bent, shown if Figure

4.57. The Force-Displacement figures are shown below and in the Appendix. Pullout resistance values at a displacement of 0.75 in. were used (as per AASHTO).

The equation for the smooth bar pullout resistance and the cross bars with their various lengths are shown in the Table 4.8. The variable x is the vertical stress desired. The equation for the cross bars shows the cross bar only. It is the cross bar pullout resistance subtracted by the smooth bar pullout resistance at 0.75 in. of displacement and the values can be seen in Table 4.7.

Fig. 4.57. 0.5 in. diameter cross bar with 8 in. length bent from the pullout test
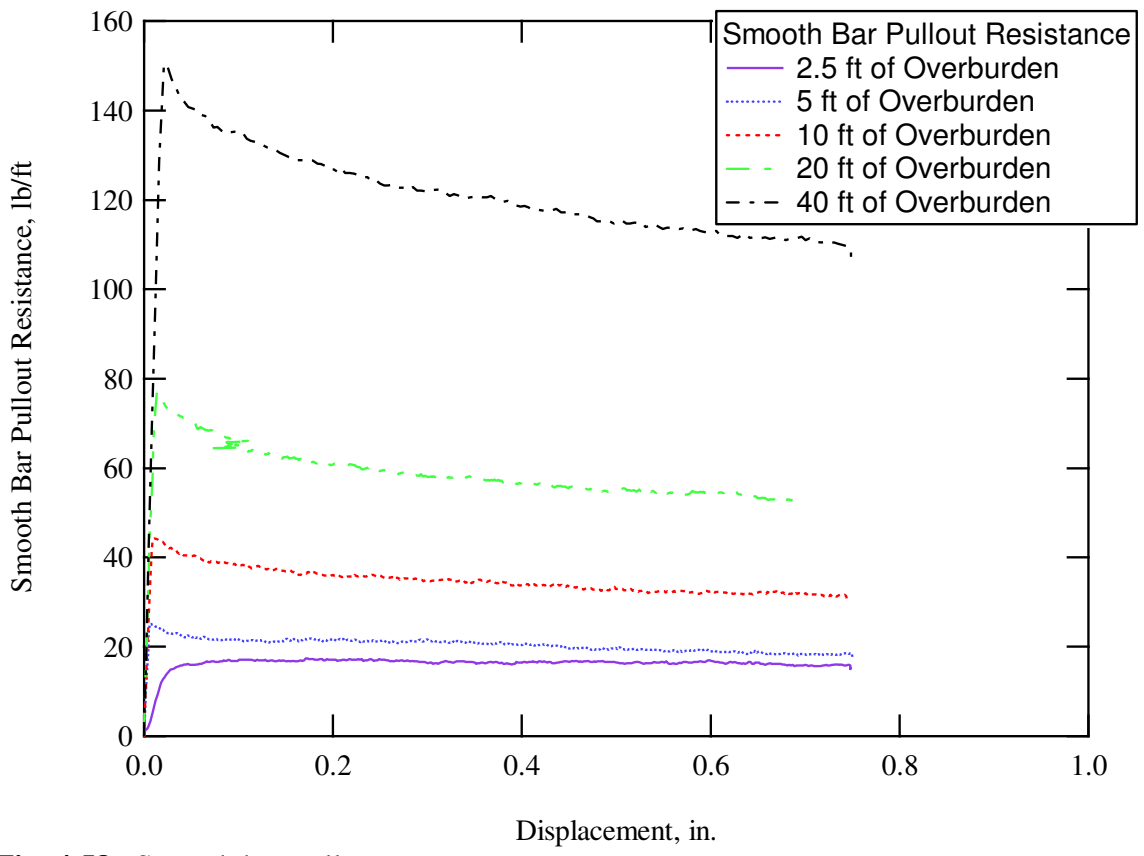
Fig. 4.58. Smooth bar pullout tests
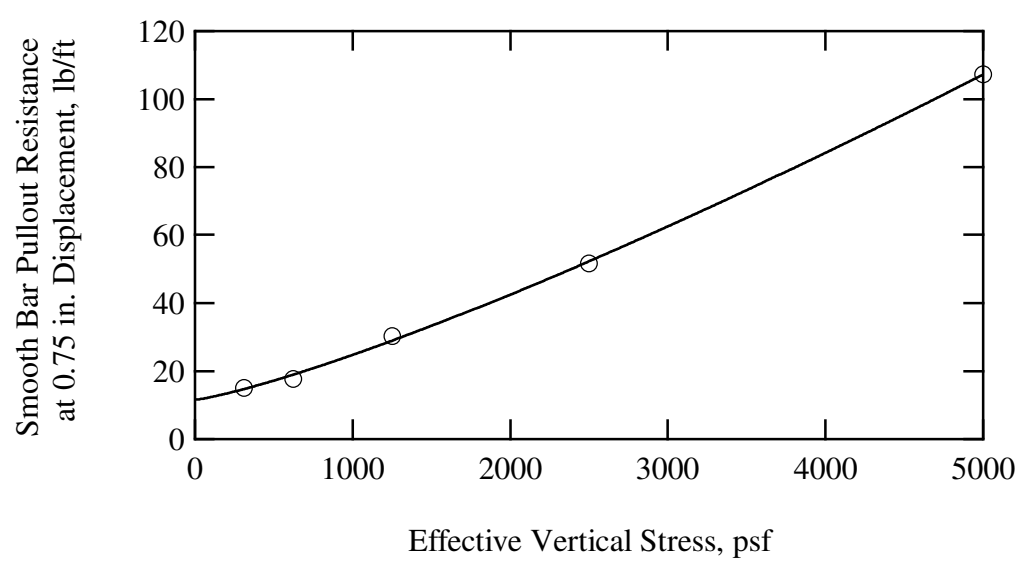
Fig. 4.59. Smooth bar pullout resistance versus effective vertical stress
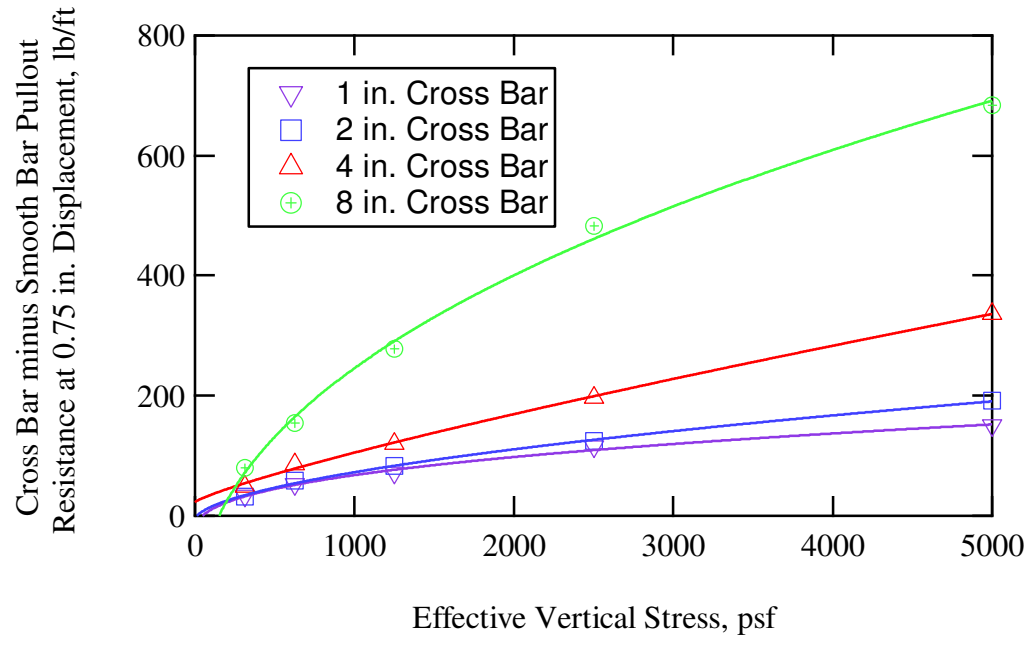
Fig. 4.60. Cross bar minus smooth bar pullout resistance versus effective vertical stress

Table 4.7. Pullout Resistance at 0.75 in. of Displacement

Pullout Resistance at 0.75 in. of displacement, lb					
Overburden depth, ft	Smooth Bar	1 in. Cross Bar	2 in. Cross Bar	4 in. Cross Bar	8 in. Cross Bar
2.5	15.1	32.8	32.0	49.4	80.1
5.0	17.6	52.7	58.2	86.3	154.6
10.0	30.3	71.1	83.4	120.6	278.1
20.0	51.6	115.4	124.2	196.8	482.8
40.0	107.3	150.2	191.7	336.9	683.8

Table 4.8. Pullout Resistance General Equations for the Smooth Bar and Cross Bars

Pullout Resistance General Equation: Pullout Resistance at 0.75 in. displacement = $Y_0 + Ax^{Power}$	
$= Y_0 + Ax^{Power}$	Type of Bar
$= 11.553 + 0.0026477x^{1.2321}$	Smooth Bar
$= -30.567 + 6.905x^{0.38459}$	1 in. Cross Bar
$= -6.6208 + 1.5824x^{0.56652}$	2 in. Cross Bar
$= 22.811 + 0.26805x^{0.82932}$	4 in. Cross Bar
$= -191.28 + 21.382x^{0.43683}$	8 in. Cross Bar

4.4.2 0.5 in. Deformed Bar Tapers and Welded Washers

The taper bars were chosen to have a 15° and 30° angle deformations. The 15° taper was expected to have more deformation than the 30° taper. The disadvantage of the 15° taper is that there is more steel in the bar which increases costs.

For this test we had 0.5 in. diameter bars that were machined to have a 15° and 30° angle deformations, shown in Figure 4.61 and Figure 4.62. We performed overburden pressures simulating a depth of 2.5 ft, 5 ft, 10 ft, 20 ft, and 40 ft on both bars. The pressures applied started with 2.5 ft then 5 ft and so on to 40 ft. After each overburden

pressure was applied the bars were pulled a distance of 0.75 in. to 1.0 in. in displacement. The Force per Length versus Deflection plots are shown thru Figure 4.63 to 4.68.

For the 40 ft of overburden on Figure 4.67, the 15º taper looks inconsistent with the other tests. This is because we had a 5,000 lb load cell connected and we needed a capacity up to 10,000 lb. The applied pressure was released as the load cell was switched out and then reapplied. For all of the 30º taper tests there was no need to change the load cell since the 10,000 lb load cell was installed from the 15 º taper tests.

The 15º and 30º tapers have a similar trend in Pullout Resistance. The figures show with a higher overburden depth there is more pullout capacity.

The welded washer bars had a 0.5 in. diameter and the welded washers had a diameter of 0.75 in. and 1.0 in, shown in Figure 4.69 and Figure 4.70. The washers were spaced at 1 in. increments for both bars.

We performed overburdens of 2.5 ft, 5 ft, 10 ft, 20 ft, and 40 ft on both bars. For the test we pulled the bar approximately 1.0 in. in displacement then applied the next higher overburden pressure until we reached the final overburden depth of 40 ft. The results are shown in Figure 4.71 to Figure 4.76.

As the effective vertical stress increases, the pullout capacity and % of allowable tension of the bar increases. From the figures we see that the 1 in. welded washer bar has more pullout resistance than the 0.75 in. welded washer bar. The 0.75 in. welded washer bar had pullout forces close to the 15º and 30º taper bars. This means that geometry does not matter.
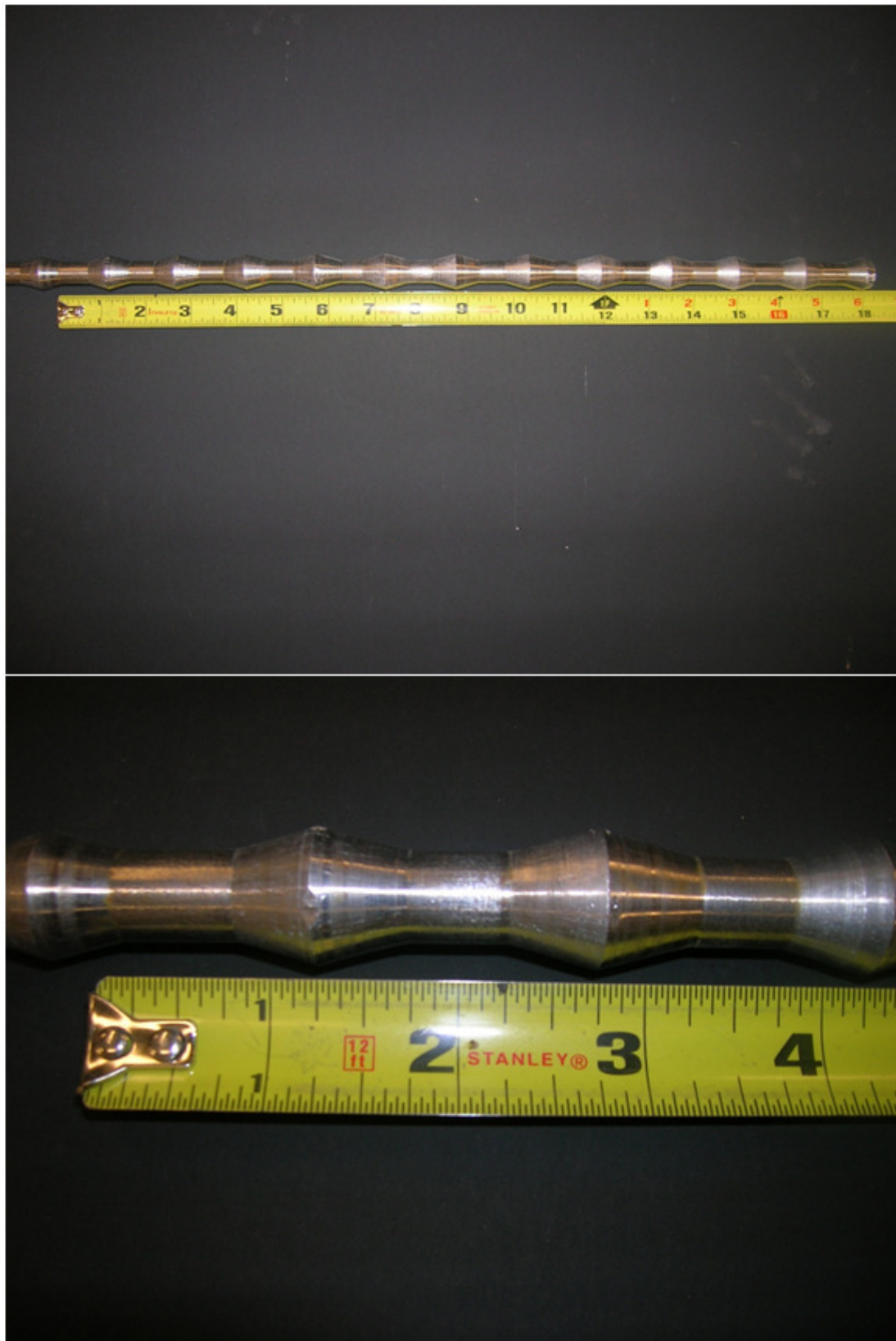
Fig. 4.61. 0.5 in. diameter bar with 15º taper

Fig. 4.62. 0.5 in. diameter bar with 30º taper
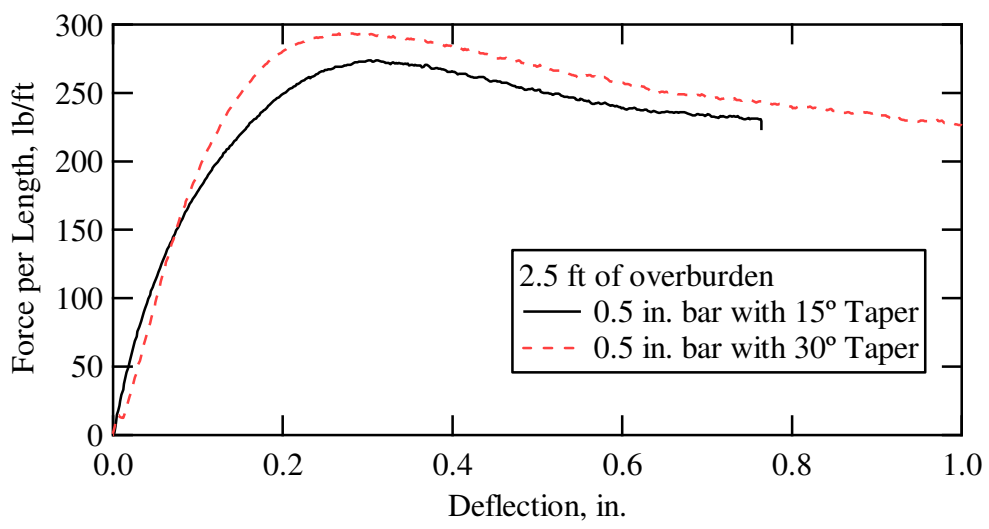
Fig. 4.63. Force-displacement curves for 0.5 in. 15° and 30° taper bars at 2.5 ft of overburden
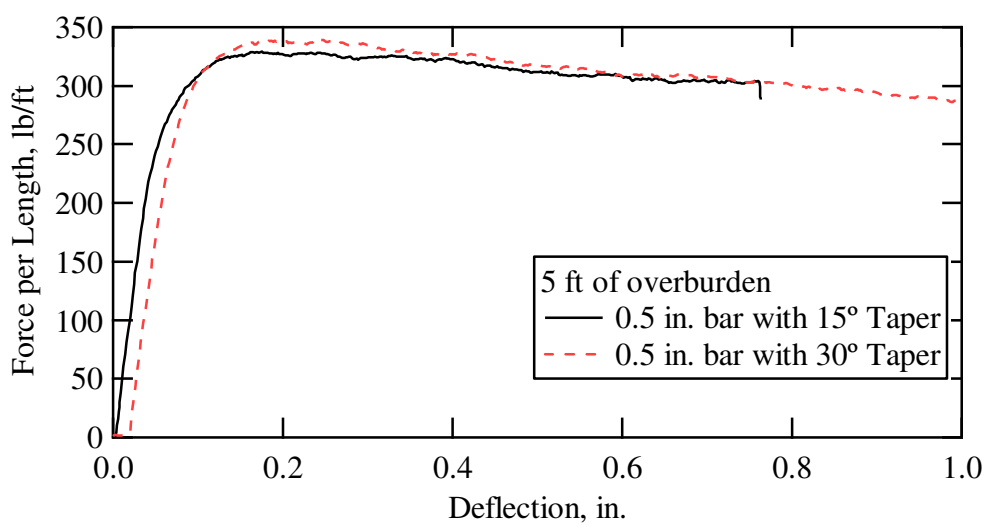
Fig. 4.64. Force-displacement curves for 0.5 in. 15° and 30° taper bars at 5 ft of overburden
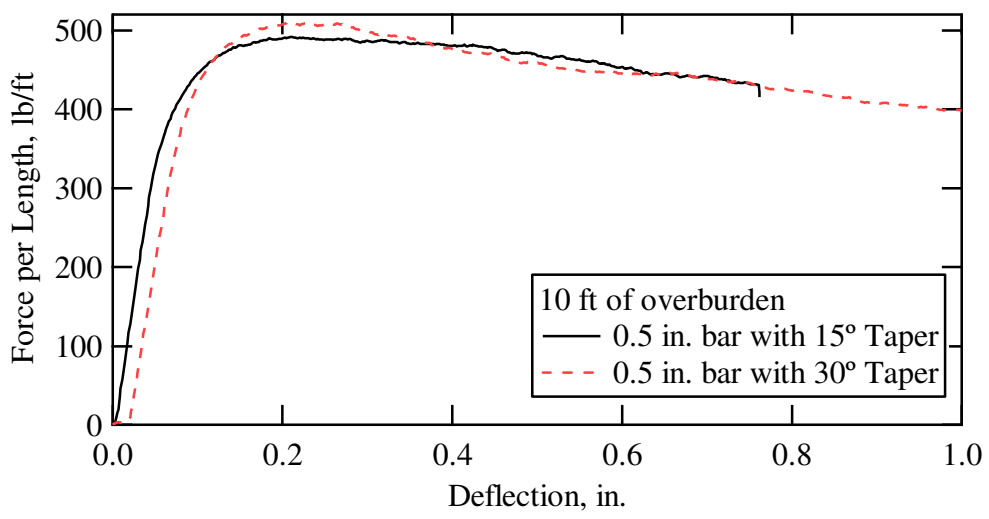
Fig. 4.65. Force-displacement curves for 0.5 in. 15° and 30° taper bars at 10 ft of overburden
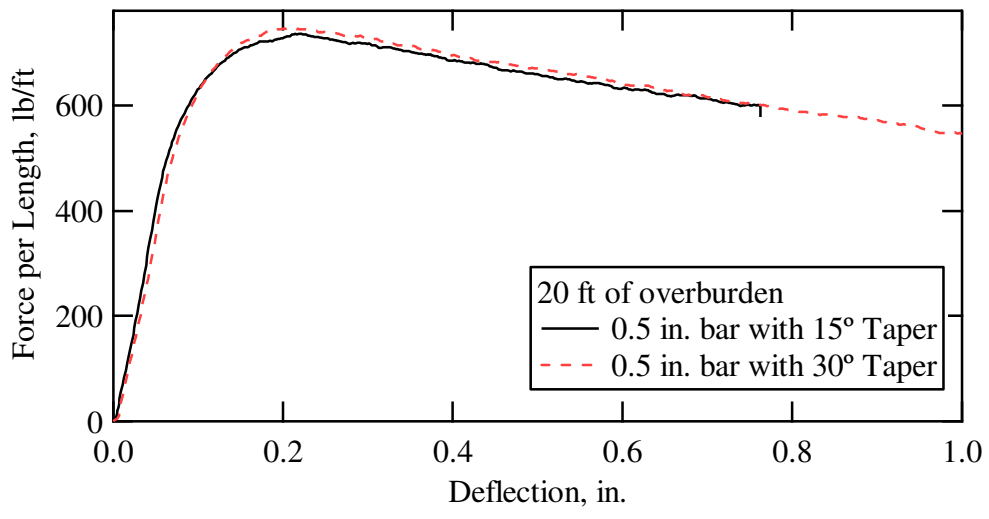
Fig. 4.66. Force-displacement curves for 0.5 in. 15° and 30° taper bars at 20 ft of overburden
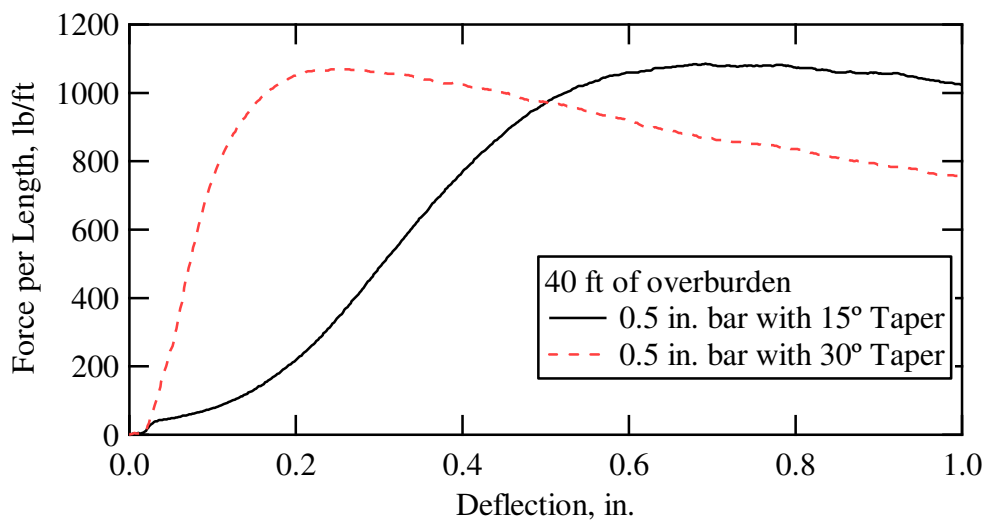
Fig. 4.67. Force-displacement curves for 0.5 in. 15° and 30° taper bars at 40 ft of overburden
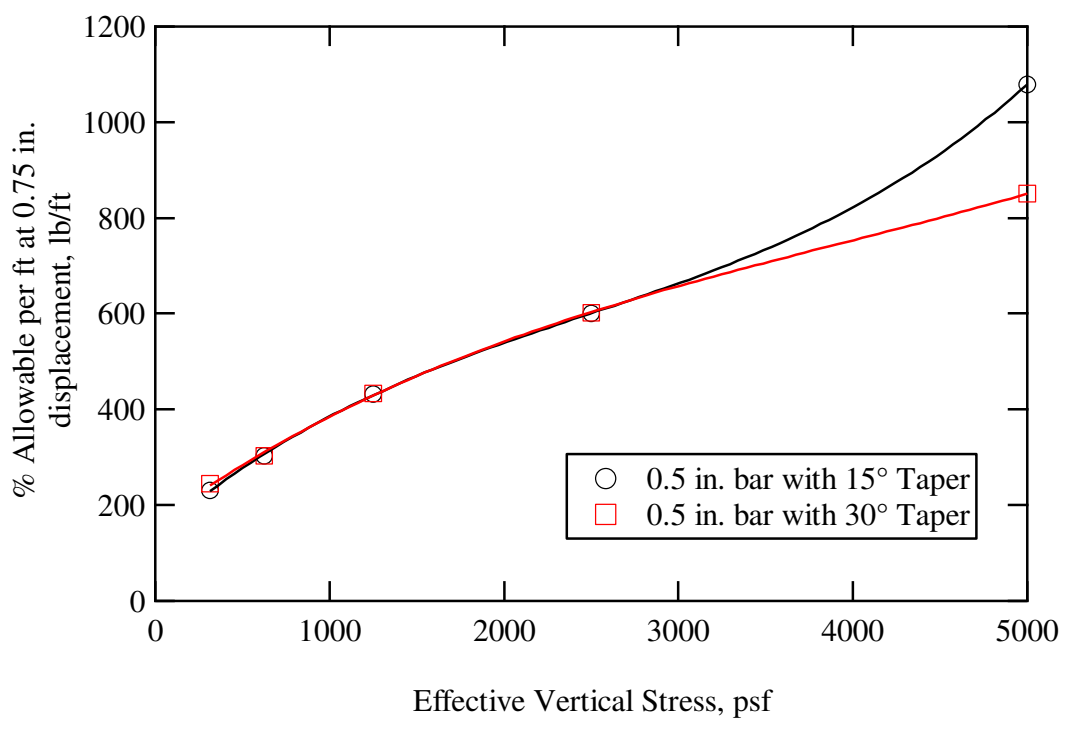
Fig. 4.68. % of allowable tension at 0.75 in. of displacement for 0.5 in. bar with 15° and 30° taper bars
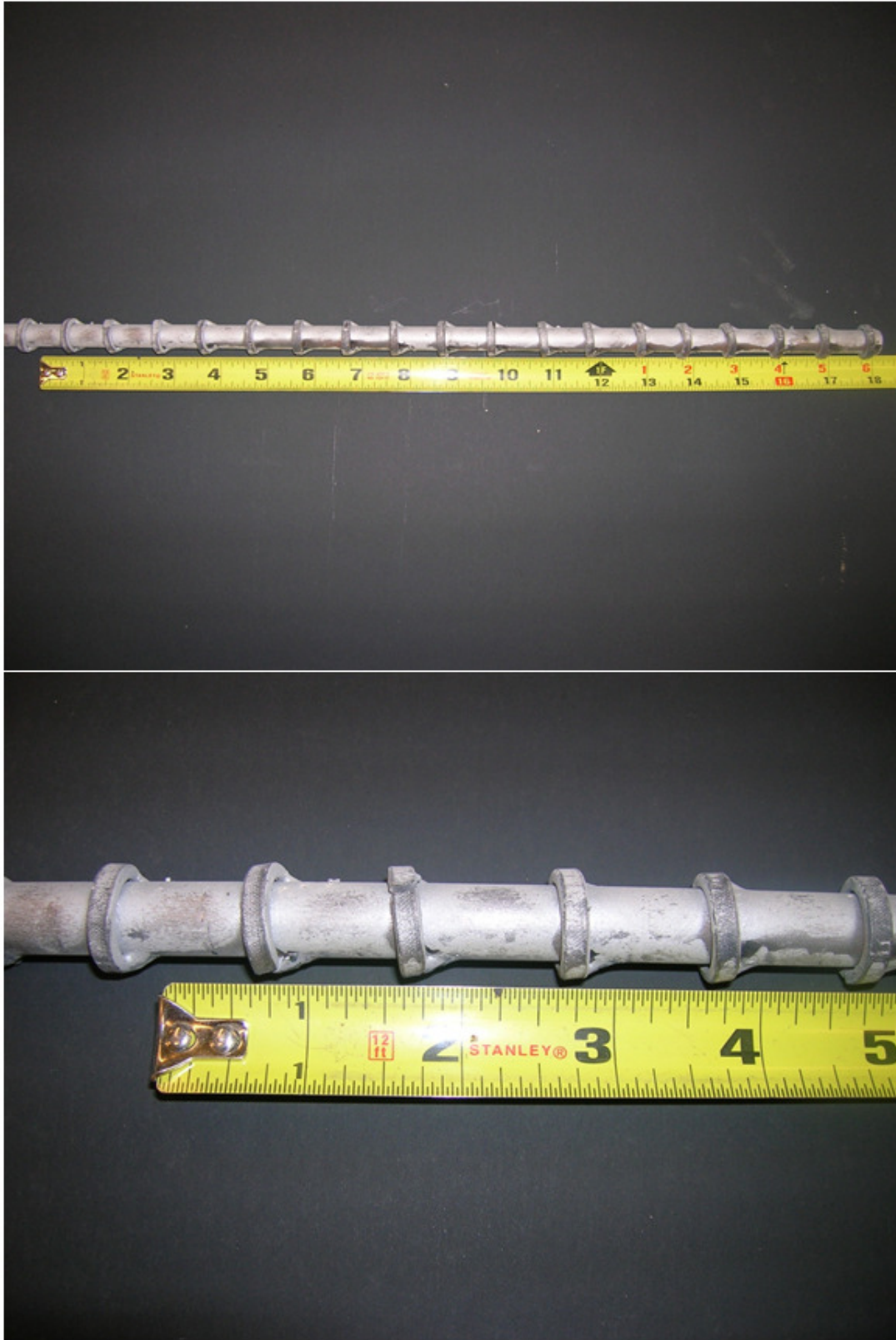
Fig. 4.69. 0.5 in. diameter bar with 0.75 in. welded washers
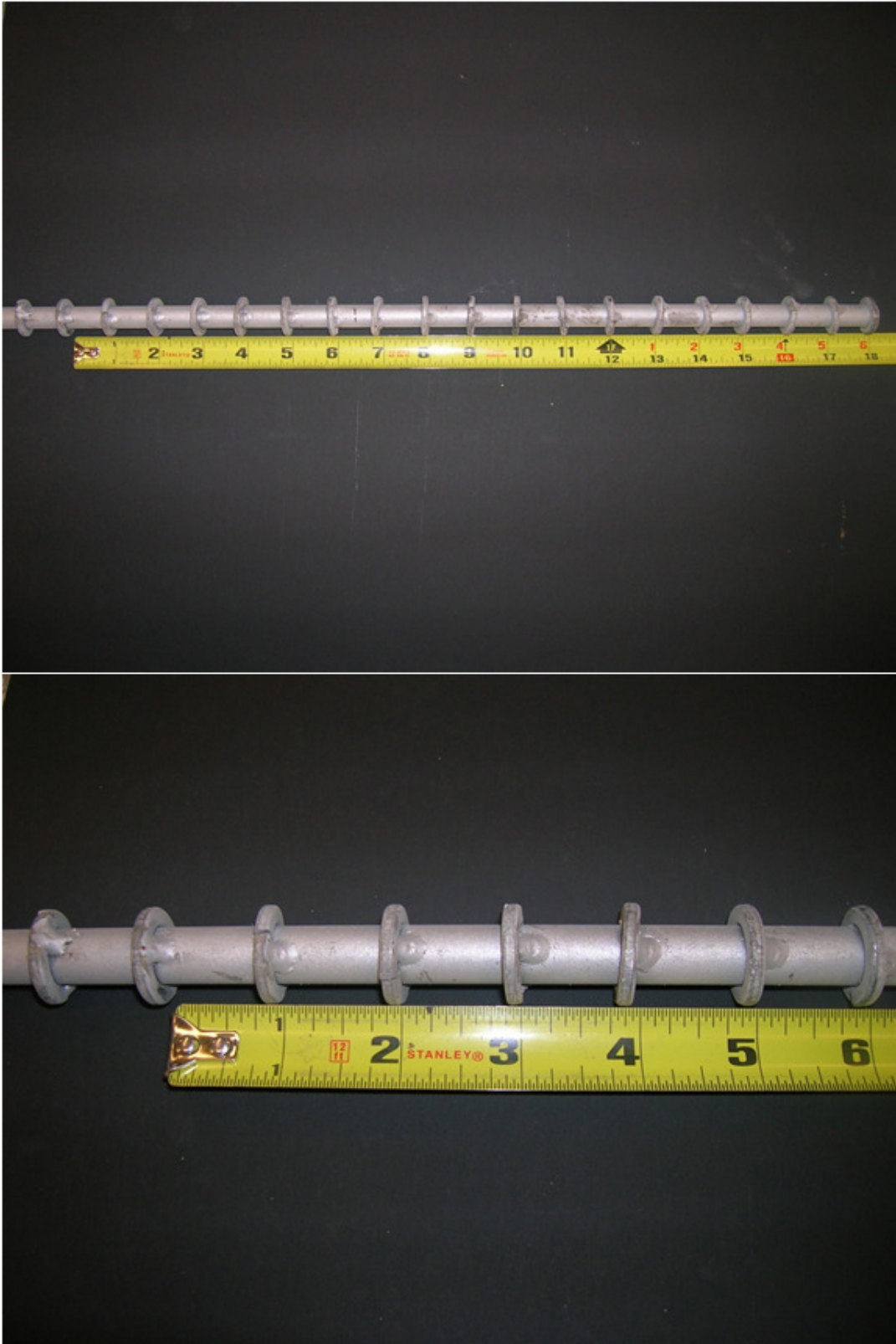
Fig. 4.70. 0.5 in. diameter bar with 1.0 in. welded washers
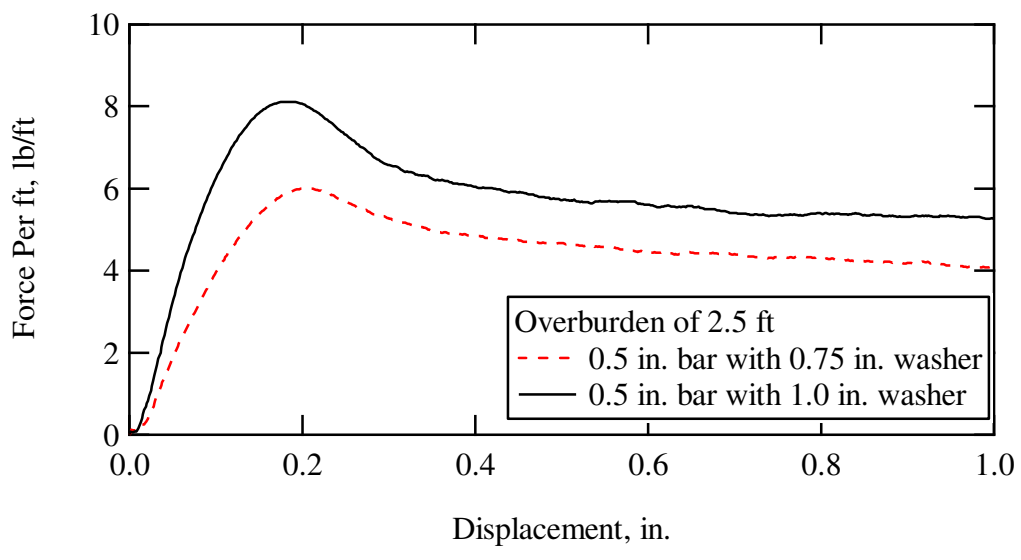
Fig. 4.71. Force-displacement curves for 0.5 in. bars with 0.75 in. and 1.0 in. washers at 2.5 ft of overburden
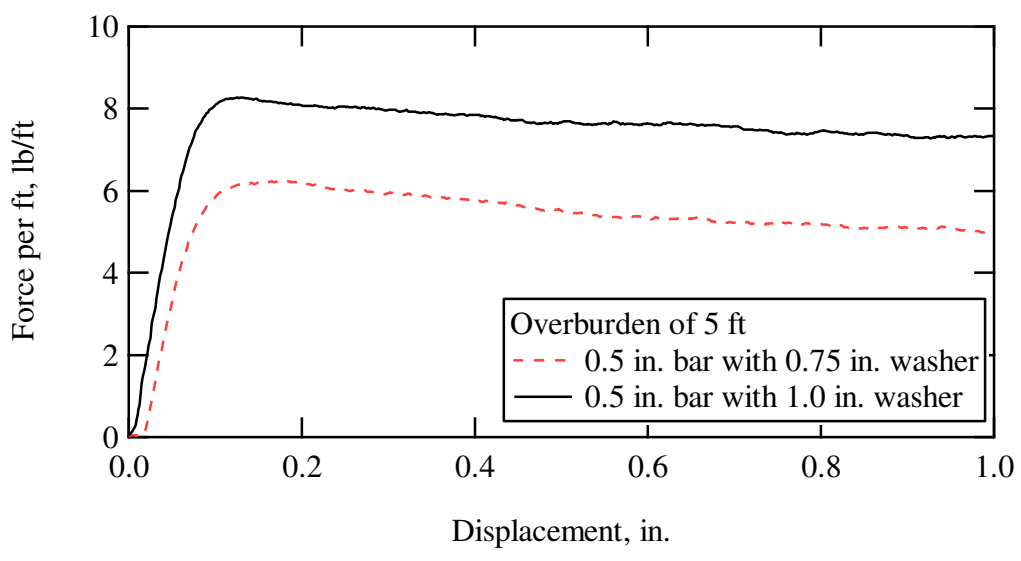
Fig. 4.72. Force-displacement curves for 0.5 in. bars with 0.75 in. and 1.0 in. washers at 5 ft of overburden
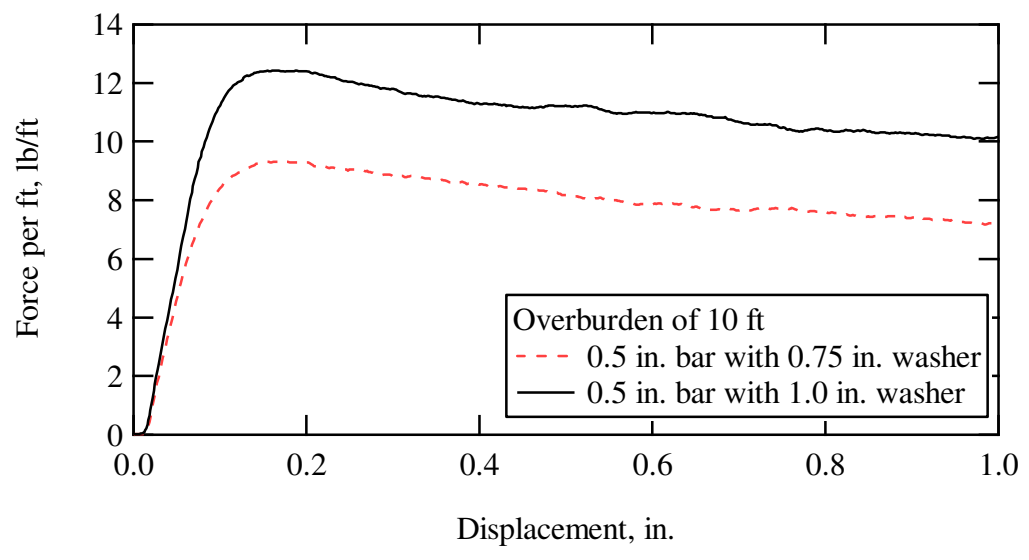
Fig. 4.73. Force-displacement curves for 0.5 in. bars with 0.75 in. and 1.0 in. washers at 10 ft of overburden
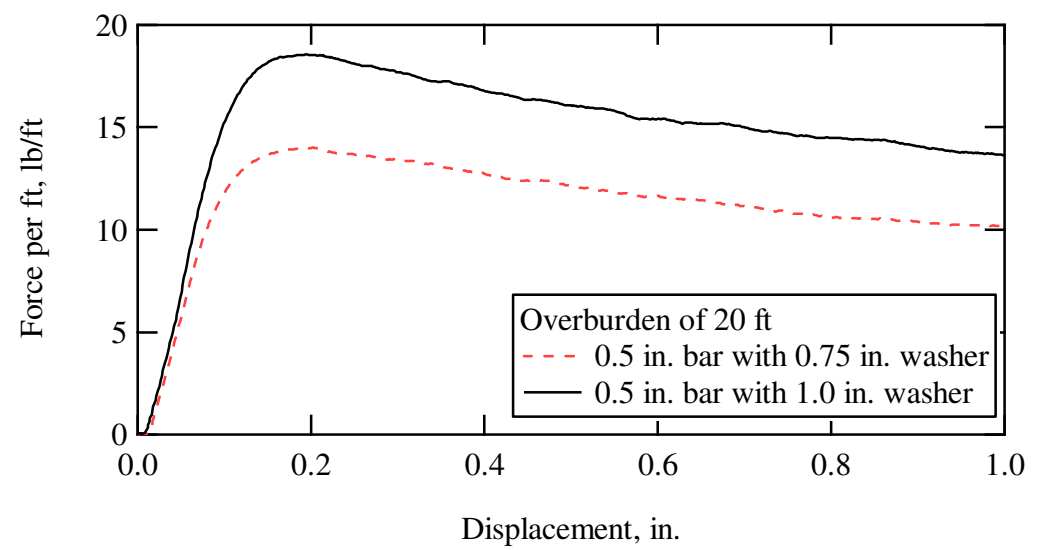
Fig. 4.74. Force-displacement curves for 0.5 in. bars with 0.75 in. and 1.0 in. washers at 20 ft of overburden
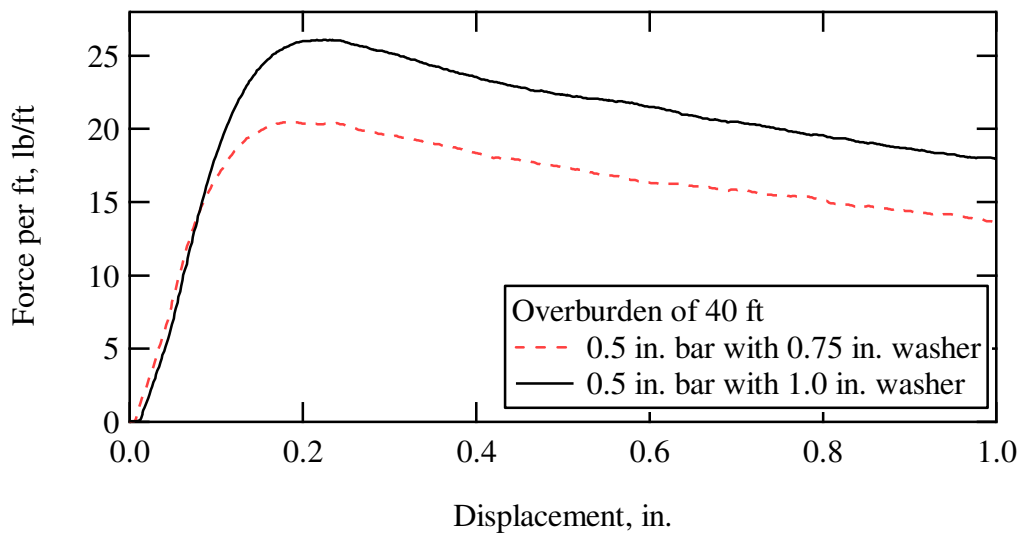
Fig. 4.75. Force-displacement curves for 0.5 in. bar with 0.75 in. and 1.0 in. washers at 40 ft of overburden
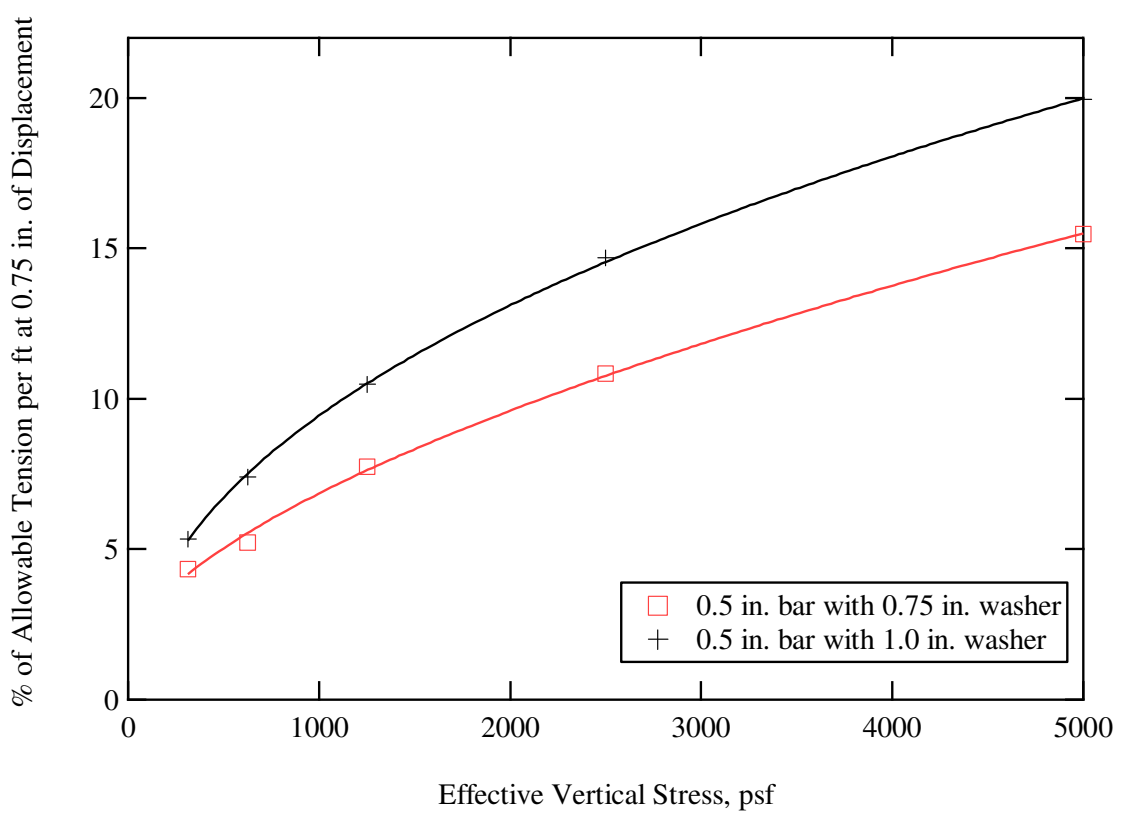
Fig. 4.76. % of allowable tension at 0.75 in. of displacement for 0.5 in. bar with 0.75 and 1.0 in. washers

4.4.3 RECO Strap

The RECO Strap is a ribbed steel strip. We used a strap with dimensions of 50 mm by 4 mm. Figure 4.77 shows the RECO Strap. We performed overburdens of 2.5 ft, 5 ft, 10 ft, 20 ft, and 40 ft on both bars. For the test we pulled the bar approximately 1.0 in. in displacement then applied the next higher overburden pressure until we reached the final overburden of 40 ft.

The results of the test are shown thru Figures 4.78 to Figure 4.89. Pullout resistance per ft was plotted versus displacement. For these values, the pullout resistance per ft was calculated by taking the force values and dividing it by the depth of embedment.

The equation for the various bars for % of Allowable Tension and Pullout Resistance are shown in Table 4.9 and Table 4.10. The variable x is the vertical stress desired. Table 4.11 and Table 4.12 show the values and ranking of the bars.

Fig.4.77. The RECO Strap bar
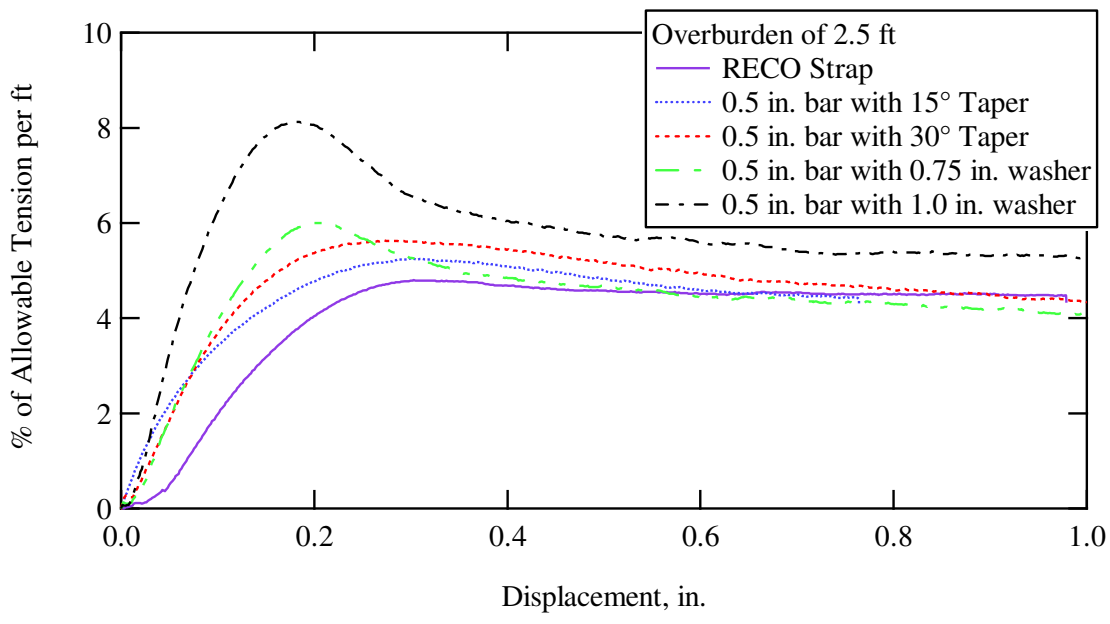
Fig. 4.78. % of allowable tension-displacement curves for all bars at 2.5 ft of overburden
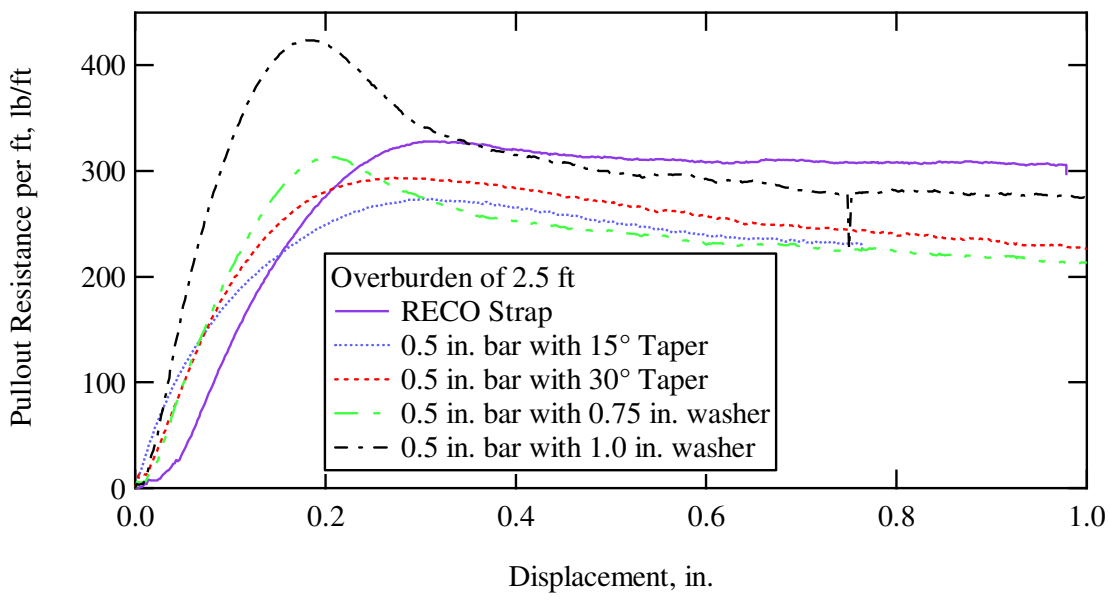
Fig. 4.79. Force-displacement curves for all bars at 2.5 ft of overburden
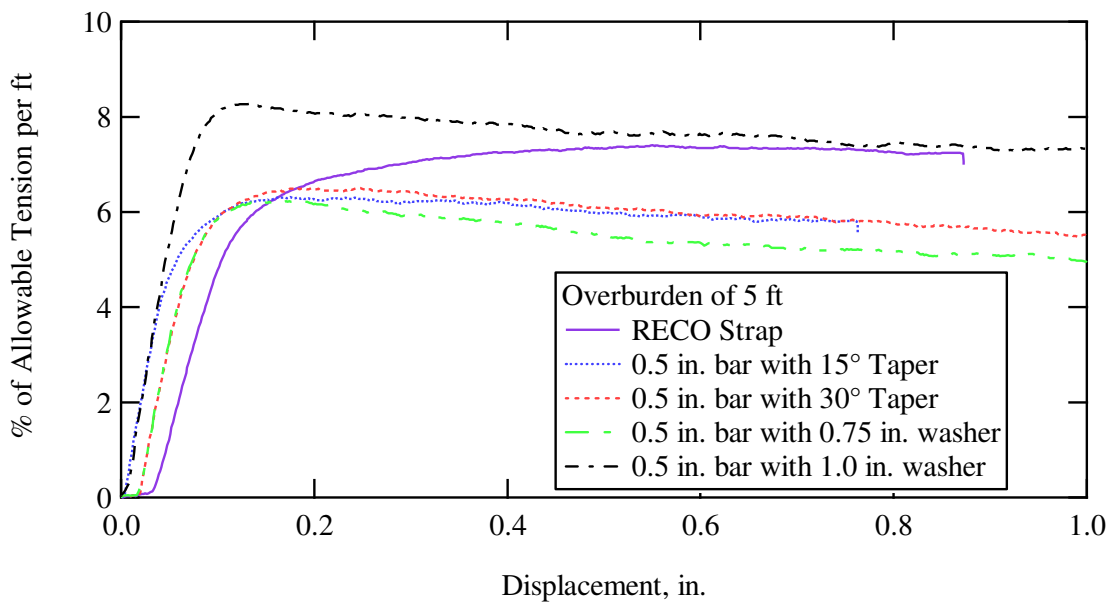
Fig. 4.80. % of allowable tension-displacement curves for all bars at 5 ft of overburden
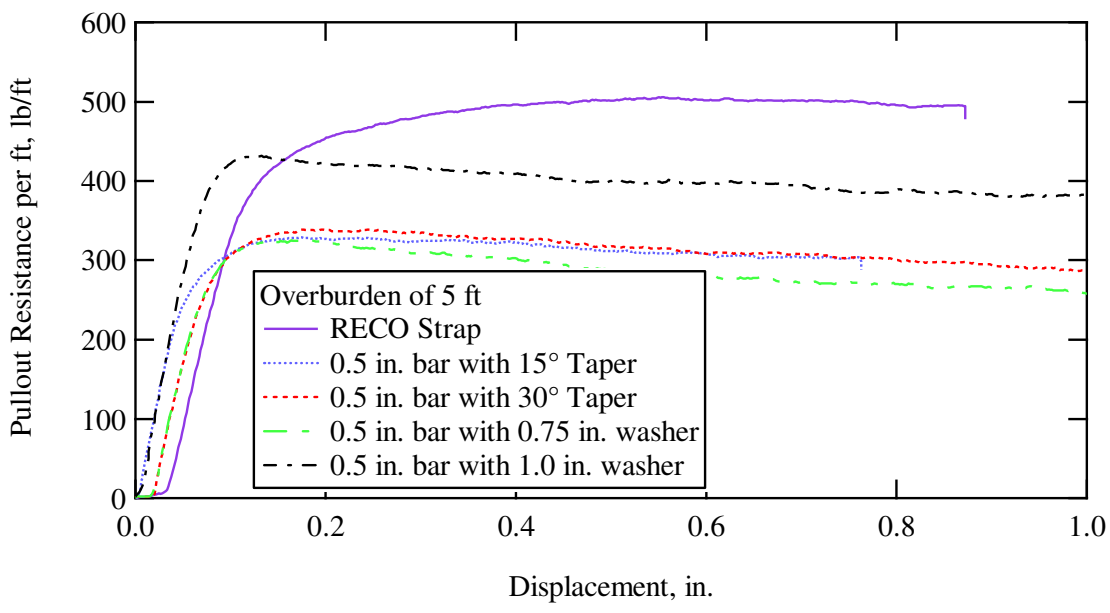
Fig. 4.81. Force-displacement curves for all bars at 5 ft of overburden
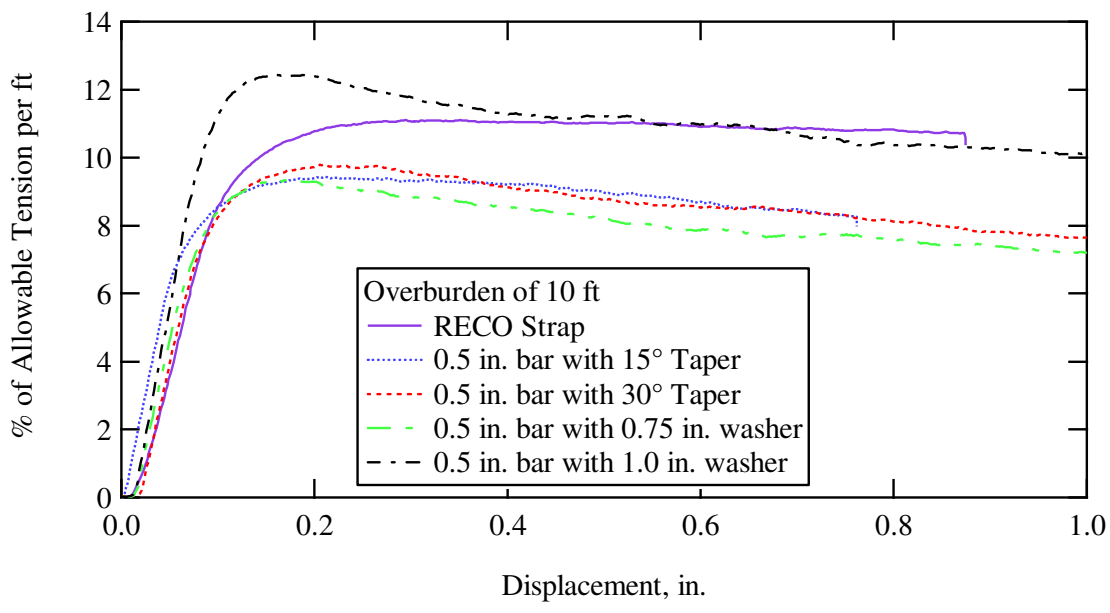
Fig. 4.82. % of allowable tension-displacement curves for all bars at 10 ft of overburden
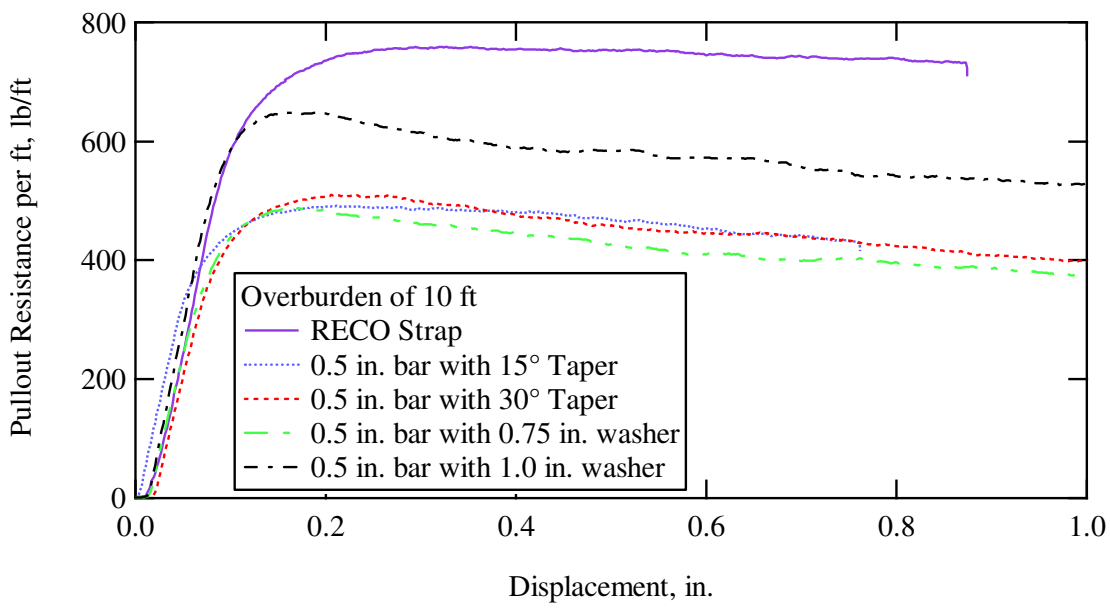
Fig. 4.83. Force-displacement curves for all bars at 10 ft of overburden
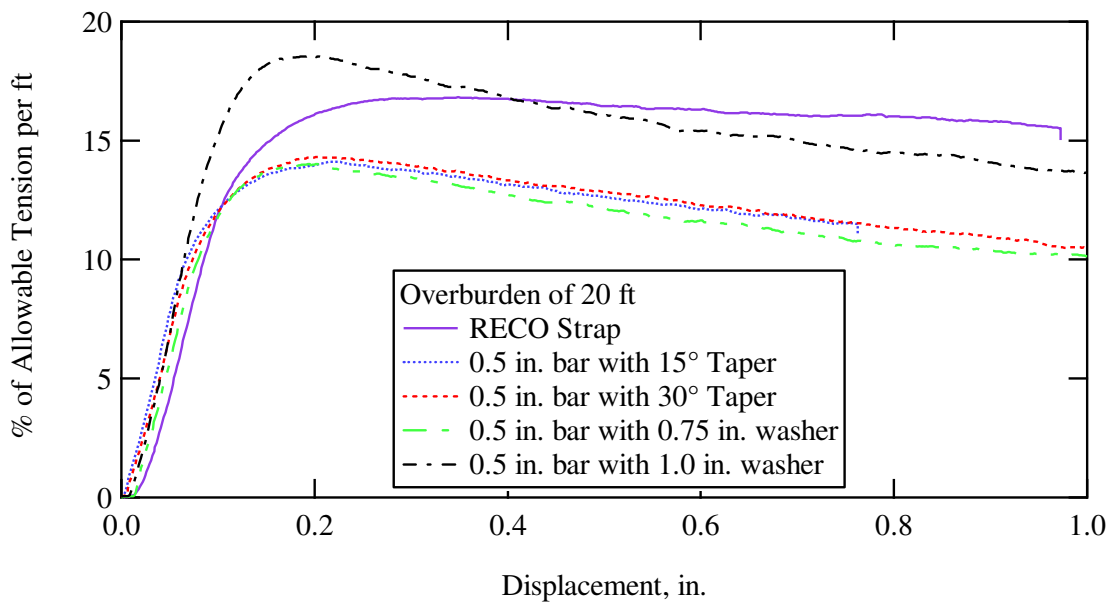
Fig. 4.84. % of allowable tension-displacement curves for all bars at 20 ft of overburden
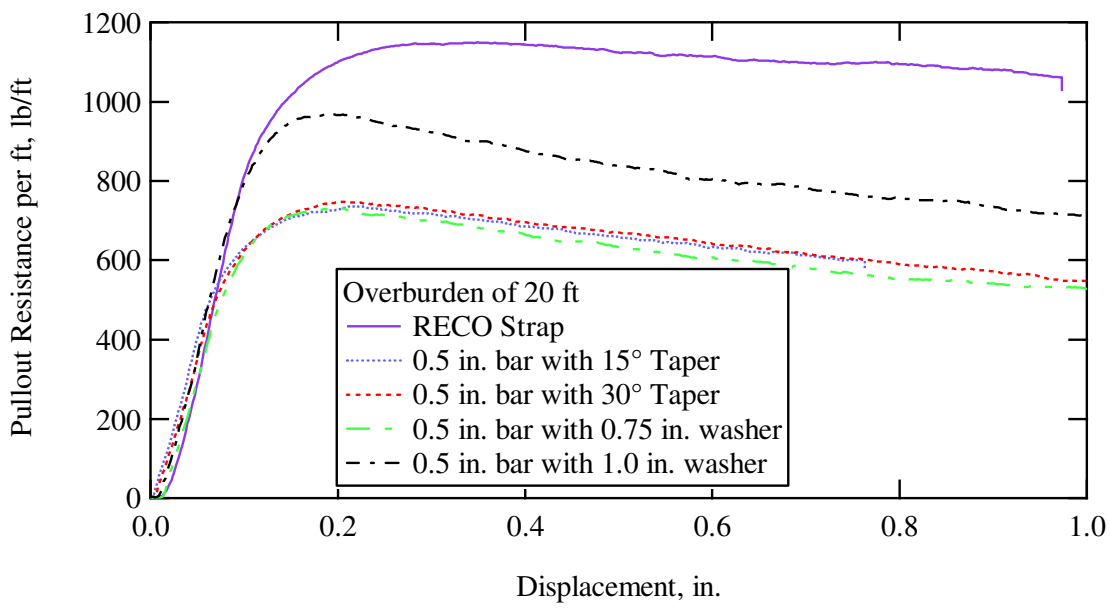
Fig. 4.85. Force-displacement curves for all bars at 20 ft of overburden
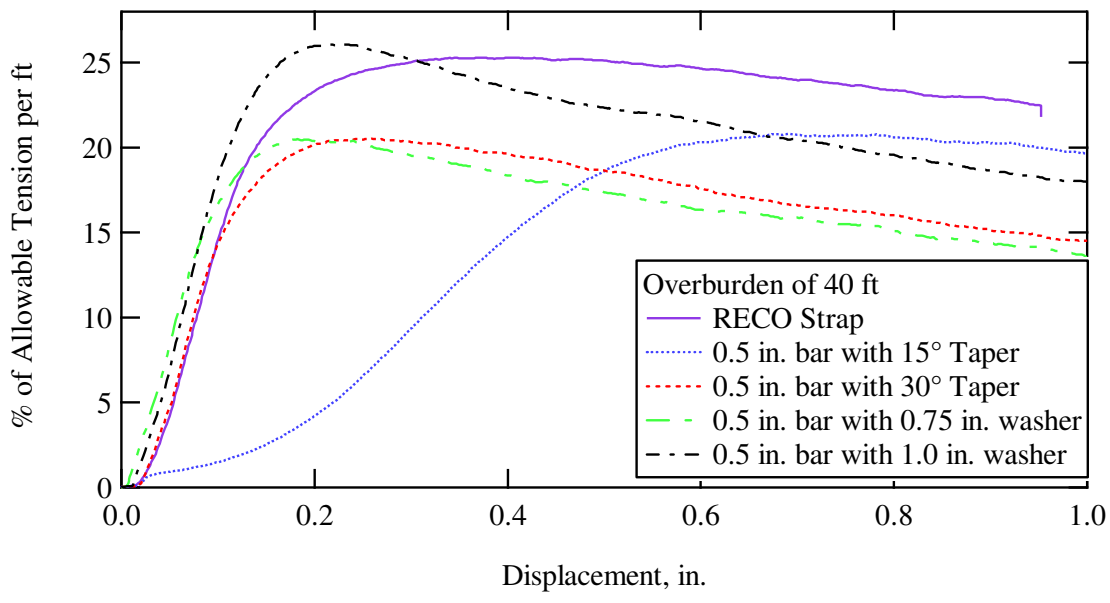
Fig. 4.86. % of allowable tension-displacement curves for all bars at 40 ft of overburden
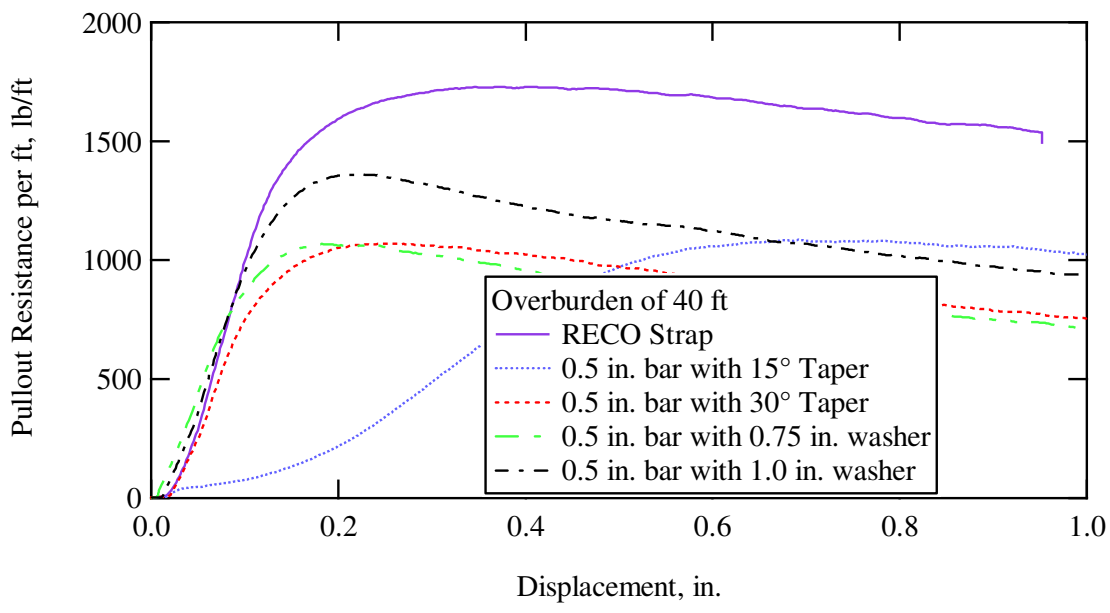
Fig. 4.87. Force-displacement curves for all bars at 40 ft of overburden
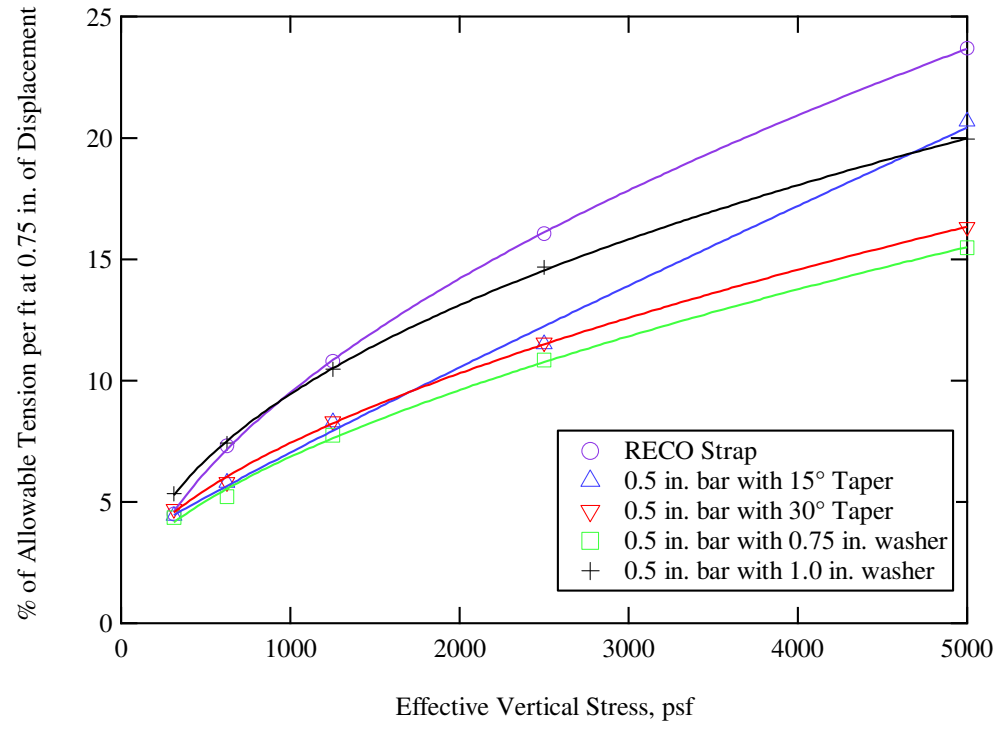
Fig. 4.88. % of allowable tension at 0.75 in. of displacement for all bars
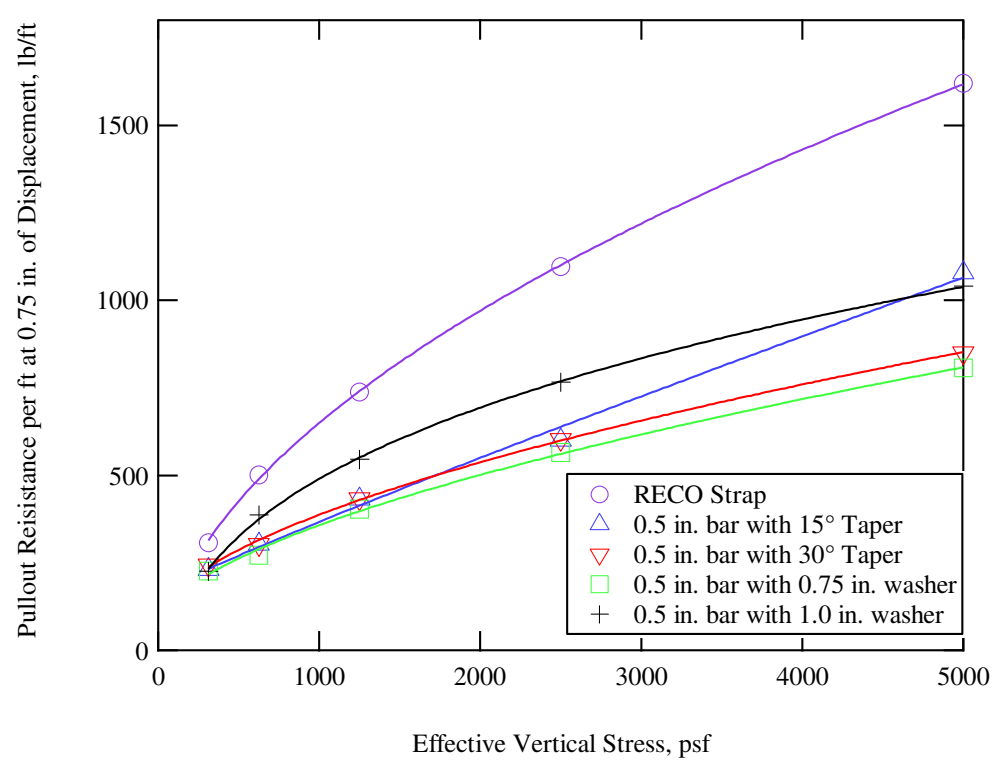
Fig. 4.89. Pullout tensions at 0.75 in. of displacement for all bars

Table 4.9. % of Allowable Tension General Equations for Various Bars

% of Allowable Tension General Equation: $$\text{\% of Allowable Tension at 0.75 in. displacement} = Y_0 + Ax^{\text{Power}}$$	
$= Y_0 + Ax^{\text{Power}}$	Type of Bar
$= -1.3028 + 0.29696x^{0.52035}$	RECO Strap
$= 3.1302 + 0.0065641x^{0.92478}$	15° Taper
$= 1.5482 + 0.11221x^{0.57314}$	30° Taper
$= 1.4538 + 0.089205x^{0.59403}$	0.75 in. washer
$= -1.111 + 0.53882x^{0.43061}$	1.0 in. washer

Table 4.10. Pullout Resistance General Equations for Various Bars

Pullout Resistance General Equation: Pullout Resistance at 0.75 in. displacement = $Y_0 + Ax^{Power}$	
$= Y_0 + Ax^{Power}$	Type of Bar
$= -89.028 + 20.293x^{0.52035}$	RECO strap
$= 163.24 + 0.34231x^{0.92478}$	15° Taper
$= 80.737 + 5.8515x^{0.57314}$	30° Taper
$= 75.814 + 4.652x^{0.59403}$	0.75 in. washer
$= -369.49 + 103.3x^{0.30669}$	1.0 in. washer

Table 4.11. % of Allowable Tension at 0.75 in. of Displacement (%, rank)

% of Allowable Tension at 0.75 in. of displacement, (%, rank)					
Overburden depth, ft	RECO Strap	15° Taper	30° Taper	0.75 in. welded washer	1.0 in. welded washer
2.5	4.51, 3rd	4.43, 4th	4.69, 2nd	4.34, 5th	5.35, 1st
5.0	7.32, 2nd	5.81, 3rd	5.81, 3rd	5.22, 5th	7.41, 1st
10.0	10.80, 1st	8.28, 4th	8.30, 3rd	7.74, 5th	10.48, 2nd
20.0	16.05, 1st	11.51, 4th	11.55, 3rd	10.84, 5th	14.69, 2nd
40.0	23.70, 1st	20.69, 2nd	16.31, 4th	15.48, 5th	19.96, 3rd

Table 4.12. Pullout Resistance at 0.75 in. of Displacement (lb, rank)

Pullout Resistance at 0.75 in. of displacement, (lb, rank)					
Overburden depth, ft	RECO Strap	15° Taper	30° Taper	0.75 in. welded washer	1.0 in. welded washer
2.5	308.0, 1st	230.9, 3rd	244.8, 2nd	226.5, 4th	226.5, 4th
5.0	500.3, 1st	302.9, 4th	303.0, 3rd	272.0, 5th	386.6, 2nd
10.0	737.8, 1st	431.9, 4th	433.0, 3rd	403.6, 5th	546.6, 2nd
20.0	1096.8, 1st	600.4, 4th	602.5, 3rd	565.2, 5th	765.9, 2nd
40.0	1619.3, 1st	1079.0, 2nd	850.6, 4th	807.5, 5th	1041.1, 3rd

4.4.4 Progressive Loading

As the USU MSE wall was built and compacted, the reinforcement experienced increasing overburden pressure and deformation. To simulate this in the lab we performed a "progressive" loading test. This test was conducted on the taper bars, welded washer bars, and RECO strap reinforcements.

The taper bar tests reached 375 lb for the overburden pressure simulating the depth of 2.5 ft and continued to in increments 375 lb for each 2.5 ft load step. The pullout resistance was unable to reach the 3375 lb increment at 22.5 ft depth so the increment was changed 250 lb and the test was started over. The 15º bar exhibited significantly more deflection than the 30º bar in these tests. For soil to be in an active state the deformation required are between 0.002*H and 0.005*H. An active state condition lessens the loads of the reinforcement. A 20 ft wall requires a range from 0.48 in. to 1.2 in. of deformation. The results of these tests are shown in Figure 4.90 and Figure 4.91. Our results show that we are much lower than the required deformations. Figure 4.91 shows that the taper bars did not reach the required range to go to an active state.

For the welded washer bars, the load to reached 250 lb for the pressure simulating the depth of 2.5 ft and continued to increase 250 lb for each 2.5 ft increment load step to 40 ft. Because of some errors in the lab with the air pressure, the 1.0 in. welded washer bar experienced a higher overburden pressure before the tests were run. The pressure was released and the correct pressure was then applied for the tests.

The progressive loading for the RECO strap started at a 390 lb load for the pressure simulating a 2.5 ft depth and continued to increases to 390 lbs for each 2.5 ft increment load step to 40 ft. Figure 4.93 compare the 15º and 30º tapers, the 0.75 in. and 1.0 in.

welded washer, and the RECO strap. The graphs compare the reinforcement in two

ways. One is called % of Allowable Tension per ft. For these graphs we calculated the

area of the RECO strap and the 0.5 in. diameter bars after 75 years of corrosion. It is

shown in Equation 4.1.

$$T_{allowable} = \sigma_{allowable} * Area_{75\ years} \qquad (4.1)$$

where $T_{allowable}$ is the allowable tension plotted on the graphs, $\sigma_{allowable}$ is 32.5 ksi, and

$Area_{75\ years}$ is the area after 75 years design life. The % of $T_{allowable}$ per ft is calculated

by the force per length of embedded bar, which is then divided by the $T_{allowable}$ value.

For these plots we credited all steel reinforcement with 15 years protection due to zinc

coating. The loss per year was 0.00047 in./yr.
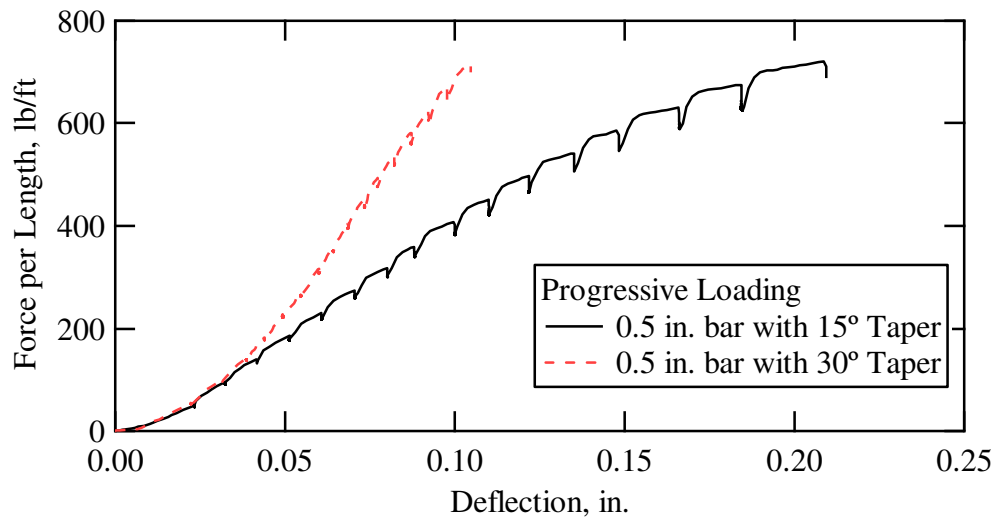
Fig. 4.90. Force-displacement curves for 0.5 in. 15º and 30º taper bars at progressive
loading
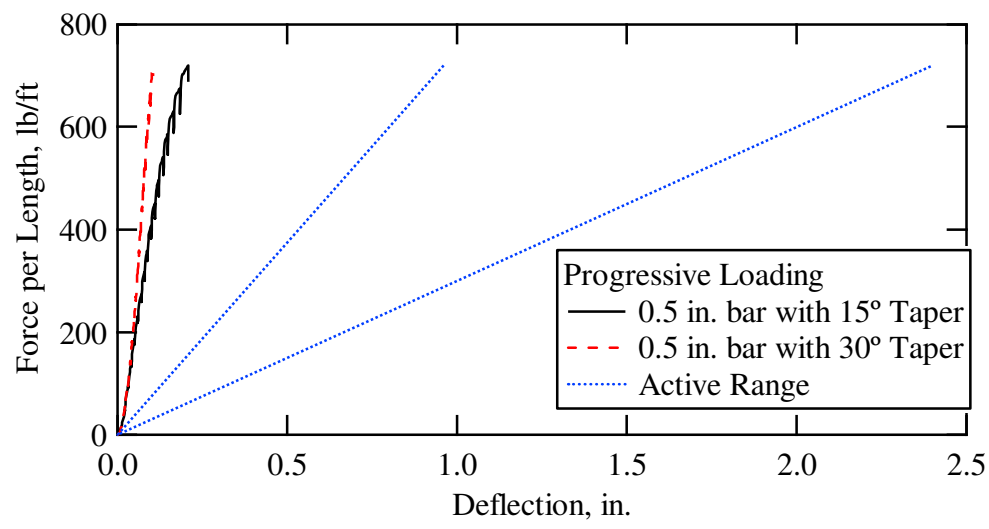
Fig. 4.91. Force-displacement curves for 0.5 in. 15° and 30° taper bars at progressive loading showing active range
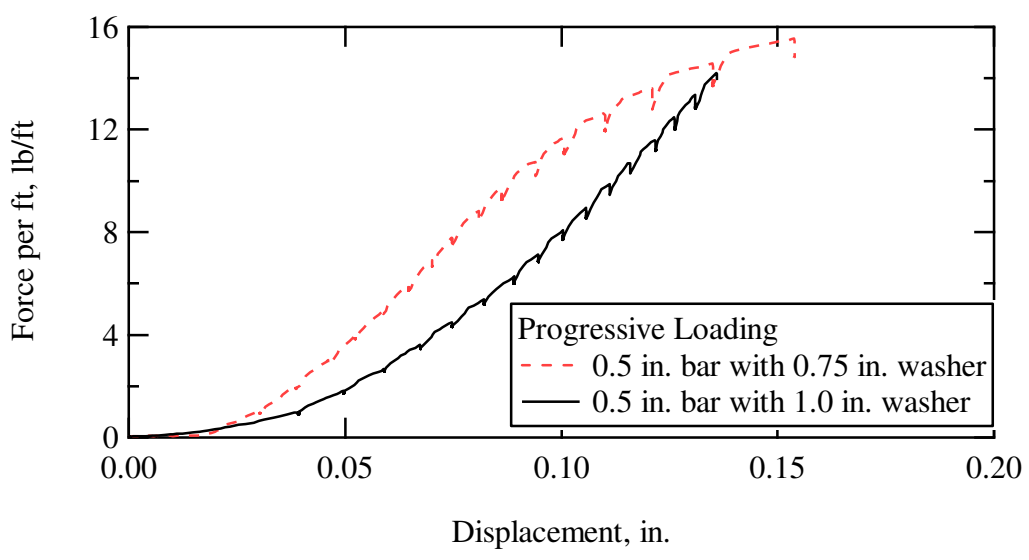
Fig. 4.92. Force-displacement curves for 0.5 in. bar with 0.75 in. and 1.0 in. washers at progressive loading
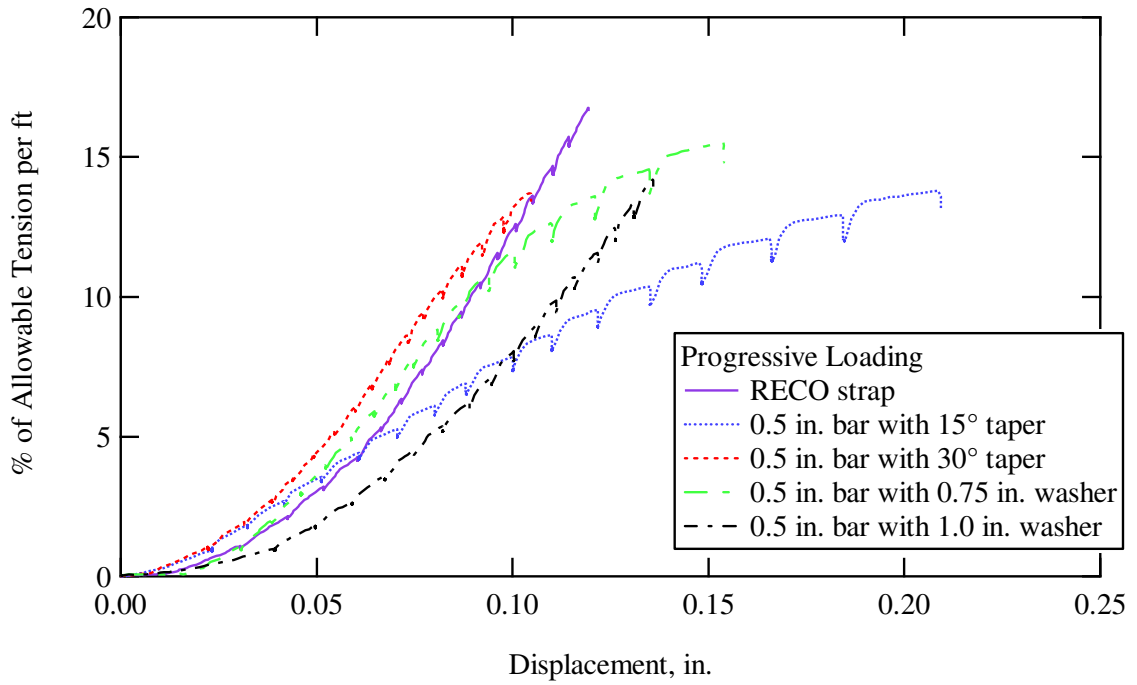
Fig. 4.93. Force-displacement curves for all bars at progressive loading

CHAPTER 5

CONNECTION CAPACITY

Concrete connections were sent to the lab to test the strength and verify the design load on the connections. For this part of the test we had two connections called a choker hook and metal bracket, shown in Fig. 5.104. The choker hook was colored red, smaller, and could be rotated around the metal ring in the cement block. The metal bracket in the cement block was rigid and unable to rotate.

We ran three tests for each connection. The first test was to pull the bars connected to the concrete slab to a tensile load approximately 6.1 kips and then returning the load to zero. The design strength is 6.1 kips. The second test was to pull the bars connected to the concrete slab tensile loading to approximately 10 kips and then returning the load to zero. This was done since our load sensor was rated to a capacity of 10 kips. Thus third test was to pull the bars connected to the concrete slab to failure in the Tenuis and Olsen machine shown in Figure 5.100. The results for the first two tests for both connections are shown in Figure 5.104. Cracking occurred in the concrete slab during the second test, which is shown in Figure 5.99.

For the final test, we connected the metal bracket connection into the Tenius and Olsen machine. The choker hook connection reached approximately 15.1 kips at failure. Failure was occurring both in the bar and in the concrete, but the bar broke first. The metal bracket reached approximately 16.4 kips before failing. This failure was also in the bar. Figure 5.105 and Figure 5.106 show the bar failures. From these test we can conclude that the concrete connections were adequate since they had greater strength than

their design. The concrete connections and bars after the final loading are shown in

Figures 5.101 to 5.103.
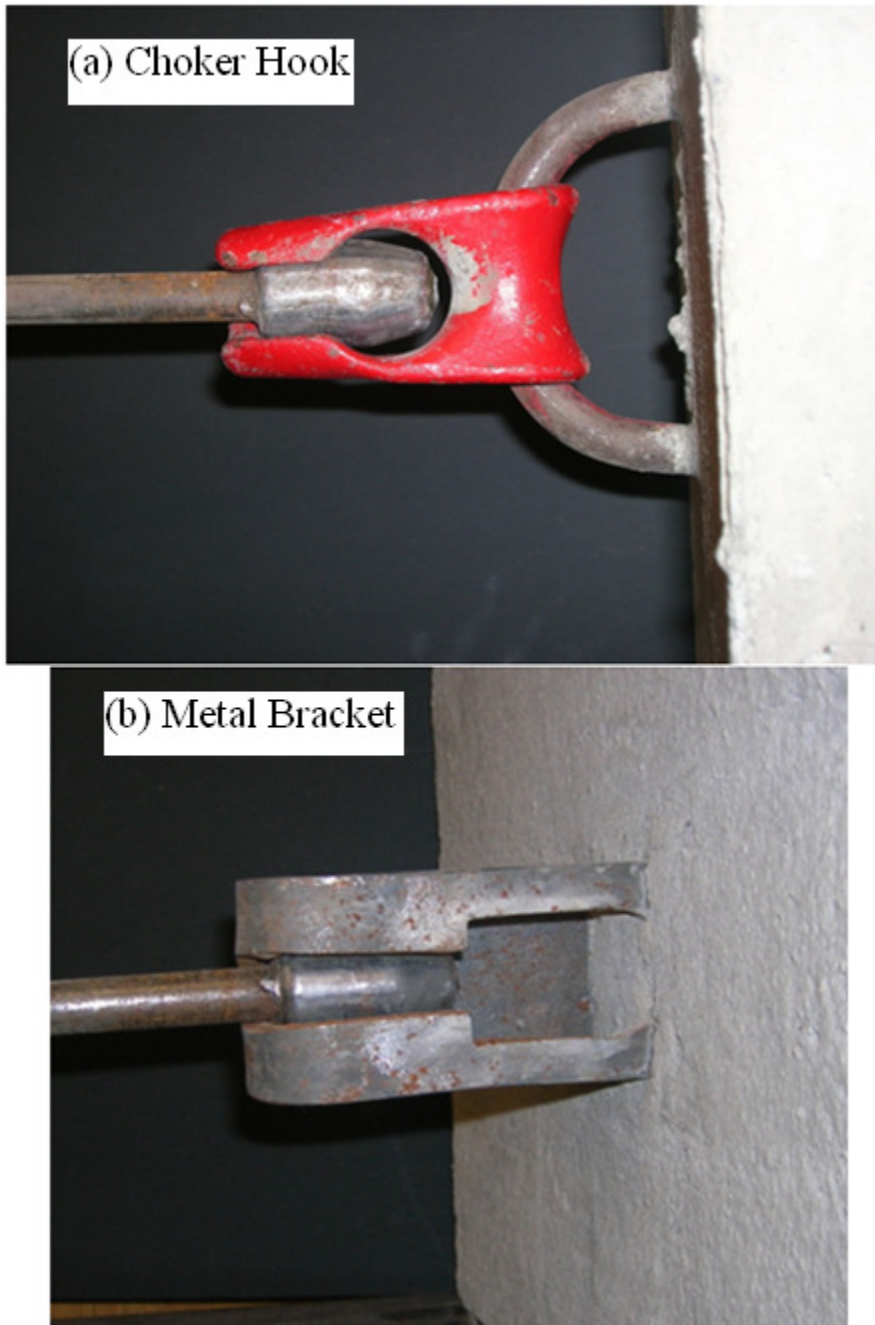
Fig. 5.94. Choker Hook (a) and Metal Braket (b) connections
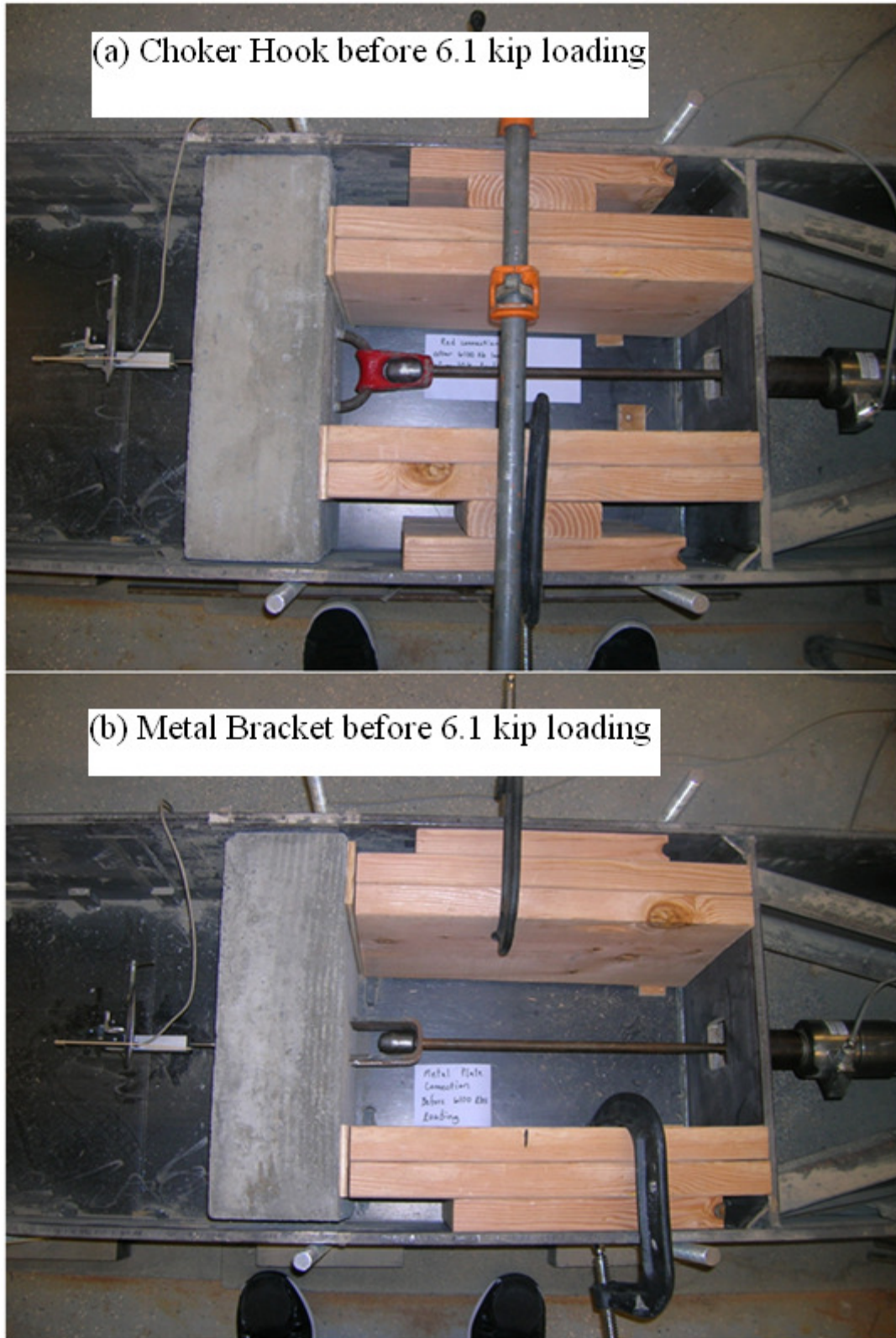
Fig. 5.95. Choker Hook (a) and Metal Braket (b) connections before 6.1 kip loading

Fig. 5.96. Choker Hook (a) and Metal Bracket (b) connections before 6.1 kip loading

Fig. 5.97. Choker Hook (a) and Metal Bracket (b) connections after 6.1 kip loading and before 10 kip loading

Fig. 5.98. Choker Hook (a) and Metal Bracket (b) connections after 10 kips loading

Fig. 5.99. Minor cracking occurring in the metal bracket connection
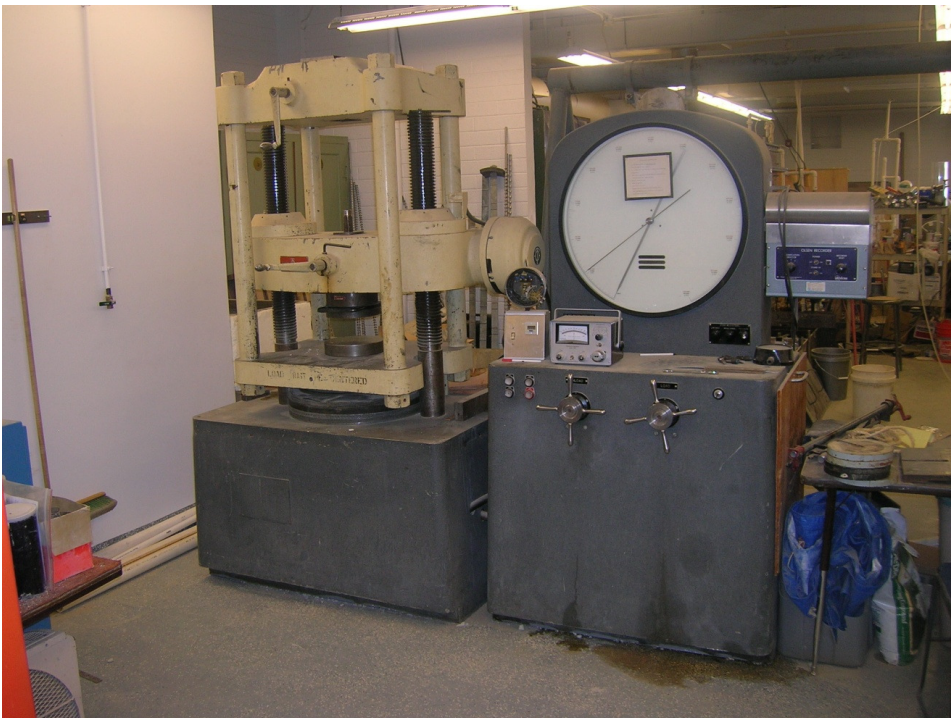
Fig. 5.100. The Tenius and Olsen machine
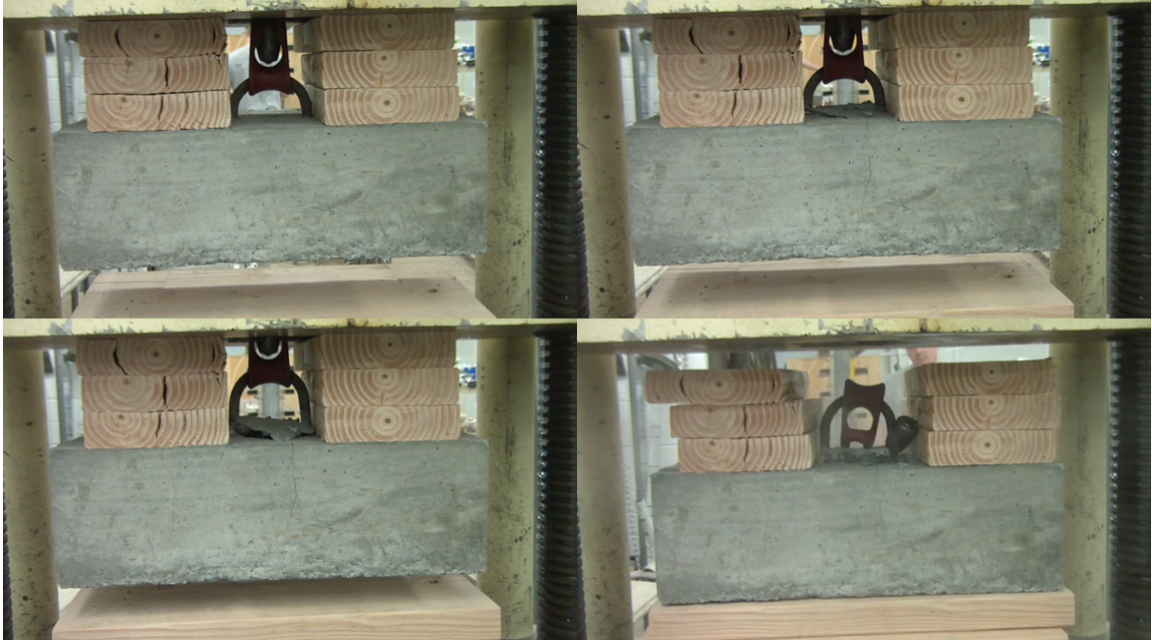
Fig. 5.101. Using Tenius and Olsen machine to pull choker hook connection to failure
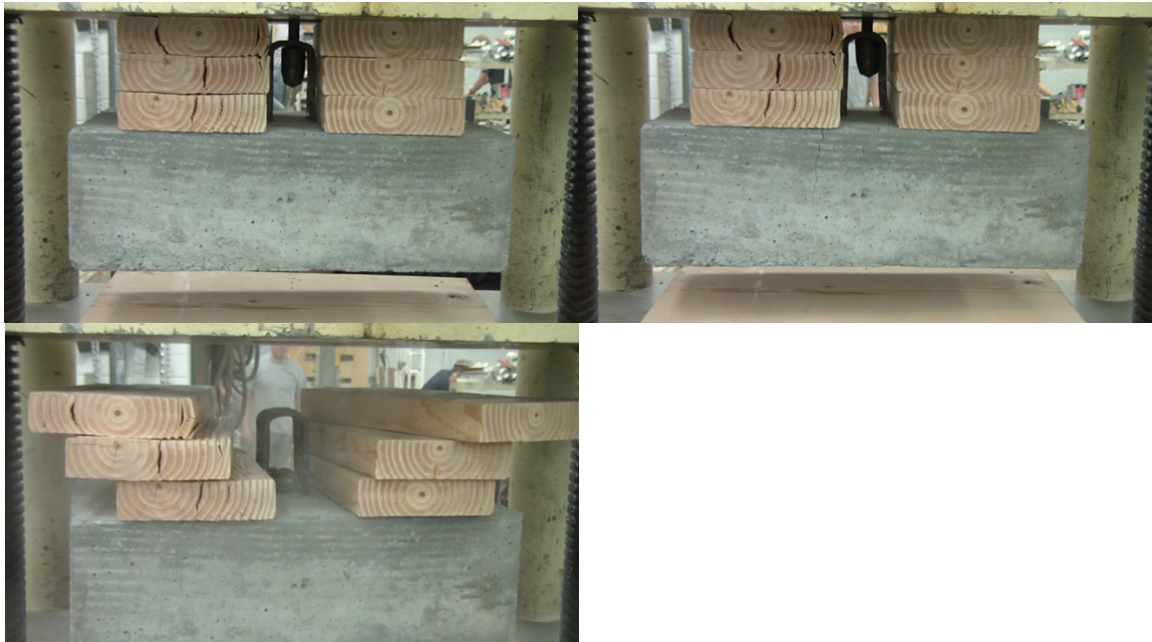
Fig. 5.102. Using Tenius and Olsen machine to pull metal bracket connection to failure

Fig. 5.103. Concrete connections after test using the Tenius and Olsen machine**.**
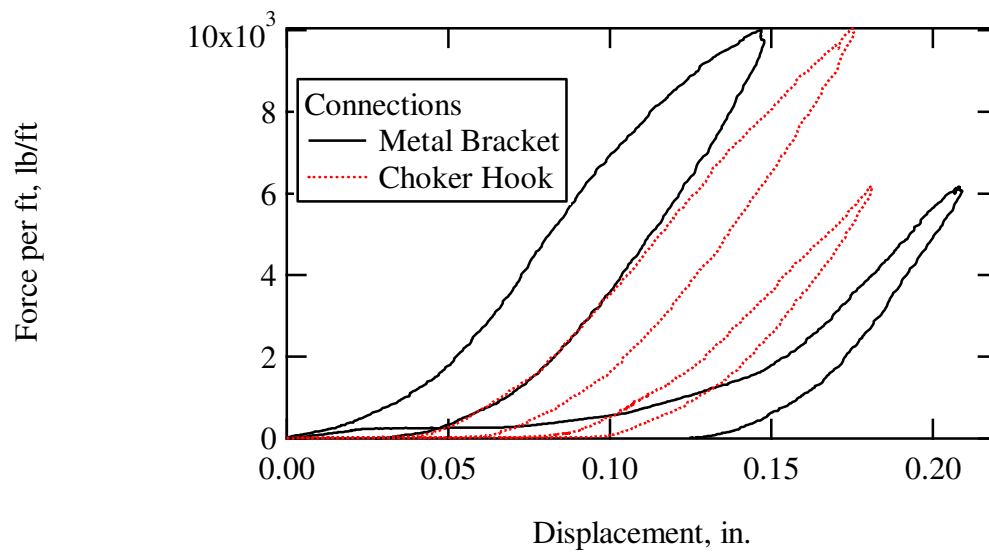
Fig. 5.104. Metal Bracket and Choker Hook Force-displacement curves

Fig. 5.105. Metal Bracket connection failure at 16.4 kips

Fig. 5.106. Red Choker Hook connection failure at 15.1 kips

CHAPTER 6

GALVANIZED CRIMPS

The purpose of galvanization metal is to prevent the corrosion of metal. This process involves applying a zinc coating to metal. Our purpose for testing the crimps was to get stiffness measurements using our pullout box and also to monitor the galvanization coating after the pullout tests.

We had three different sizes of galvanized crimps. Each crimp bar had a diameter of 0.5 in. The different sizes of crimps include a 2, 2.5, and 3 in. crimp shown in Figures 6.107 thru Figure 6.114. The crimps were loaded to their design capacity of 6.1 kips (6100 lbs) in the pullout box, shown in Figure 6.115.

The results of the pullout and stiffness tests are shown in Figures 6.107 and 6.108, respectively. Both the 3.0 in. and 2.5 in. crimp straightened when loaded to their design strength of 6.1 kips. They did not experience any cracking of their galvanization coating. Thus, the 3.0 in. and 2.5 in. crimps will perform well to their design strength and maintaining the integrity of the galvanization shown in Figure 6.116. However, the 2.0 in. crimp experienced some cracking which can be seen in Figure 6.117. The 2.0 in. crimp will not perform well to its design strength while maintaining the galvanization coating.
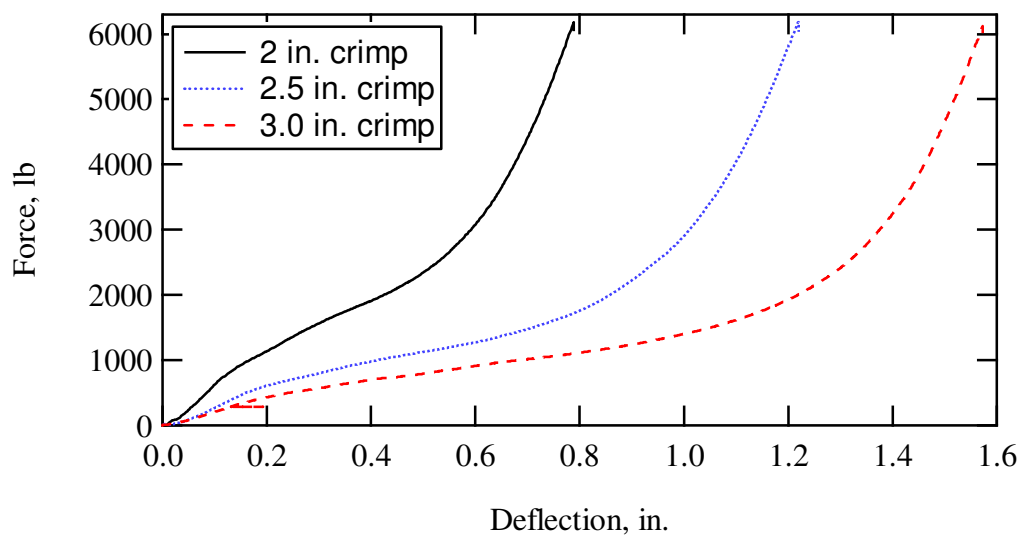
Fig. 6.107. Force versus deflection curves for the 2, 2.5, and 3 in. galvanized crimp
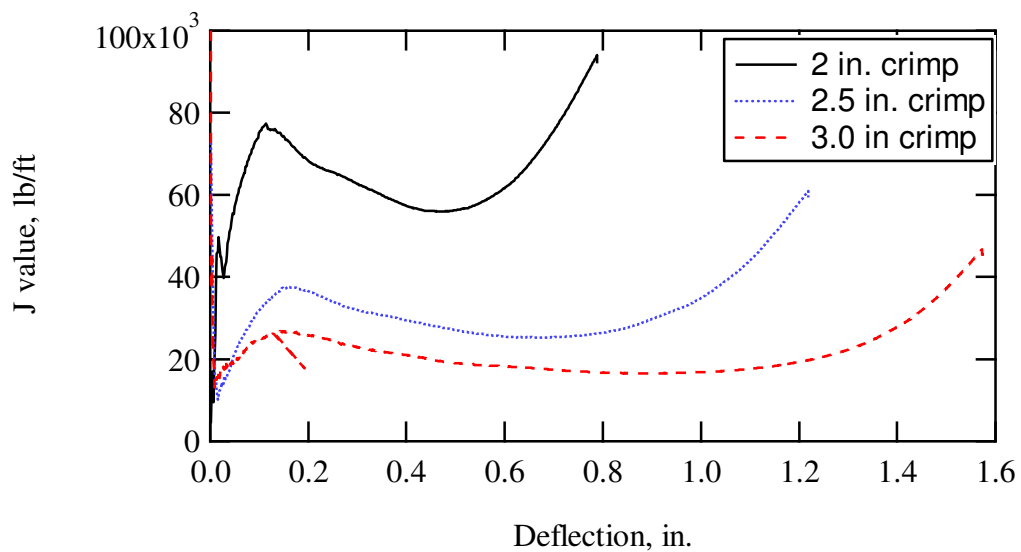
Fig. 6.108. J values versus deflection for the 2, 2.5, and 3 in. galvanized crimp
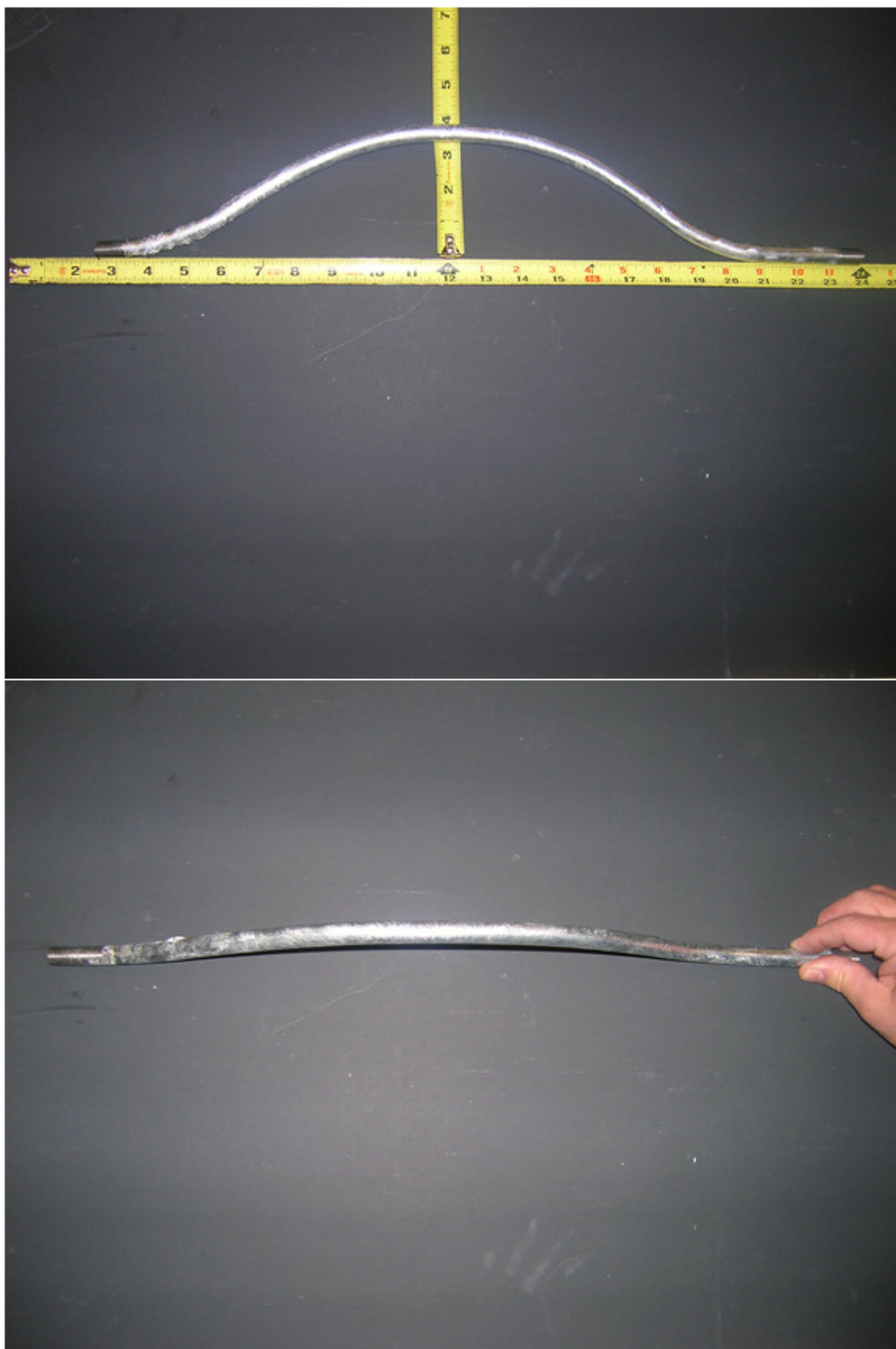
Fig. 6.109. 3.0 in. galvanized crimp
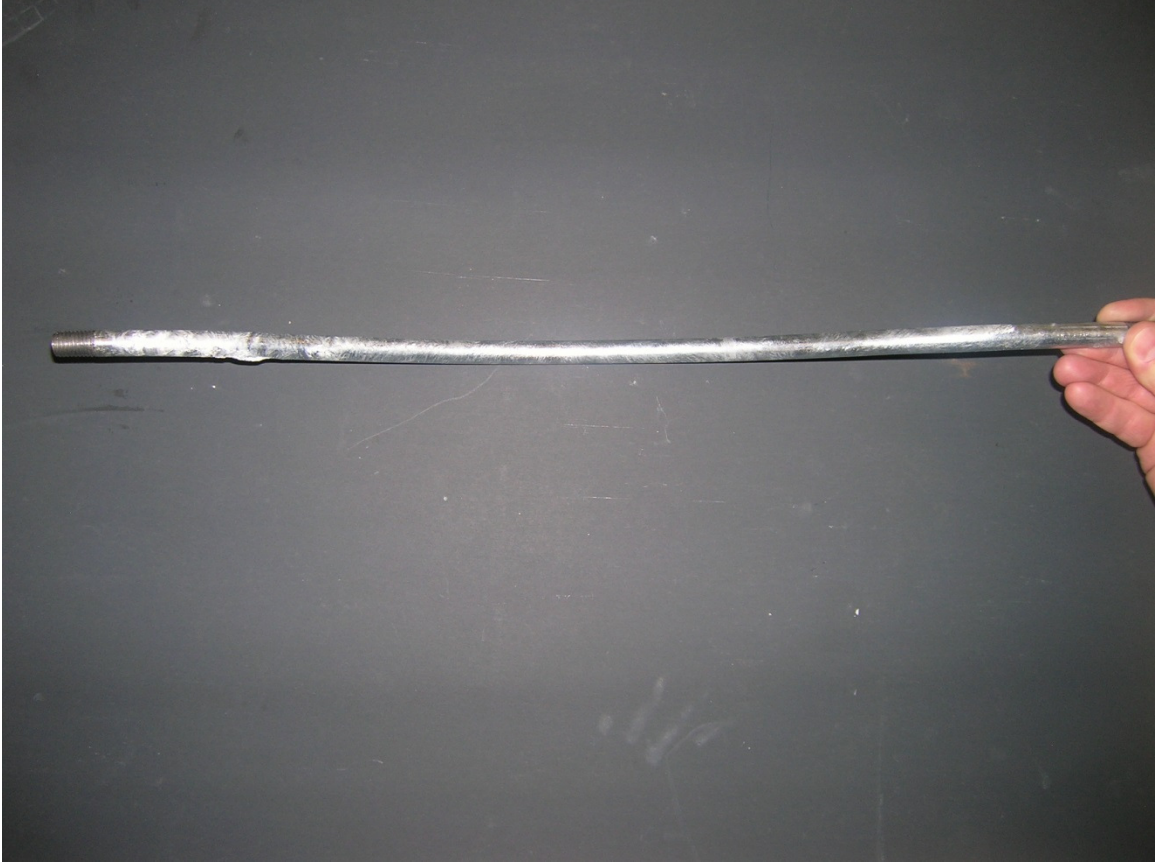
Fig. 6.110. 3.0 in. galvanized crimp
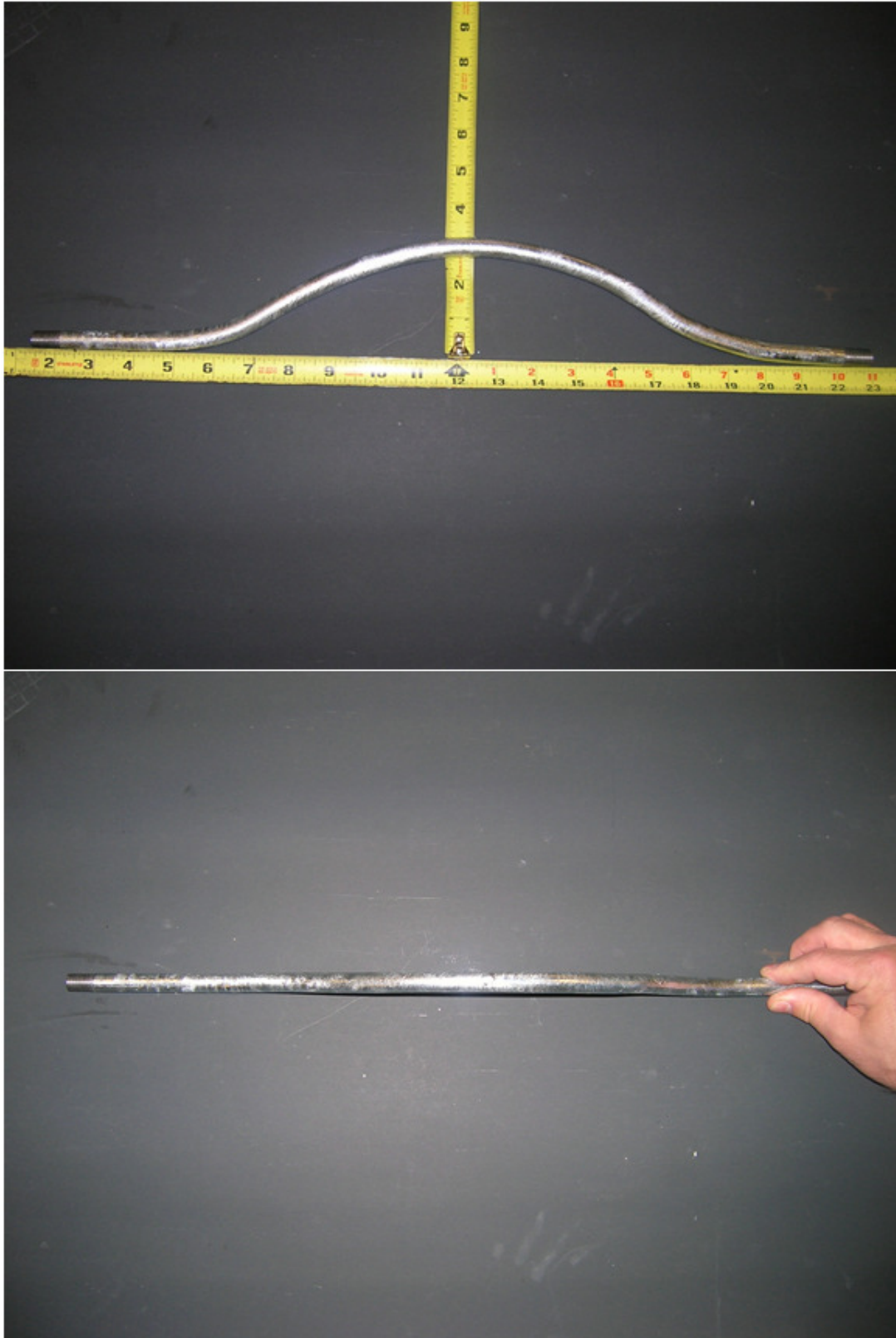
Fig. 6.111. 2.5 in. galvanized crimp

Fig. 6.112. 2.5 in. galvanized crimp
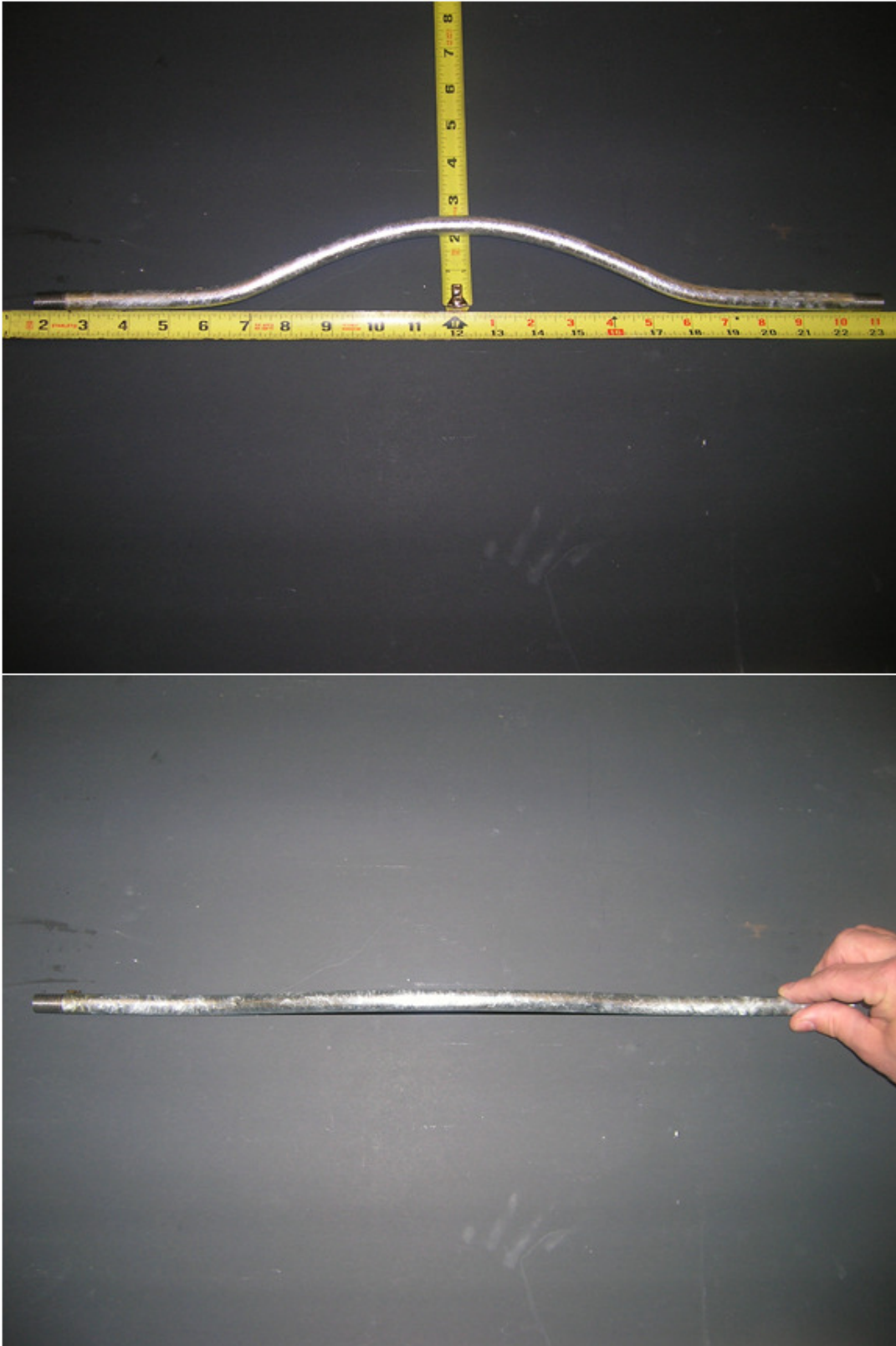
Fig. 6.113. 2.0 in. galvanized crimp

Fig. 6.114. 2.0 in. galvanized crimp
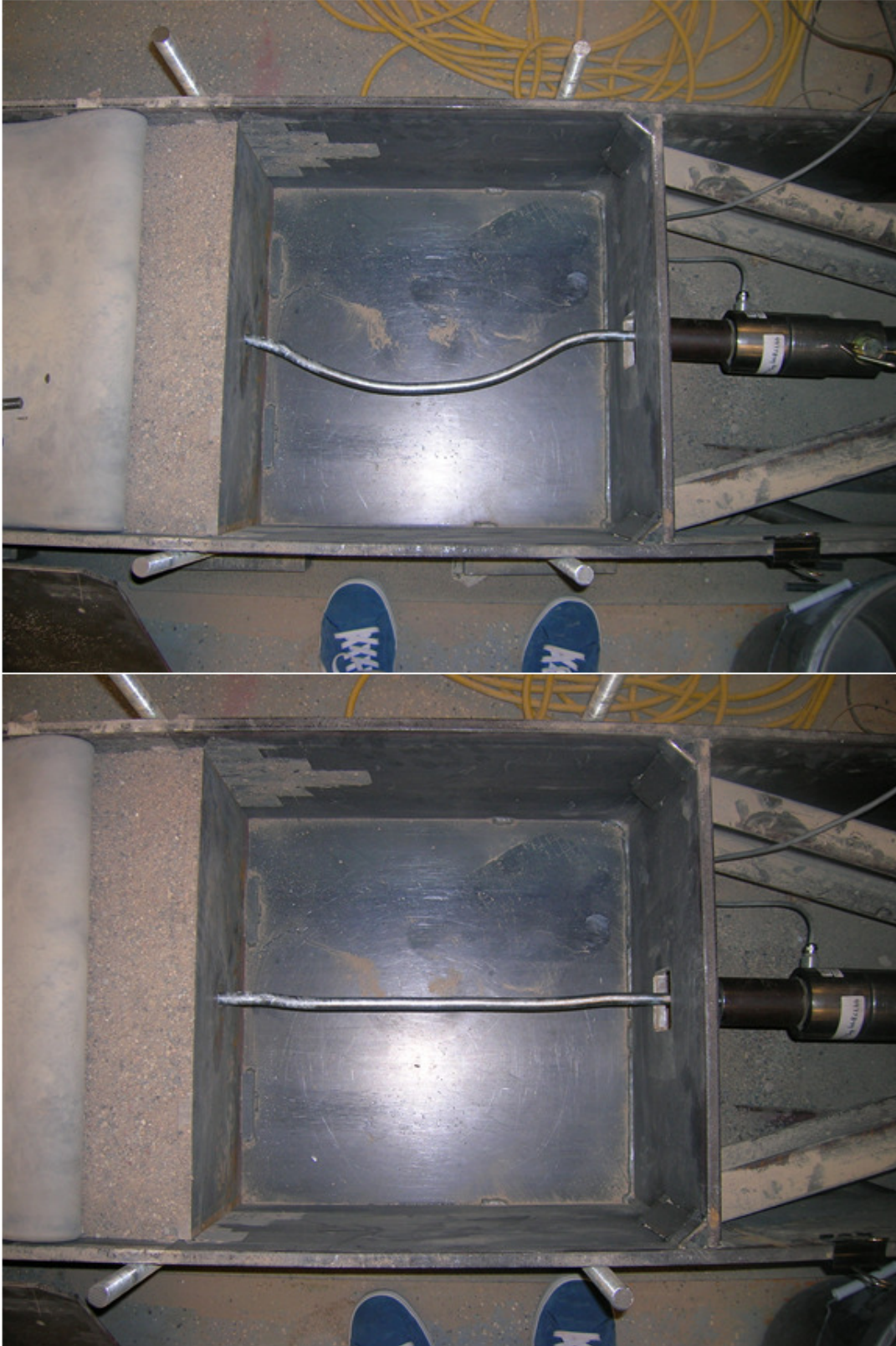
Fig. 6.115. 3.0 in. galvanized crimp before and after pullout test
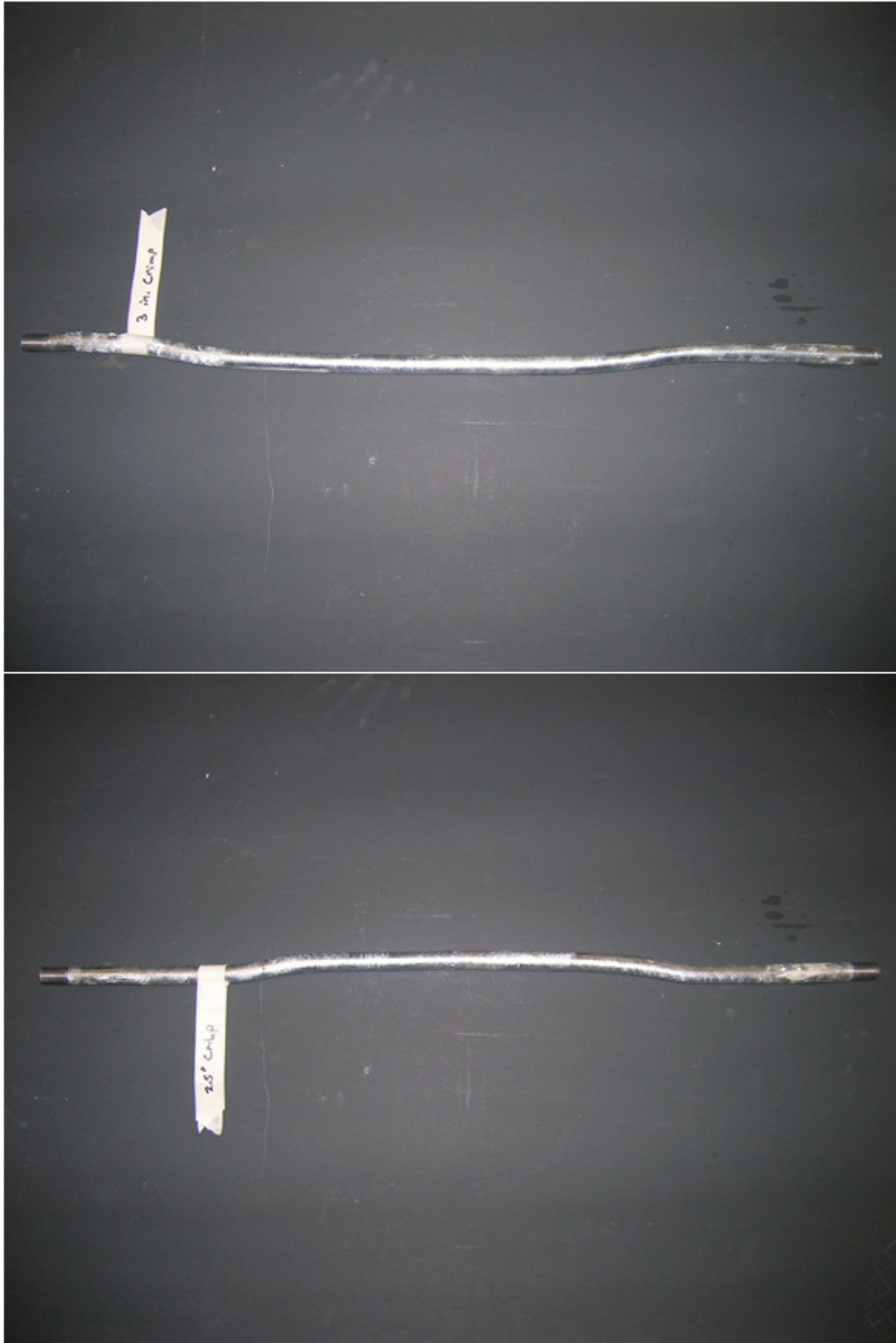
Fig. 6.116. 3.0 and 2.5 in. galvanized crimps straightened after pullout test
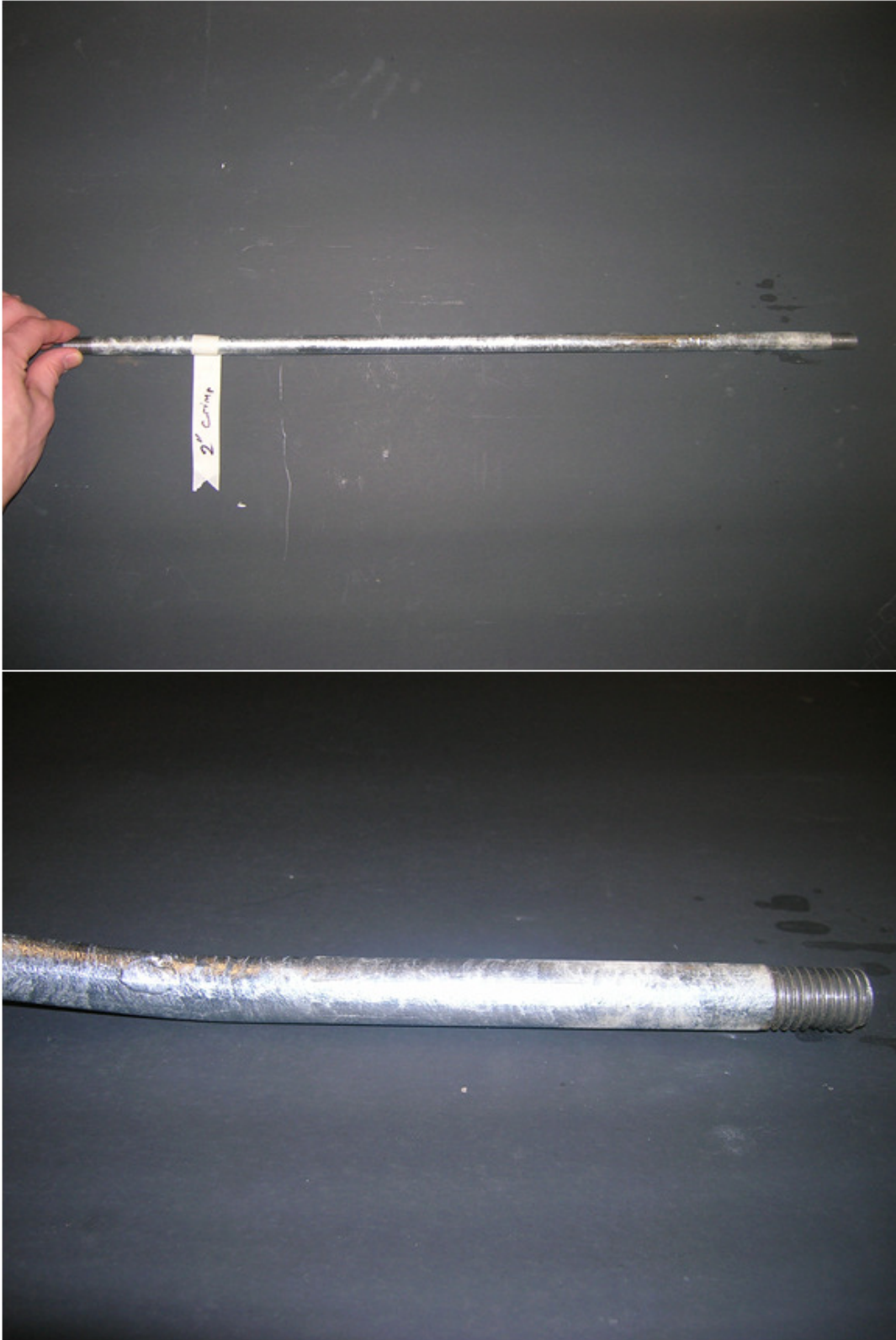
Fig. 6.117. Cracking of galvanization coating in 2.0 in. crimp

CHAPTER 7

SUMMARY, CONCLUSIONS, AND RECCOMMENDATIONS

In this research, we exhumed the crimps from the USU MSE wall. Digging with an

excavator and our shovel often caused damage. A water hose aided in extracting the

crimps and there were no damaged crimps following this process. We measured

deflections of crimps that were in the USU MSE prototype wall. We did lab

measurements on the stiffness of the crimps. From the measured deflections and the lab

measurement tests we predicted the stiffness in the USU MSE wall. The predicted K-

Stiffness value was $\frac{S_{global}}{Pa} = 12.73$.

We performed pullout tests on the crimps to assist in the prediction of the stiffness of

the wall. We also performed pullout test on metal reinforcement including 0.5 in.

diameter bars having a cross bar length of 8, 4, 2, 1 in. and no cross bar (smooth bar), 0.5

in. diameter bars having a 15° and 30° taper, 0.5 in. diameter bars have a 0.75 and 1.0 in.

diameter welded washer spaced every inch, and a RECO strap. The pullout resistance for

the cross bars shows the value measured subtracted by the smooth bar pullout resistance.

Thus, it shows only the crossbar itself. The results for the pullout tests are shown.

The results show the longer the cross bar and higher the overburden depth the more

pullout resistance was obtained. However, the 1 in. cross bar was most efficient. The 1

in. welded washer was the best for depths of 2.5 and 5.0 ft for % of Allowable Tension at

0.75 in. of displacement. The RECO Strap performed the best for the 10 ft, 20 ft, and

40ft depths in the % of Allowable Tension at 0.75 in. of displacement. The RECO Strap

performed the best for all depths in Pullout Resistance at 0.75 in. of displacement. The

15º and 30º taper bars and 0.75 in. welded washer had pullout forces that were close. This means that geometry does not matter. The values we obtained from the pullout test on the different bars can be used in MSE designs.

We tested the concrete connection capacity and found that its allowable strength was greater than the design strength. The choker hook connection failed at a load of 15.1 kips. The metal bracket connection failed at a load of 16.4 kips. The design load for both connections were 6.1 kips. They performed well above their design strength.

We performed pullout tests on the 0.5 in. diameter galvanized crimp to obtain stiffness values and monitored the integrity of the galvanization by watching for cracking. We had a 2 in., 2.5 in., and 3 in. crimp on a 0.5 in. diameter galvanized bar to test. The design strength of these bars was 6.1 kips. The shorter height of the crimp, the higher the stiffness obtained. However, the 2 in. crimp had cracking in the galvanization. Thus, it did not perform to its design strength while maintaining the integrity of the galvanization. The 2.5 in. and 3 in. crimps did not have galvanization cracking.

My recommendation is that more pullout tests should be done. In this research, only one soil type is used, which is washed mortar sand. It would be beneficial to continue performing pullout tests on different shapes and geometries of reinforcement and to have more soil types that are commonly used in MSE walls, furthering the understanding of pullout behavior in MSE walls.

Table 7.13. % of Pullout Resistance at 0.75 in. of Displacement (lb)

Pullout Resistance at 0.75 in. of displacement, (lb)					
Overburden depth, ft	Smooth bar	1 in. Cross bar	2 in. Cross bar	4 in. Cross bar	8 in. Cross bar
2.5	15.1	32.8	32.0	49.4	80.1
5.0	17.6	52.7	58.2	82.3	154.6
10.0	30.3	71.1	83.4	120.6	278.1
20.0	51.6	155.4	124.2	196.8	482.8
40.0	107.3	150.2	191.7	336.9	683.8

Table 7.14. % of Allowable Tension at 0.75 in. of Displacement (%, rank)

% of Allowable Tension at 0.75 in. of displacement, (%, rank)					
Overburden depth, ft	RECO Strap	15° Taper	30° Taper	0.75 in. welded washer	1.0 in. welded washer
2.5	4.51, 3rd	4.43, 4th	4.69, 2nd	4.34, 5th	5.35, 1st
5.0	7.32, 2nd	5.81, 3rd	5.81, 3rd	5.22, 5th	7.41, 1st
10.0	10.80, 1st	8.28, 4th	8.30, 3rd	7.74, 5th	10.48, 2nd
20.0	16.05, 1st	11.51, 4th	11.55, 3rd	10.84, 5th	14.69, 2nd
40.0	23.70, 1st	20.69, 2nd	16.31, 4th	15.48, 5th	19.96, 3rd

Table 7.15. Pullout Resistance at 0.75 in. of Displacement (lb, rank)

Pullout Resistance at 0.75 in. of displacement, (lb, rank)					
Overburden depth, ft	RECO Strap	15° Taper	30° Taper	0.75 in. welded washer	1.0 in. welded washer
2.5	308.0, 1st	230.9, 3rd	244.8, 2nd	226.5, 4th	226.5, 4th
5.0	500.3, 1st	302.9, 4th	303.0, 3rd	272.0, 5th	386.6, 2nd
10.0	737.8, 1st	431.9, 4th	433.0, 3rd	403.6, 5th	546.6, 2nd
20.0	1096.8, 1st	600.4, 4th	602.5, 3rd	565.2, 5th	765.9, 2nd
40.0	1619.3, 1st	1079.0, 2nd	850.6, 4th	807.5, 5th	1041.1, 3rd

REFERENCES

Chen, C.-W., Wu, J.Y. (2012). "Effects of wetting on the pullout resistance of geogrids in compacted silty sand." EJGE, 17, 2529-2540.

Cherdsak Suksiripattanapong, S. H. (2012). "Pullout resistance of bearing reinforcement embedded in coarse-grained soils." Geotextiles and Geomembranes, 44-54.

Horpibulsuk, S.N. (2010). "Pullout resistance of bearing reinforcement embedded in sand." Soils and Foundations, 50(2), 215-226.

Jensen, J. A. (2013). "Analysis of full scale mechanically stabilized earth (MSE) wall using crimped steel wire reinforcement." MS thesis, Div. of Geotechnical Engr., Utah State University. Logan. Utah.

Tin, N. (2010). "Factors affecting kinked steel grid reinforcement in MSE structures." Geotextiles ans Geomembranes, 9, 172-180.

APPENDIX

Table A.16. Deflection Measurements from Layer 1

Inter val	Row												Avera ge Lengt h
	1	2	3	4	5	6	7	8	9	10	1 1	12	
1	n/a	n/a	n/a	n/a	n/a	n/a	n/a	n/a	n/a	n/a	n/a	n/a	n/a
2	5.11 5	5.01 8	5.16 65	5.11 7	5.32 65	5.04 5	X	X	4.86 2	5.0 6	X	4.8 65	5.063 889
3	5.09 25	5.01 35	5.16 7	5.00 8	5.2	5.11 2	X	X	4.84 15	5.1 79	X	4.8 87	5.055 611
4	5.12 4	5.02 3	5.01	4.91 35	5.13 2	4.97 35	X	X	4.98 9	5.1 79	X	X	5.043
5	4.98 75	4.77 35	4.72 85	4.77 8	5.31 75	4.61 4	X	X	4.83 7	X	X	X	4.862 286

Table A.17. Deflection Measurements from Layer 2

	Layer 2 (in.)												
	Row												Average Length
Interval	1	2	3	4	5	6	7	8	9	10	11	12	
1	n/a	n/a	n/a	n/a	n/a	n/a	n/a	n/a	n/a	n/a	n/a	n/a	n/a
2	5.062	5.127	5.053	5.087	5.182	5.1875	5.186	5.149	5.176	5.096	5.235	5.235	5.147958
3	4.781	4.747	5.0025	5.201	4.882	4.934	5.287	4.981	4.904	5.031	5.082	4.848	4.973375
4	4.9265	4.7875	5.0185	4.96	5.072	5.236	4.987	4.948	4.873	4.971	4.997	4.959	4.977958
5	5.083	4.664	4.7975	4.6975	4.662	4.9	4.705	4.702	4.672	4.94	4.482	4.725	4.7525

Table A.18. Deflection Measurements from Layer 3

	Layer 3 (in.)												
	Row												Average Length
Interval	1	2	3	4	5	6	7	8	9	10	11	12	
1	n/a	n/a	n/a	n/a	n/a	n/a	n/a	n/a	n/a	n/a	n/a	n/a	n/a
2	X	5.342	5.229	5.223	5.237	5.235	5.087	5.157	5.263	5.417	5.105	5.207	5.227455
3	X	5.3425	5.207	5.15	5.174	5.206	5.142	5.079	5.175	5.396	5.244	5.206	5.211045
4	X	5.07	5.049	5.139	5.025	5.292	5.097	5.009	5.12	5.396	5.252	5.194	5.149364
5	5.267	4.822	4.81	5.209	4.923	5.487	4.742	4.761	4.725	5.086	4.852	4.796	4.956667

Table A.19. Deflection Measurements from Layer 4

Interval	1	2	3	4	5	6	7	8	9	10	11	12	Average Length
						Row							
1	n/a	n/a	n/a	n/a	n/a	n/a	n/a	n/a	n/a	n/a	n/a	n/a	n/a
2	X	X	X	5.404	5.275	5.29	5.314	5.102	5.492	X	X	5.144	5.288714
3	X	X	X	5.441	5.22	5.192	5.15	5.184	5.354	X	X	4.951	5.213143
4	X	X	X	5.389	4.925	4.555	4.738	4.704	4.992	5.048	X	4.757	4.8885
5	X	X	X	5.486	5.333	5.026	4.659	4.573	4.565	4.558	X	4.915	4.889375

Table A.20. Deflection Measurements from Layer 5

	Row												Average Length
Interval	1	2	3	4	5	6	7	8	9	10	11	12	
1	n/a	n/a	n/a	n/a	n/a	n/a	n/a	n/a	n/a	n/a	n/a	n/a	n/a
2	5.354	5.14	5.26	5.278	5.258	5.166	5.173	5.746	5.142	5.214	5.313	X	5.276727
3	5.375	X	X	X	5.124	5.196	5.175	4.908	5.231	5.028	5.12	X	5.144625
4	X	5.425	4.669	4.64	4.661	4.626	4.635	4.645	4.638	4.756	4.744	X	4.7439
5	X	5.168	4.939	4.512	5.062	4.55	4.561	4.56	4.451	4.639	4.604	X	4.7046

Table A.21. Deflection Measurements from Layer 6

	Row												Average Length
Interval	1	2	3	4	5	6	7	8	9	10	11	12	
1	5.229	5.251	4.968	4.812	4.77	4.994	4.758	5.071	5.292	4.933	5.326	5.204	5.050667
2	5.099	5.122	5.079	5.027	4.944	5.07	5.092	5.144	5.073	4.974	5.208	5.221	5.08775
3	4.96	4.927	4.958	4.704	4.806	4.9	4.862	5.805	4.846	8.864	4.771	5.681	5.340333
4	4.667	4.731	4.731	4.637	4.679	4.652	4.738	4.682	4.672	4.767	4.771	4.632	4.696583
5	n/a	n/a	n/a	n/a	n/a	n/a	n/a	n/a	n/a	n/a	n/a	n/a	n/a

Table A.22. Deflection Measurements from Layer 7

Interval	\multicolumn{12}{c}{Layer 7 (in.)}	Average Length
	Row	
	1	2	3	4	5	6	7	8	9	10	11	12	
1	5.335	5.177	5.058	4.934	4.802	4.982	5.068	5.237	5.092	5.135	5.043	4.877	5.062917
2	5.178	5.176	5.247	5.319	4.959	5.168	5.244	5.232	5.095	5.088	5.085	4.967	5.1465
3	4.874	4.919	4.894	4.745	4.764	4.949	5.063	5.121	4.931	4.959	4.75	4.769	4.894833
4	4.637	4.587	4.61	4.555	4.618	4.633	4.597	4.747	4.675	4.638	4.567	4.487	4.612583
5	n/a	n/a	n/a	n/a	n/a	n/a	n/a	n/a	n/a	n/a	n/a	n/a	n/a

Table A.23. Deflection Measurements from Layer 8

	Row												Average Length
Interval	1	2	3	4	5	6	7	8	9	10	11	12	
1	4.999	5.008	5.101	5.273	5.125	5.172	5.083	5.219	4.475	4.517	4.525	4.529	4.918833
2	4.936	4.962	5.006	5.114	5.024	5.105	4.888	5.286	4.755	4.968	5.038	5.068	5.0125
3	4.689	4.625	4.678	4.759	4.688	4.727	4.613	4.773	5.389	5.235	5.349	5.321	4.903833
4	4.573	4.491	4.508	4.504	4.503	4.441	4.45	4.525	4.923	5.175	5.166	5.129	4.699
5	n/a	n/a	n/a	n/a	n/a	n/a	n/a	n/a	n/a	n/a	n/a	n/a	n/a

Table A.24. Deflection Measurements from Layer 9

	Row												Average Length
Interval	1	2	3	4	5	6	7	8	9	10	11	12	
1	4.912	5.42	4.93	4.817	4.723	4.883	5.137	4.844	5.097	4.832	4.724	4.785	4.925333
2	4.573	5.201	4.707	4.733	4.634	4.689	4.617	4.69	4.682	4.631	4.686	4.719	4.7135
3	4.53	4.641	4.512	4.612	4.621	4.616	4.569	4.54	4.515	4.534	4.508	4.689	4.573917
4	4.889	4.467	4.483	4.475	4.49	4.479	4.466	4.667	4.564	4.534	4.508	4.521	4.54525
5	n/a	n/a	n/a	n/a	n/a	n/a	n/a	n/a	n/a	n/a	n/a	n/a	n/a

Layer 9 (in.)

Table A.25. Deflection Measurements from Layer 10

	Row												Average Length
Interval	1	2	3	4	5	6	7	8	9	10	11	12	
1	4.784	4.215	4.731	4.702	4.524	4.719	4.738	4.76	4.665	3.846	4.82	4.849	4.61275
2	4.64	4.798	4.573	4.46	4.508	4.578	X	4.534	4.523	4.36	4.521	4.614	4.555364
3	4.421	4.47	4.472	4.405	4.495	4.66	4.501	4.468	4.562	4.47	4.48	4.443	4.48725
4	4.429	4.41	4.412	4.36	4.447	4.448	4.438	4.363	4.427	4.442	4.286	4.394	4.404667
5	n/a	n/a	n/a	n/a	n/a	n/a	n/a	n/a	n/a	n/a	n/a	n/a	n/a

Table A.26. Layer 1 Crimp Measurements

Layer 1 (in.)		
Interval	Average Length	Interval Average Deflection
1	n/a	n/a
2	5.064	0.632
3	5.056	0.624
4	5.043	0.611
5	4.862	0.430
	Sum of Average Deflection =	2.297
	Layer Average Deflection =	0.574

Table A.27. Layer 2 Crimp Measurements

Layer 2 (in.)		
Interval	Average Length	Interval Average Deflection
1	n/a	n/a
2	5.148	0.716
3	4.973	0.541
4	4.978	0.546
5	4.753	0.321
	Sum of Average Deflection =	2.124
	Layer Average Deflection =	0.531

Table A.28. Layer 3 Crimp Measurements

Layer 3 (in.)		
Interval	Average Length	Interval Average Deflection
1	n/a	n/a
2	5.227	0.795
3	5.211	0.779
4	5.149	0.717
5	4.957	0.525
	Sum of Average Deflection =	2.817
	Layer Average Deflection =	0.704

Table A.29. Layer 4 Crimp Measurements

Layer 4 (in.)		
Interval	Average Length	Interval Average Deflection
1	n/a	n/a
2	5.289	0.857
3	5.213	0.781
4	4.889	0.457
5	4.889	0.457
	Sum of Average Deflection =	2.552
	Layer Average Deflection =	0.638

Table A.30. Layer 5 Crimp Measurements

	Layer 5 (in.)	
Interval	Average Length	Interval Average Deflection
1	n/a	n/a
2	5.277	0.845
3	5.144	0.713
4	4.744	0.312
5	4.705	0.273
	Sum of Average Deflection =	2.142
	Layer Average Deflection =	0.535

Table A.31. Layer 6 Crimp Measurements

	Layer 6 (in.)	
Interval	Average Length	Interval Average Deflection
1	5.051	0.619
2	5.088	0.656
3	5.340	0.908
4	4.697	0.265
5	n/a	n/a
	Sum of Average Deflection =	2.447
	Layer Average Deflection =	0.612

Table A.32. Layer 7 Crimp Measurements

Layer 7 (in.)		
Interval	Average Length	Interval Average Deflection
1	5.063	0.631
2	5.147	0.715
3	4.895	0.463
4	4.613	0.181
5	n/a	n/a
	Sum of Average Deflection =	1.989
	Layer Average Deflection =	0.497

Table A.33. Layer 8 Crimp Measurements

Layer 8 (in.)		
Interval	Average Length	Interval Average Deflection
1	4.919	0.487
2	5.013	0.581
3	4.904	0.472
4	4.699	0.267
5	n/a	n/a
	Sum of Average Deflection =	1.806
	Layer Average Deflection =	0.452

Table A.34. Layer 9 Crimp Measurements

Layer 9 (in.)		
Interval	Average Length	Interval Average Deflection
1	4.925	0.493
2	4.714	0.282
3	4.574	0.142
4	4.545	0.113
5	n/a	n/a
	Sum of Average Deflection =	1.030
	Layer Average Deflection =	0.258

Table A.35. Layer 10 Crimp Measurements

Layer 10 (in.)		
Interval	Average Length	Interval Average Deflection
1	4.613	0.181
2	4.555	0.123
3	4.487	0.055
4	4.405	-0.027
5	n/a	n/a
	Sum of Average Deflection =	0.332
	Layer Average Deflection =	0.083
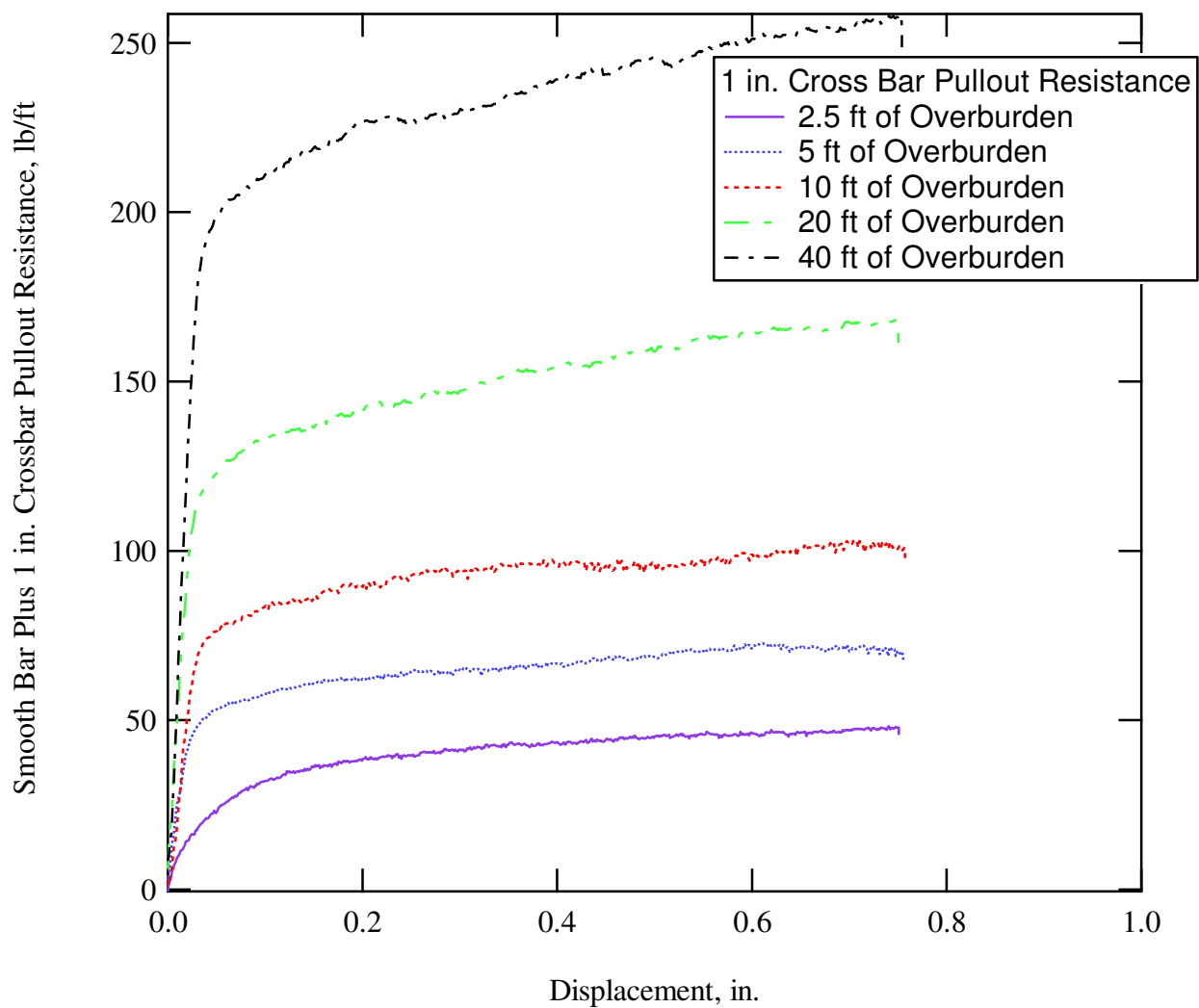
Fig. A.118. Smooth bar plus 1 in. cross bar pullout resistance
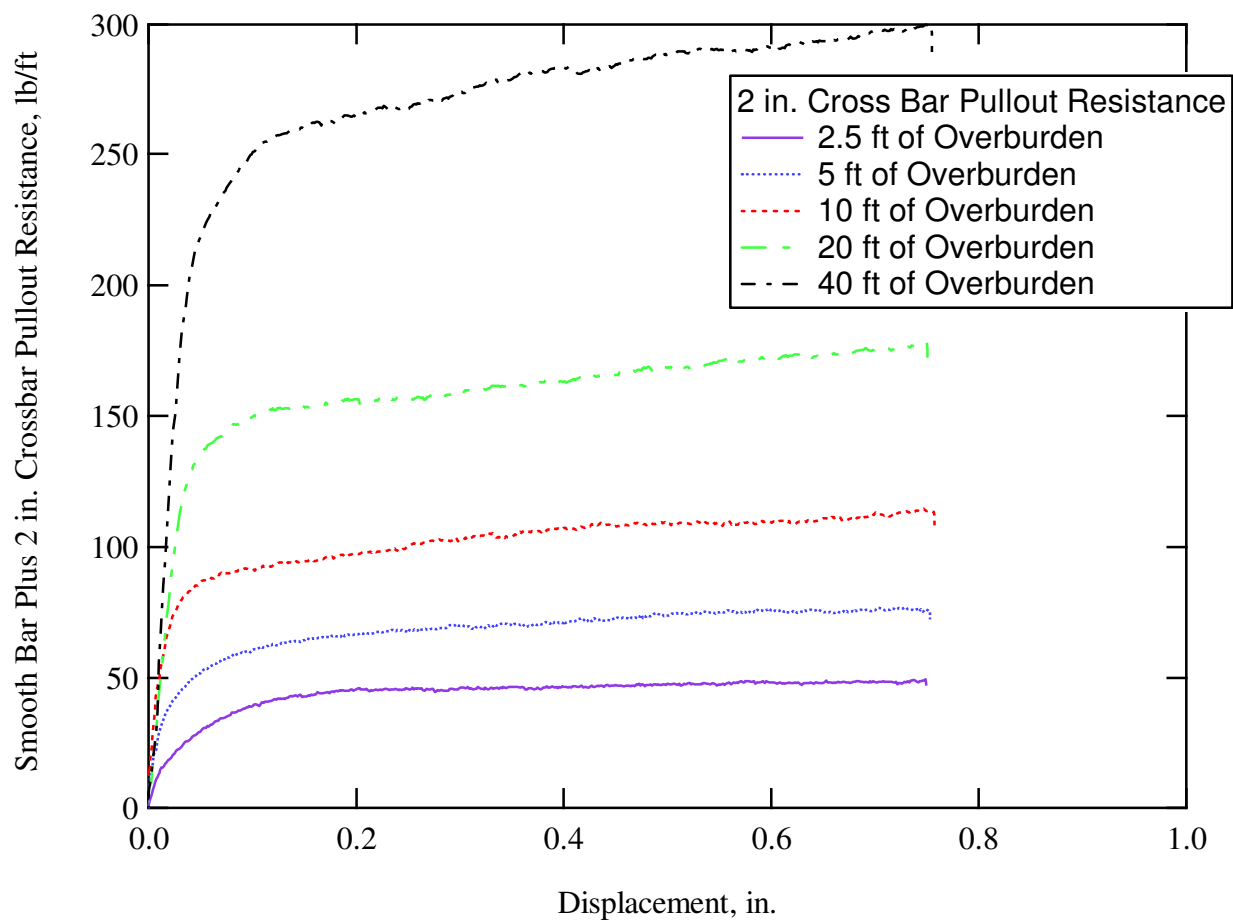
Fig. A.119. Smooth bar plus 2 in. cross bar pullout resistance
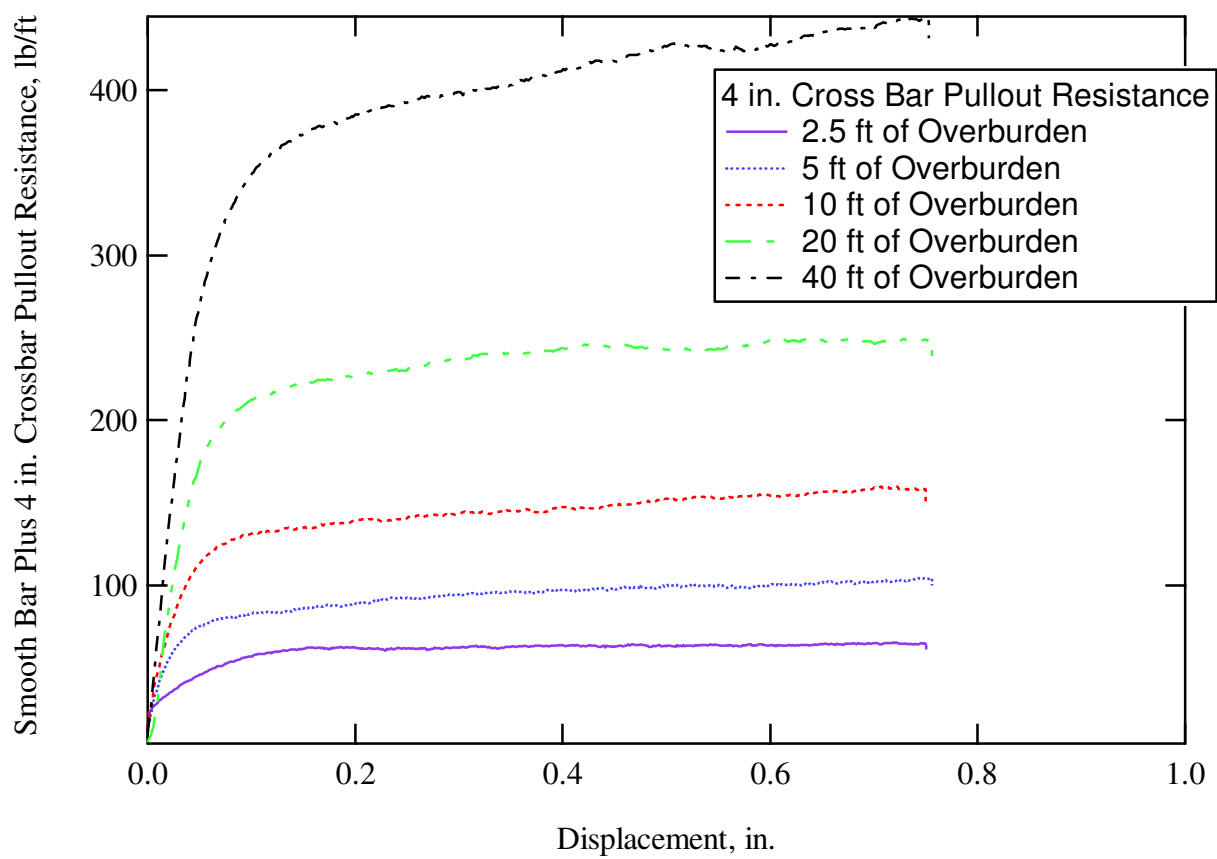
Fig. A.120. Smooth bar plus 4 in. cross bar pullout resistance
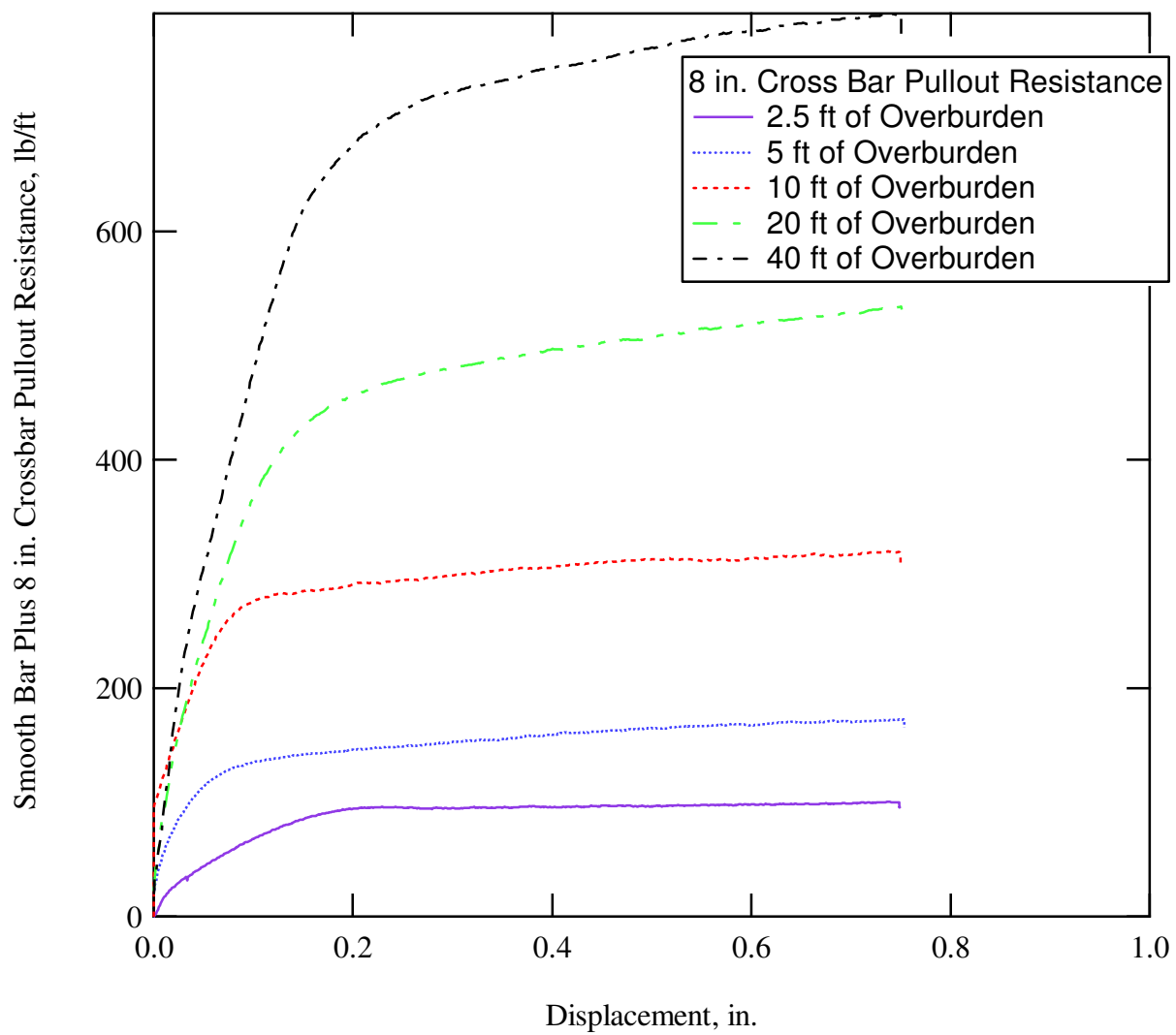
Fig. A.121. Smooth bar plus 8 in. cross bar pullout resistance